A New Decarboxylase:

A Mechanistic Characterization of PrFMN Decarboxylase FDC1

By

Kyle Louis Ferguson

A dissertation submitted in partial fulfillment of
The requirements for the degree of
Doctor of Philosophy
(Chemistry)
in the University of Michigan
2018

Doctoral Committee:

Professor E. Neil G. Marsh, Chair
Assistant Professor Kristin Koutmou
Associate Professor Bruce A. Palfey
Professor Nils G. Walter

kferge@umich.edu

ORCID: 0000-0002-8317-756X

Dedication

I would like to dedicate this body of work to my grandfathers, Charles Frank Iantorno and Tom Ferguson, for instilling me with a lifelong love of learning and curiosity, to my grandmothers Kathy Ferguson and Ariadne Iantorno for their constant encouragement, to my parents Tina & Kevin Ferguson for giving me the drive to discover and for their continued support to pursue science, and to my brothers Rob, Andrew, and Ryan for all their support.

Acknowledgements

First and foremost, I would like to take this opportunity to thank Prof. E. Neil G. Marsh, my advisor, for his invaluable guidance and support. I have truly learned an incredible amount from him about scientific writing, experiment design, and how to become a productive and independent scientist. I would like to thank him for his patience and understanding during this herculean endeavor.

I would like to thank my committee members Prof. Bruce Palfey, Prof. Kristin Koutmou, and Prof. Nils Walter for their suggestions, guidance, and assistance in my thesis. I would personally like to extend my thanks to Prof. Brandon Ruotolo, Dr. Joseph Eschweiler, and Chunyi Zhao for their assistance with mass spectrometry.

I am grateful to Dr. Fengming Lin for laying the ground work for this project, and to Dr. Tadeuz Orgozalek, Dr. Matthew Waugh, and Dr. Aaron Sciore and the rest of the Marsh lab for their patience and effort in training me on the various equipment and making lab a fun and enjoyable place to work. Finally, I would like to offer a special thanks to Dr. Gabriel Roman, for supporting and teaching me as well as convincing me to join the Marsh lab.

I would like to thank the members of the University of Michigan's Mass Spectrometry and Nuclear Magnetic Resonance facilities. I would like to thank the undergraduates and the graduate students I trained on this project including David Boyer, Eden Koo, Ryan McGinnis, KaKa Ho, Matthew Goodrich, and April Kaneshiro for working with me and putting up with me as well as for their invaluable contributions during their time they worked on this project.

I'd thank all of my friends especially Jake Boissanault, Kyle Williams, Sam Esarey, April Kanashiro, and Evan Stevenson for helping keep me sane during the course of this project. Your

advice and friendship was what helped propel me through the snowy winter months here in Michigan. Finally, I would like to thank my family for all their love and support.

TABLE OF CONTENTS

List of Tables

List of Figures

List of Appendices

List of Abbreviations, Acronyms, and Symbols

[E] – enzyme concentration
Δfdc1 – FDC1 knock out in *S. cerevisiae*
Δfdc1/Δpad1 – FDC1 and PAD1 knocks out in *S. cerevisiae*
Δpad1 – PAD1 knock out in *S. cerevisiae*
ΔubiX – UbiX knockout gene
µL – microliter
µm – micrometer
µM – micromolar
µM – micromollar
A – Alanine
ACMSD – α-amino-β-carboxymuconate-ε-semialdehyde decarboxylase
BAPAD – *B. amyloliquenfaciens* phenolic acid decarboxylase
ChEBI – chemical entities of biological interest
cm - centimeter
D_2O – deuterium oxide
DCl – deuterated chloride
DFT – density functional theory
DMAP – dimethyl ally phosphate
DMSO – dimethylsulfoxide
DNA – Deoxyribonucleic acid
dNTP – deoxyribose adenine triphosphates
dsDNA – double stranded DNA
E – Glutamic Acid
ε^o - extinction coefficient
EpiD - phosphopantothenoylcysteine decarboxylase for *E. coli*
EtOAc- Ethylacetate
eV – electron volts
FA – Ferulic Acid
FDC1 – Ferulic acid decarboxylase from *Saccharomyces cerevisiae*
fdc1- ferulic acid decarboxylase 1 encoding gene
FMN_{ox} – Oxidized Flavin mononucleotide
FMN_{red} – Reduced Flavin mononucleotide
FNVB – 2,2 fluoronitrovinylbenzene
GC – Gas chromatography
GC-MS – Gas chromatography with a mass spectrometry
H_2O – water
HOMO – highest occupied molecular orbital
HPLC – High pressure liquid chromatography
hr(s) – hours

IPTG – Isopropyl β-D-1-Thiogalactopyranoside
k_{cat} – turnover number
kDa – kilodalton
$KHCO_3$ – potassium bicarbonate
KIE – Kinetic Isotope Effects
K_M – Michaelis Constant
kV – kilovolts
L – Liter
LC-ESI-MS – liquid chromatography electron spray ionization mass spectroscopy
LC-MS – Liquid chromatography mass spectrometry
LFER – Linear Free Energy Analysis
log – log based 10
LPPAD – *Lactobacillus plantarum* phenolic acid decarboxylase
LUMO – lowest unoccupied molecular orbital
m – meter
M – molar
MeOD – 1-deuterated methanol
Mg – magnesium
mg – milligram
min – minute
mm – milimeter
mM – milimolar
MMCD – methylmalonyl CoA decarboxylase
mol% – molar percentage
MrsD – phosphopantothenoylcysteine decarboxylase for *E. coli*
MS^2 – Tandem mass spectrometry
NADH – Nicotinamide Adenine Dinucleotide
NADPH – Nicotinamide Adenine Dinucleotide Phosphate
NaOD – sodium deuteroxide
NEB – New England Biolabs
NH_4HCO_3 – ammonium bicarbonate
nm – nanometer
NMR – Nuclear Magnetic Resonance
ºC – Degrees Celsius
OhbA1 – *Aspergillus niger* ferulic acid decarboxylase
OHCUD – 2-oxo-4-hydroxy-4-carboxy-5-ureidoimidazoline decarboxylase
OMPCD – orotidine 5' – monophosphate decarboxylase
PAD – Phenolic Acid Decarboxylase
PAD1 – Phenolic Acid Decarboxylase from *Saccharomyces cerevisiae*
pad1– phenolic acid decarboxylase 1 encoding gene
PBS – phosphate buffer saline buffer
PCR – Polymerase chain reaction
pD – Negative log of deuterium ion concentration
PDB – protein data bank
pFDC – pET28b FDC1 plasmid
pH – Negative log of hydrogen ion concentration

PPC – phosphopantothenoylcysteine decarboxylase
PrFMN – prenylated Flavin mononucleotide
Q – Glutamine
R –Arginine
SDS-PAGE – Sodium dodecylsulfate polyacrylamide gel electrophoresis
SKIE – Solvent Kinetic Isotope Effects
TCA – *trans*-cinnamic acid
TCA – *trans*-cinnamic acid
TCEP – tris(2-carboxyethyl)phosphine
tPAD1 – PAD1 with the first 58 amino acids truncated from the sequences
TrisHCl – Tris(hydroxymethyl)aminomethane hydrochloride
U.V.-vis – Ultra Violet visible spectroscopy
ubiD – ubiquinone synthase D encoding gene
UbiD – Ubiquinone synthase D from *E. coli*
ubiX – ubiquinone synthase X encoding gene
UbiX – Ubiquinone synthase X from *E. coli*
V – volts
ν – velocity of the reaction
V/K – k_{cat}/K_M
WT – Wild type protein
ρ - rho
σ – Hammett electron substituent constant
σ- – negative Hammett electron substituent constant
σ+ – positive Hammett electron substituent constant
χ – mole fraction

Abstract

The large number of inexpensive carboxylic acids found in nature has spurred research to convert carboxylic acids to an assortment of other functional groups for a range of purposes. To accomplish this, researchers employ a variety of strategies ranging from heat and heavy metals to biocatalysts. Ferulic acid decarboxylase (FDC1) from *Saccharomyces cerevisiae* is a member of the UbiD family of decarboxylase enzymes. The UbiD family of proteins consists of prenylated flavin (PrFMN)-dependent enzymes that catalyze the reversible decarboxylation of a wide variety of aromatic carboxylic acids. The UbiD family attracted interest as a biocatalyst to produce chemical feedstocks from renewable sources and as a potential target for antimicrobial research.

The UbiD enzyme, FDC1, and its associated protein partner, PAD1, were identified as being responsible for the detoxification of aromatic carboxylic acids in fungi. How PAD1/FDC1 work together to facilitate the decarboxylation of toxic aromatic acids remains an open question. The genes encoding PAD1 and FDC1 were independently expressed in *E. coli* with the PAD1 homolog UbiX knocked out. Independently, FDC1 and PAD1 were unable to decarboxylate phenylacrylic acids. Moreover, PAD1 failed to decarboxylate any of the phenylacrylic acids by itself. In contrast FDC1 was able to recover its decarboxylase activity upon the addition of PAD1 or its homolog UbiX, indicating FDC1 was solely responsible for the decarboxylase activity. Co-expression of FDC1 and PAD1 coupled with the sole purification of FDC1 exhibited spectral characteristics of a reduced flavin in an aerobic system. This increased the k_{cat} by 8-fold.

The holo-FDC1 crystal structure (PDB 4ZAC) provided insight into the decarboxylation mechanism of FDC1. FDC1 was proposed to perform a unique and controversial 1,3-dipolar cycloaddition mechanism. To address the controversial nature of the proposed mechanism KIE and a Hammett analysis were utilized to ascertain whether FDC1 undergoes the proposed mechanism or a completely different mechanism. The solvent isotope effects, normal secondary isotope effects, and the negative slope of the Hammett analysis are consist with the rate-determining step being the breakdown of the PrFMN-product adduct through a non-concerted cyclo-elimination reaction, and provides evidence in favor of the novel 1,3-dipolar cycloaddition mechanism.

The proposed mechanism involves the formation of a novel pentacyclic intermediate through a novel 1,3-dipolar cycloaddition mechanism between PrFMN and the β -γ double bond of the substrate, which serves to activate the substrate towards decarboxylation. In order to trap this hypothesized intermediate, a mechanism-based inhibitor 2-fluoro-2-nitro-vinylbenzene (FNVB) was used to trap the putative cyclo-addition intermediate. Upon incubating FNVB with FDC1, there was a red-shift in the flavin spectrum which is reminiscent of an uncharged N5, C4α dialkyl flavin adduct and is consistent with a 1,3-dipolar cycloadduct. Finally by pushing the equilibrium of the FDC1 reaction to favor the formation of product-PrFMN adducts: $_{7}$dstyrene-PrFMN and styrene-PrFMN intermediates were isolated and characterized by Tandem Native Mass Spectrometry.

FDC1 decarboxylates phenylacrylic acids by forming a novel 1,3-dipolar cycloaddition adduct, followed by a Grob fragmentation, protonation of the intermediate, re-cyclization between the PrFMN and the product, then finally product release. This work lays the

groundwork for developing new biocatalysts from these UbiD decarboxylases and the development of a new class of antifungal or antibiotics drugs.

Chapter 1

Introduction

1. Sustainability

As the global population approaches the United Nations prediction of 9 billion by 2050, perhaps the most significant and imminent challenge facing humanity is that of sustainability. In the last one hundred and fifty years, the exponential growth of our population, globalization of communication, and economic networks has been driven by fossil fuels, ancient carbon reserves derived from animals and plant matter long decayed[1]. These resources are finite and will likely deplete by the end of the current century. The increasing scarcity of these resources will result in an increase in international conflicts over what little of these resources remain. To avert the

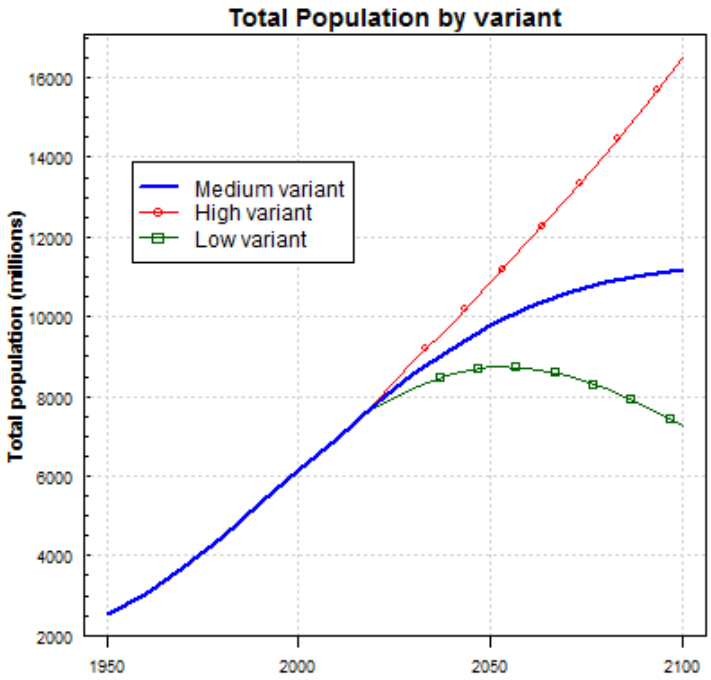

Figure 1.1-United Nations projected world population growth mode. The blue line shows the median, the green and red lines are based on high and low predictions[1].

political and economic catastrophe that would result upon the depletion of fossil fuels, sustainable solutions are urgently needed. A major focus of these efforts is developing alternative synthetic solutions for a variety of high-value compounds derived from fossil fuels including, alkanes, polyaromatic compounds, and vinylbenzene derivatives.

1.1. Carboxylic Acids as a Renewable Chemical Feedstock

Carboxylic acids are available inexpensively from a wide variety of synthetic and natural sources such as lignin. Lignin is a class of organic polymers, particularly prevalent in plant cell walls and vascular tissue, consisting of primarily cross-linked phenolic polymers, which when broken down under oxidative conditions yield a wide array of aromatic carboxylic acids. They are easy to store and handle and have long served as a versatile connection point in the construction of carbon frameworks, and as a chemical feedstock for the production of valuable commodity chemicals[2]. Carboxylic acids are highly prevalent in biomass, which currently make up the greatest proportion of renewable raw materials in the chemical industry[2-5]. These materials offer a sustainable feedstock that provides a large number of possibilities that exceed the opportunities provided by petrochemistry[6]. Currently more than 90% of the oleochemical reactions involving these biorenewable materials involve carboxylate groups. To utilize these materials, synthetic chemists employ numerous biotechnological and chemical techniques to transform these materials into commodity chemicals including polymer building blocks and food preservatives.

One valuable class of carboxylic acids are phenylacrylic carboxylic acids, which are prevalent in lignin biomass. Phenylacrylic acids need to be depolymerized from the lignin biomass and then be decarboxylated, which often involves chemically harsh or energetically costly processes, both of which will be detailed later in this chapter. Finally, the phenylacrylic

acids are transformed into commodity chemicals such as polystyrene, which currently constitutes a growing $40 billion market[6-8]. Styrene and styrene derivatives serve as monomers for a variety of polymers including: high impact plastics, styrene sulfonate polymers for medical uses, and as a general building material. Other valuable vinyl benzene derivatives include vinyl guaiacol, a food preservative, and vinyl phenol, which serves as a building block to a wide variety of anthromycin derivatives, which can be used as a food additive or as an n-junction material in dye-sensitized solar cells. Carboxylic acids provide a cheap, stable, and renewable chemical feedstock for a variety of commodity compounds and are thus of great interest to the chemical industry[8].

1.2. Chemical Synthetic Strategies for Aromatic Carboxylic Acid Decarboxylation

A conventional strategy to decarboxylate materials from renewable chemical feedstocks to valuable products is to heat these compounds up to 150 ºC-200 ºC in the presence of sodium hydroxide or another base. However many aliphatic and aromatic carboxylic acids only give yields approximating 5-10%, which is ineffective for mass scale production[9-11].

In order to decarboxylate a wider variety of substrates, chemists and chemical engineers often use a heavy metal catalyst to stabilize the carbanion that results from decarboxylation. A range of aryl and heteroaryl decarboxylation yields were improved using a copper(I)oxide and 1,10-phenanthroline at 5 mol% catalytic loading; this resulted in an increase in yield from 5-10% upwards to 98% yield over the timescale of minutes. Further improvement of yields was accomplished using different heavy metals such as palladium or platinum[11, 12]. Unfortunately, all the conventional chemical decarboxylation processes that possess high yields suffer from several disadvantages including using heavy metal catalysts, being energetically costly, and requiring harsh organic solvents such as quinoline[10]. These disadvantages prevent

these decarboxylation processes from being industrially sustainable, thus spurring the search for a low-cost alternative to decarboxylate aromatic carboxylic acids to produce aromatic compounds.

1.2. Biochemical Strategies for Aromatic Carboxylic Acid Decarboxylation

1.2.1. Advantages of Using Enzymes for Decarboxylation

Enzymes offer solutions to the problems of conventional chemical synthetic routes. Enzymes are very efficient catalysts catalzye reactions 10^8-10^{12} times faster than those of the corresponding non-catalyzed reactions and are thus exceed the rate enhancement values that chemical catalysts are capable of achieving[13, 14]. Therefore, chemical catalysts are generally employed at a 0.1-1 mol% of catalyst loading, whereas most enzymatic reactions can be performed with a mole percentage of 0.001-0.0001 mol%. However, enzyme preps are usually significantly more expensive than small molecule catalysts. Enzymes are environmentally benign unlike the metal catalysts that present in conventional synthesis, and act under environmentally benign conditions. Enzymes exhibit the highest activity in near physiological conditions in water, typically around pH 7, and preferably around 30 ºC. This minimizes the problems of undesired side-reactions such as decomposition, isomerization, racemization, and rearrangement. In synthetic decarboxylation chemistry, the high temperatures required result in the destruction of other sensitive groups including amino, ether, ester, and other carboxylic acid groups. Enzymes, on the other hand, act on a single functional group, while leaving other sensitive functionalities intact. In addition, due to their complex three-dimensional structure, enzymes can distinguish between functional groups that are chemically identical but situated in different positions within the same substrate molecule[4, 14].

1.2.2. Problems with Biocatalysts

Enzymes exhibit a few general disadvantages as well as a few specific disadvantages in the area of aromatic carboxylic acid decarboxylation. Enzymes require narrow operation parameters, requiring conditions near their optimal temperature and pH. Therefore, if a reaction proceeds slower than industrially desired under these narrow parameters, there is only a small window for alteration. Elevated temperatures and extreme pH values lead to the deactivation of the protein, as do high salt concentration. Hence these narrow operation conditions prevent radical changes. Enzymes also often exhibit their highest catalytic activity in water, but due to the high boiling point, high heat of vaporization, and its tendency to promote corrosion, water is often considered to be the least suitable solvent for organic reactions. Furthermore, the majority of organic compounds exhibit poor solubility in water. Thus, enzyme reactions that perform organic transformations either need to use a biphasic solvent system or perform the organic reaction in organic solvents. Both of these cases often result in enzymes exhibiting lesser activity relative to native reaction conditions, usually by an order of magnitude.

Aromatic carboxylic acid decarboxylases seem to be prone to the tight binding of substrate and product molecules. This tight binding causes a drop in the reaction rate at elevated substrate or product concentrations. This drop in the reaction rate limits the efficiency of the process. While substrate tight binding can be easily solved by introducing substrate at a steady rate, product inhibition can be more complex to solve. Specifically, aromatic acid decarboxylases seem to be prone to product inhibition.

1.2.3. How can Aromatic Carboxylic Acid Decarboxylases be Improved?

To solve the issue of product inhibition, researchers explored the use of an organic phase in a biphasic reactor to remove the more lipophilic products. Agitation of the reactor causes the

more lipophilic products to cross the aqueous/organic membrane thus removing the product from the aqueous phase where the enzymatic reaction occurs.

A second issue is that most enzymes are often unable to operate at temperatures above 37 ºC. Higher temperatures would increase the activity, and the yield of these enzymes, and thus make more appealing catalysts for these decarboxylation processes. Fortunately, success in addressing these issues was made through the advent of site-specific mutagenesis by Michael Smith. Site-specific mutagenesis provides a method by which enzymes can be redesigned using structure and sequence information which result in enhanced properties[15]. A notable success story involves the enhancement of the thermostability of xylanase from *Aspergillus niger* BCC14405. By substituting surface serine and threonine residues with arginine, researchers were able to increase the activity of the enzyme at 50 ºC from 15% of its native activity to 80% of its native activity[16].

Consequently, a technique that has gained much support in addressing issues unique to enzymes is rational design. Rational design involves precise changes in amino acid sequence and protein structure based on precise knowledge of the structure and mechanism of these enzymes[17]. Phenylacrylic acid decarboxylases such as the PAD family or the UbiD family could be targets for rational design. With the crystal structure available for several UbiD/UbiX derivative enzymes, as well as some initial characterization of mechanism for the PAD family [18-21], it is certainly feasible to use rational design to improve these decarboxylase enzymes.

1.2.4. Whole-cell Conversion of Phenylacrylic Acids

Numerous whole-cell platforms exist to decarboxylate a variety of phenylacrylic acids including *Saccharomyces cerevisiae*, *Escherichia coli*, *Aspergillus niger*, and *Bacillus pumilus*.

These systems have either been studied to investigate decarboxylation pathways to break down phenylacrylic acids or engineered to improve their activity[22-32].

One of the earliest systems studied was the breakdown of ferulic acid by *A. niger*. Ferulic acid is one of the most abundant phenolic compounds, present in most plants, and is well known for its antioxidant and antifungal properties. As a result, bacteria and fungi present in ruminant animals developed mechanisms to breakdown ferulic acid[26, 33, 34]. Baqueiro-Pena provided an analysis on how two strains of *A. niger*, the diploid strain DAR2 and the wildtype strain, break down ferulic acid. The main difference was that the wild type produced both vanillic acid and vinyl guaiacol, while the diploid mainly produced vinyl guaiacol. This suggested that the diploid strain of *A. niger* more readily performed a non-oxidative decarboxylation of ferulic acid to vinyl guiacol. Baquiero-Pena hypothesized that the decarboxylation of ferulic acid was part of a detoxification system similar to that of *Paecilomyces variotii* or *Pestalotia palmarum* which is designed to maintain ferulic acid and similar inhibitory compounds under a threshold concentration[25]. The breakdown of these inhibitory compounds was dependent on the presence of two gene products PadA1 and OhbA1, which are orthologs to the gene products UbiX and UbiD respectfully and are responsible for the decarboxylation of 3-octaprenyl-4-hydroxybenzoic acid[27]. Substrate profiling in *A. niger* indicated that OhbA1/PadA1 decarboxylase system exhibits broad activity with a number of aromatic and sorbic acid analogs, indicating that this decarboxylation system is promiscuous in order to protect the fungus from the many xenotoxins that it may encounter[27].

The first engineered whole-cell system that catalyzed the decarboxylation of ferulic acid to 4-vinyl guaiacol was in *B. pumilus* in a two phase aqueous-organic system[28]. Whole-cells expressing the ferulic acid decarboxylase appeared to require no cofactor and exhibited specific

activity of 0.22 µM/min and a K_M of 7.9 mM for ferulic acid. Ferulic acid has a high water solubility, whereas its decarboxylated product, vinyl guaiacol, is poorly soluble. However, vinyl guaiacol has been reported to inhibit the enzyme. In an effort to increase the yield of vinyl guaiacol, Lee et al. decided to employ a 2-phase reaction system to remove the product of the reaction; this resulted in a considerable (300%) increase in activity[28].

In an effort to lower the costs of these whole-cell systems, McKenna et al. devised a novel synthetic route for styrene from renewables using glucose as the substrate[22, 35]. The proposed styrene pathway utilizes endogenously synthesized L-phenylalanine as the precursor metabolite that could be converted to styrene in two enzymatic steps (Figure 1.2). First, L-phenylalanine is converted to TCA through deamination, as catalyzed by phenylalanine ammonia lyase (PAL). The second step in the proposed styrene biosynthesis pathway involves the decarboxylation of TCA by a ferulic acid decarboxylase (FDC1) from *S. cerevisiae* to yield styrene as its final product. TCA decarboxylase activity in *S. cerevisiae* is dependent on the overexpression of two gene products PAD1 and FDC1. FDC1 from *S. cerevisiae* shares significant genetic similarity with previously established OhbA1 and UbiD enzymes of *A. niger* and *E. coli* respectively[27,22, 35].

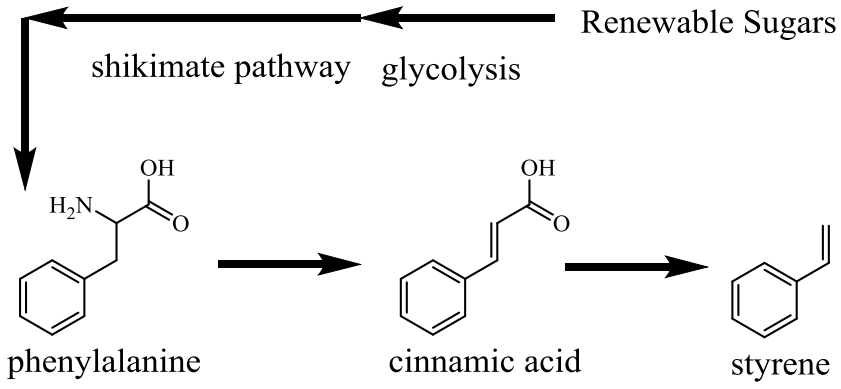

Figure 1.2 Pathway from renewable sugar to styrene proposed by McKenna et al[22].

These whole-cell platforms to decarboxylate phenylacrylic acids, unfortunately, suffer from critical flaws that preclude the use of these biocatalysts from industrial use. These whole-cell platforms are too slow to compete with the industrial processes with k_{cat}/K_M values ranging in the 10^{-1}-10^{1} $M^{-1}s^{-1}$ far below the desired value range of 10^{5} $M^{-1}s^{-1}$, which is the threshold for most biocatalyst to compete with conventional industrial catalyst[13, 14].

1.2.5. Single Enzyme Decarboxylation: Phenylacrylic Acid Decarboxylation

In order to solve some of the problems discussed, researchers isolated the phenylacrylic acid decarboxylases from these various species to characterize, study, and asses their suitability for industrial use[36]. From this effort emerged two distinct decarboxylase families: the PAD family that required no cofactors and the UbiD family which appears to utilize a FMN-binding domain, but still participates in non-oxidative decarboxylation. Isolated enzymes typically exhibit higher average activity than whole-cell preparations and thus, may be better suited to industrial applications. Phenylacrylic acid decarboxylases and UbiD decarboxylases have been isolated from a variety of sources, but the best studied examples are PAD from *Bacillus amyloliquefaciens* and FDC from *A. niger* and *S. cerevisiae*.

1.3 The PAD Family of Enzymes

The PAD family of enzymes is involved in the breakdown of lignin[37]. Plant matter is a major component of many ruminant animal diets. The breakdown of plant matter results in a high concentration of two common compounds *p*-coumaric acid and ferulic acid which are toxic to many gut microbes[26, 33, 34, 38]. The mechanism by which these enzymes decarboxylate *p*-hydroxyphenylacrylic acid derivatives (Figure1.3) was described for the PAD enzyme from *Lactobacillus plantarum*[31, 39, 40]. The first step of the catalytic mechanism is the abstraction of a proton from the phenolic group of *p*-coumaric acid by glutamate 71. Tautomerization to the

quinone form allows the β-carbon to abstract a proton from most likely water to form a *p*-quinone methide intermediate. In the second step, the *p*-quinone methide intermediate undergoes decarboxylation, liberating carbon dioxide and forming a vinylogous double bond[39, 40].

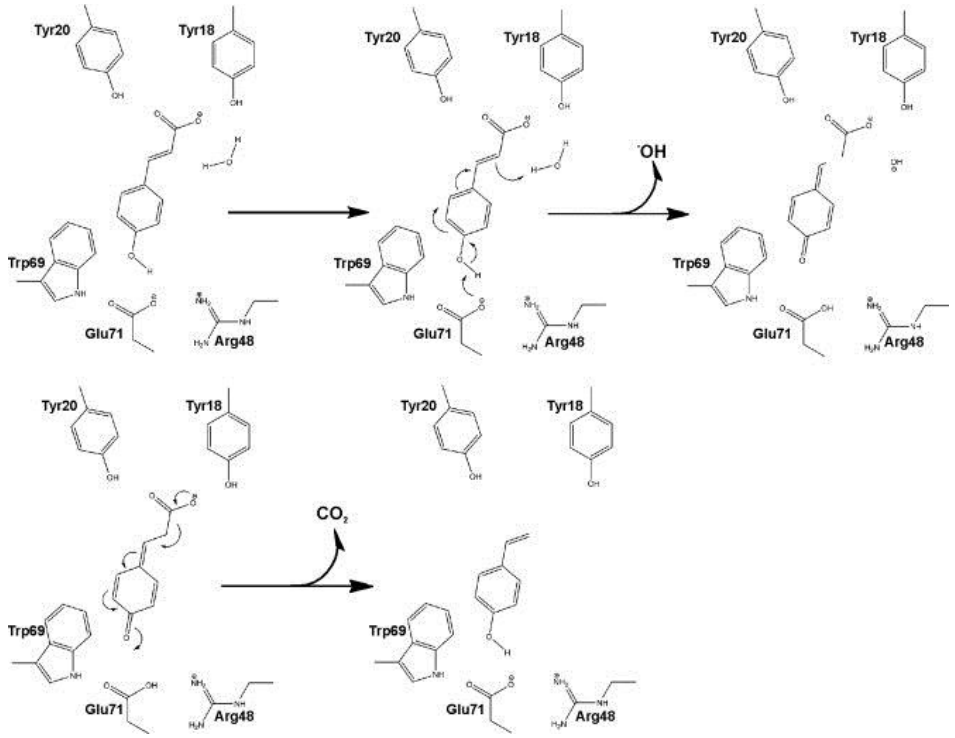

Figure 1.3 Proposed decarboxylation mechanism of PAD family members *Lactobacillus plantarum*[39,40].

Phenolic acid decarboxylase from *B. amyloliquefaciens* was identified as a member of the PAD family of enzymes based on a sequence-based subgroup analysis. This involved using *B. subtilis* as a seed sequence for PSI-BLAST of which the top 250 were collected after the 10th iteration. Multiple alignment sequences were performed and scored using a BLOSUM62 scoring matrix, the top 8 scoring corresponding proteins were chosen and expressed[41]. This analysis was designed to select enzymes to exhibit better decarboxylase activity over previously established PAD enzymes. This approach identified 8 target sequences likely to have higher activity over previously described purified PAD enzyme. The analysis identified PADs from *B. amyloliquenfaciens, Bacillus coaglulans, Citrobacter sp., Lactobacillus fermentum, L.*

plantarum, *Lactobacillus sakai*, *Pediococcus pentosaceus*, and *Streptomyces sviceus*, which were chosen for study[30].

B. amyloliquenfaciens PAD along with 7 other PAD sequences were cloned in *E. coli* BL21 DE3. Only 5 of the PAD sequences, BAPAD, PPPAD, LFPAD, LPPAD, and LSPAD, had activity. BAPAD had the highest activity (366 μmol min^{-1} mg^{-1} enzyme) and was chosen for further characterization[30]. BAPAD was active in a pH range of 4.0-6.0 at 37 ºC with the pH optimum being 5.8. BAPAD appeared to require no cofactor[30]. BAPAD catalyzed the decarboxylation of a range of phenylacrylic acids including *p*-coumaric acid, ferulic acid, and caffeic acid. However, BAPAD showed no activity for substrates without the *p*-hydroxy group such as *m*-coumaric acid, *o*-coumaric acid, and cinnamic acids, nor did it possess activity for substrates with additional methoxy groups in the two meta positions such as sinapinic acid. Steady-state kinetics of BAPAD showed a K_M value of 0.7 mM pCA, a k_{cat} value of 6000 s^{-1}, and a k_{cat}/K_M value of $8.6x10^6$ $M^{-1}s^{-1}$. These values are the highest reported values in the literature to date[30].

BAPAD, like many previously described whole-cell systems, suffers from competitive product inhibition. In aqueous systems, *p*-hydroxystyrene builds up, ultimately inhibiting BAPAD and lowering the yield of the reaction to 22.7%. The K_i of BAPAD was determined to be 20 mM *p*-hydroxystyrene. In order to overcome product inhibition, water-immiscible organic solvents were employed to remove products from the reaction. The highest conversion yield, 88.4%, was achieved by using a biphasic system with 1-octanol as the organic phase. BAPAD, to date, is the most catalytically efficient non-oxidative decarboxylase to date[30].

1.4. The UbiD/UbiX and FDC1/PAD1 Decarboxylation System

The UbiD family was first identified and named after the *E. coli* UbiD protein, which is proposed to decarboxylate 3-octaprenyl-4-hydroxybenzoate, an intermediate in the biosynthesis pathway of ubiquinone in bacteria[19, 42-45]. UbiD-like enzymes and their corresponding UbiX-like counterparts have often been reported to act in tandem to facilitate various decarboxylation processes. UbiD homologs have also been determined to be part of an alternative biosynthetic pathway in cyanobacteria to produce menaquinone from 1,4-dihydroxy-6-naphthoate[46]. The structure of UbiD from *Pseudomonas aeruginosa* has also recently been elucidated. UbiD shares some distinct structural homology to a family of NADH:FMN oxidoreductases, as well as the flavin-dependent EpiD and MrsD cysteine decarboxylases[20, 47]. The crystal structure of *P. aeruginosa* UbiD only showed magnesium bound to the enzyme, rather than a flavin. The UbiD homolog FDC1 from *S. cerevisiae* exhibits a range of differences from UbiD including the location of metal ions, the location of the active sites, and its reported oligomerization state. The UbiD family of proteins as a whole (Figure 1.4) exhibit a significant variation of substrate scope and previous studies indicate that members of the UbiD family form oligomers, either with other UbiD-like proteins or distinct subunits[18, 19].

Members of the UbiD family catalyze a wide range of reversible decarboxylation reactions (Figure 1.4). In nature, these enzymes are involved in a wide array of biochemical processes ranging from breaking down xenotoxins in *S. cerevisiae* and *A. niger* to being responsible for the decarboxylation of 3-octaprenyl-4-hydroxybenzate in the bacterial ubiquinone biosynthetic pathway. Due to the lack of mechanistic characterization efforts concerning the UbiD family of enzymes, FDC from *S. cerevisiae* is currently the best characterized due to its readily available substrates and its relative stability[48].

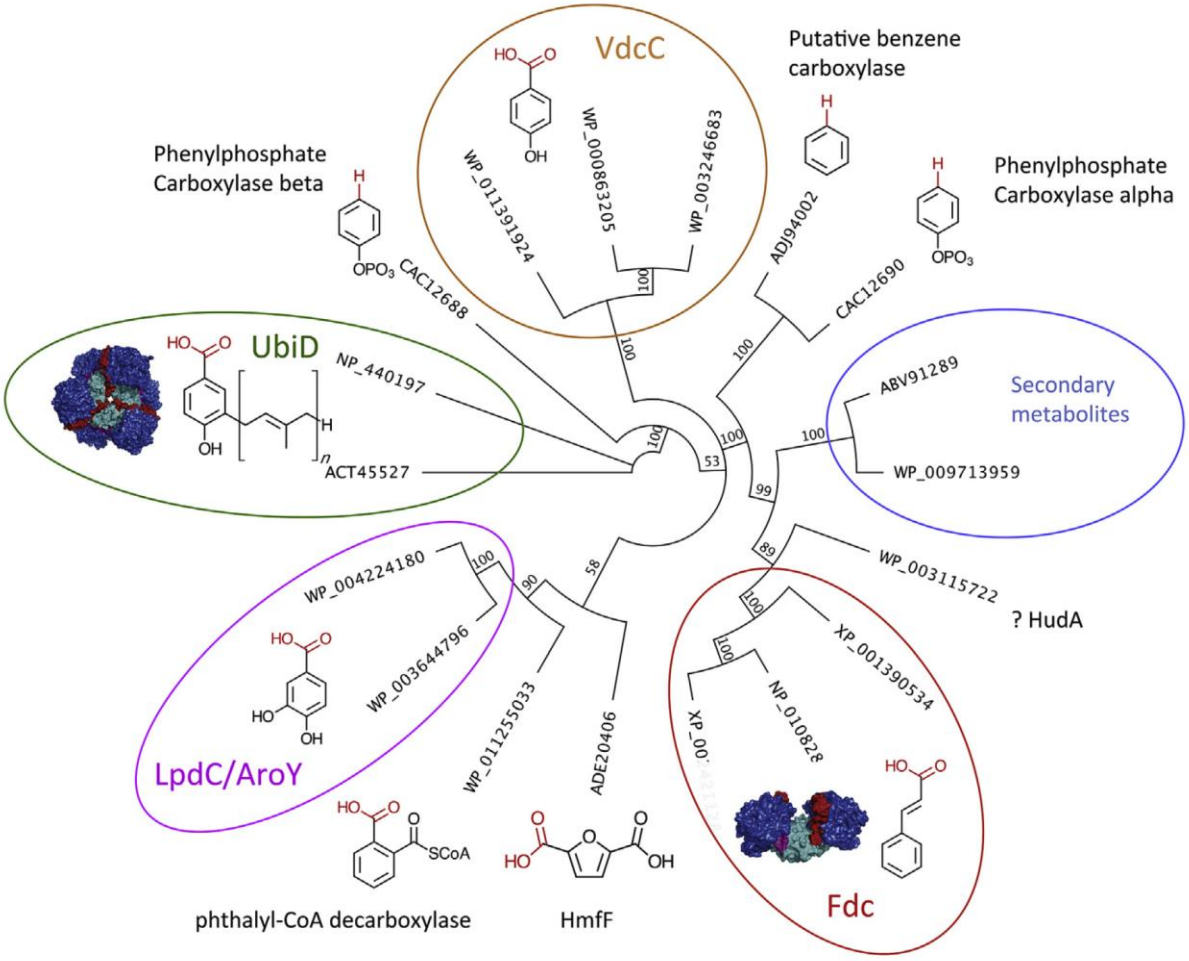

Figure 1.4 Proposed phylogenic analysis of the proposed UbiD family of enzymes[48]

1.5. *In vivo* Study of FDC1/PAD1 from *Saccharomyces cerevisiae*

Antimicrobial compounds such as phenylacrylic acid and sorbic acid are commonly incorporated into foodstuff to act as preservatives or flavor enhancers. These antimicrobial compounds are also present in plant cell walls, which protect plants from invading fungi by lowering cytosolic pH[27, 33, 34, 38, 49]. Despite these efforts, numerous fungi evolved mechanisms to detoxify their environments of these xenotoxins[27, 34, 38, 40]. FDC1 and PAD1 are involved in the non-oxidative degradation of phenylacrylic and sorbic acids to styrene and 1,3-pentadiene respectively, conferring resistance to *S. cerevisiae* and *A. niger.* FDC1 and PAD1 break down these antimicrobial compounds through decarboxylation to produce carbon dioxide and the vinylbenzene product[23, 24].

Genetic manipulation experiments to breakdown these inhibitory compounds intially suggested that PAD1 was solely responsible for processing these inhibitory compounds. Deteling *pad1* eliminated styrene and 1,3-pentadiene production *in vivo,* suggesting that PAD1 was responsible for the decarboxylase activity observed in the wild type strains[24]. A separate study in which the *fdc1* gene was introduced to sake yeast (a species that lacks the *fdc1* gene) resulted in the development of resistance to ferulic acid, cinnamic acid, and sorbic acid, suggesting that FDC1 was requried for the degradation of phenylacrylic compounds[24]. Genomic analysis of *fdc1* and *pad1* indicated that these two genes were located in close proximity to each other on chromosomes IV and VI in *S. cerevisiae* and *A. niger* respectively[24]. Knockout strains Δ*fdc1*, Δ*pad1* and Δ*fdc1*/Δ*pad1* in *S. cerevisiae* were analyzed for decarboxylase activity against *p*-coumaric acid, *trans*-cinnamic acid, and ferulic acid. All three knockout strains lacked decarboxylase activity, indicating that both genes were required for decarboxylase activity. Similar results were observed in *A. niger*. This established

that FDC1 and PAD1 were both required for decarboxylase activity. However, no biochemical studies were conducted to characterize the relationship between FDC1 and PAD1.

1.6. Decarboxylation Mechanism

Historically, the decarboxylation mechanism by which the UbiX/UbiD or PAD1/FDC1 systems broke down carboxylic acids to their vinyl products were generally considered to be 1 of 3 possibilities. Based on the crystal structure of UbiD from *P. aeruginosa* possessing an Mg^{2+} [19, 24], a hypothesis was put forth indicating that this decarboxylase could perform a non-oxidative, metal-dependent decarboxylation[50]. The crystal structure of UbiX resembled a flavin-dependent, non-oxidative cysteine decarboxylase, such as MrsD, therefore suggesting this enzyme may behave as a flavin-dependent decarboxylase[20, 47]. However, because neither enzyme had an established active site, there was also the alternative hypothesis that these enzymes catalyzed decarboxylation in a cofactor-independent manner.

However, as this thesis will detail later on, these hypothesized mechanisms were based on a fundamental misunderstanding of the relationship between the UbiD/UbiX enzyme families as well as the lack of knowledge regarding the existence of the prenylated flavin (PrFMN) that is required to perform the described non-oxidative decarboxylation[51-57].

1.6.1 Non-oxidative Metal Decarboxylation Mechanism

The published crystal structure of UbiD from *P. aeruginosa* possesses a magnesium ion [24], which could indicate that UbiD undergoes a non-oxidative metal-dependent decarboxylation. One representative enzyme that performs this mechanism is α-amino-β-carboxymuconate-ε-semialdehyde decarboxylase (ACMSD), which is involved in the tryptophan metabolism[58]. ACMSD enzymes are a member of the aminohydrolase superfamily, which

mediates non-hydrolytic carbon bond cleavage. The most analyzed ACMSD is from *Pseudomonas fluorescens* where the substrate enters the active site with its C2 carboxylate in close proximity to a zinc ion (Figure1.5)[11,58]. A conserved histidine residue mediates deprotonation of a water molecule coordinated to the zinc ion, creating a hydroxide. The hydroxide attacks the β-carbon of the substrate to hydrolyze the enoic acid moiety. Release of carbon dioxide occurs simultaneously with the elimination of the hydroxide, facilitated by the histidine[58, 59].

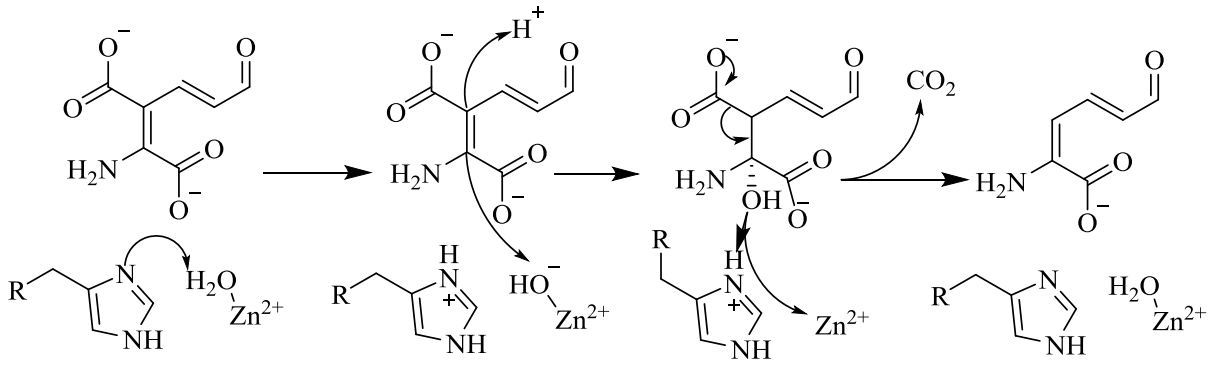

Figure 1.5 Metal dependent non-oxidative decarboxylation mechanism of ACMSD from *P. fluorescens*[58]

1.6.2. Flavin-based Decarboxylation Mechanism

UbiX from *P. aeruginosa* was shown to bind FMN and is structurally homologous to MrsD and EpiD, which are FMN-dependent decarboxylases that are part of the phosphopantothenoylcysteine (PPC) decarboxylase family, commonly referred to as the cysteine-dependent decarboxylase family[20, 21, 47]. These enzymes require substrates to possess a cysteine group to facilitate decarboxylation, a chemical motif distinctly missing in the substrates of UbiD/UbiX and FDC1/PAD1. MrsD, EpiD, and a PPC decarboxylase from *Arabidopsis thaliana* involved in coenzyme A biosynthesis, have shown that flavin-mediated decarboxylation occurs through the same general states (Figure 1.6)[59]. FMN facilitates the oxidation of the cysteine to generate a thioaldehyde intermediate along with formation of

FMN_{red}[60, 61]. The generation of the thioaldehyde adduct promotes spontaneous decarboxylation through internal delocalization of the carbanion to the cysteinyl sulfur, which creates a double bond between the α, β carbons and reconstitutes the thiol group. In EpiD and MrsD this concludes turnover, but *At*PPC decarboxylase continues the reaction by catalyzing the reduction of the C-C double bond using a proton donated by a conserved cysteine residue and the hydride stored on the flavin, returning the flavin to its oxidized form[59].

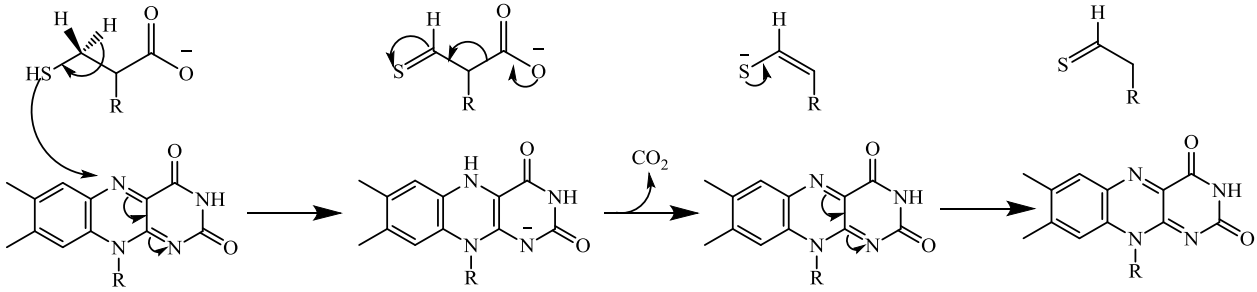

Figure 1.6 Flavin-dependent, non-oxidative cysteine decarboxylase mechanism of EpiD

1.6.3. Cofactor-Independent Decarboxylation

The UbiD/UbiX decarboxylation system has been previously described as cofactor-independent. Cofactor-independent decarboxylase systems encompass a relatively small class of enzymes. These include 2-oxo-4-hydroxy-4-carboxy-5-ureidoimidazoline decarboxylase (OHCUD) which is involved in oxidative ureide degradation during purine catabolism, and methylmalonyl-CoA decarboxylase (MMCD), a member of the crotonase family[62,59]. The decarboxylation occurs stepwise for both enzymes. Three crystal structures of OHCUD in complex with a substrate analog, product, and inhibitor suggest that the proximal active site carboxylic acid side chain is responsible for destabilizing the substrate ground state through electrostatic repulsion to facilitate carbon dioxide release (Figure 1.7)[62, 63].

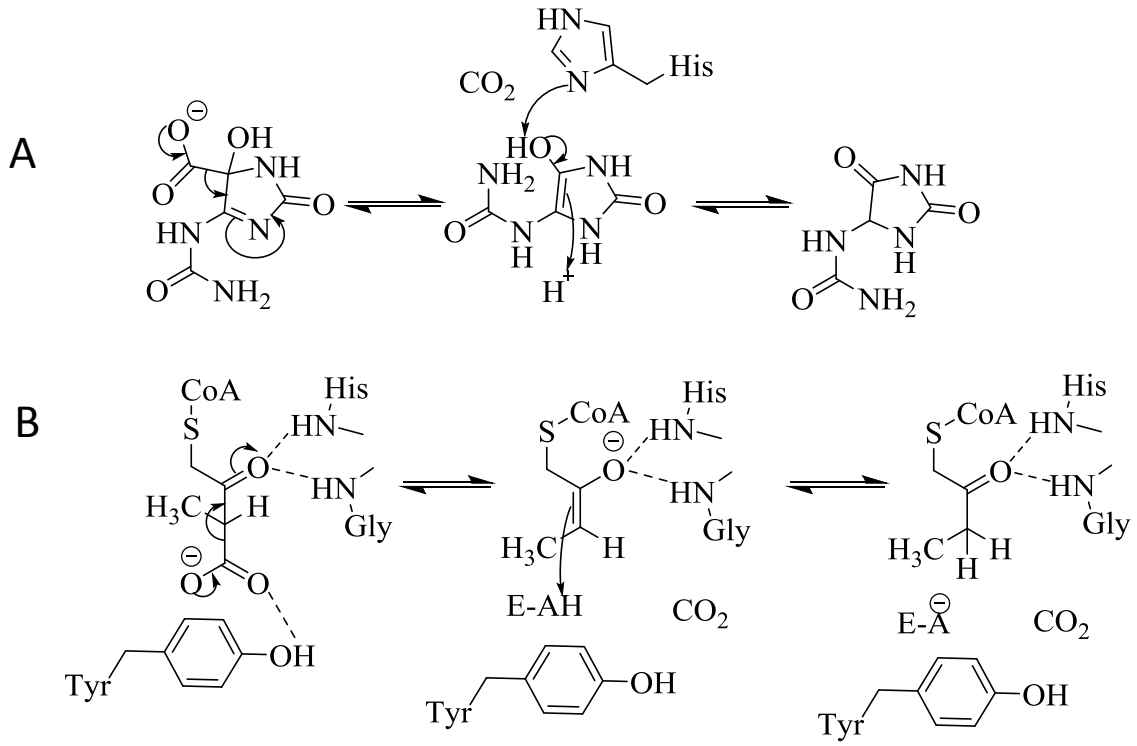

Figure 1.7 (A) OHCUD and (B) MMCD non-cofactor dependent decarboxylation mechanism

One of the most studied cofactor-independent decarboxylases, orotidine 5'-monophosphate decarboxylase (OMPCD), is involved in pyrimidine biosynthesis. OMPCD is capable of increasing the non-enzymatic rate by a factor of 10^{17}, making OMPCD one of the most proficient enzymes known[64]. Numerous studies have investigated the mechanism and have found that the negative charge of a proximal carboxylic amino acid destabilizes the substrate ground state through electrostatic repulsion, as accepted for OHUCD and MMCD. The negative charge accumulating on the C6 is stabilized by a conserved lysine residue, which protonates the carbon concomitant with carbon dioxide release avoiding the high-energy carbanion transition state is generated (Figure 1.8). The carbanion is stabilized through transfer of the negative charge to the carbonyl O4. This is supported by interaction with a backbone amide, analogous to the MMDC[65,64].

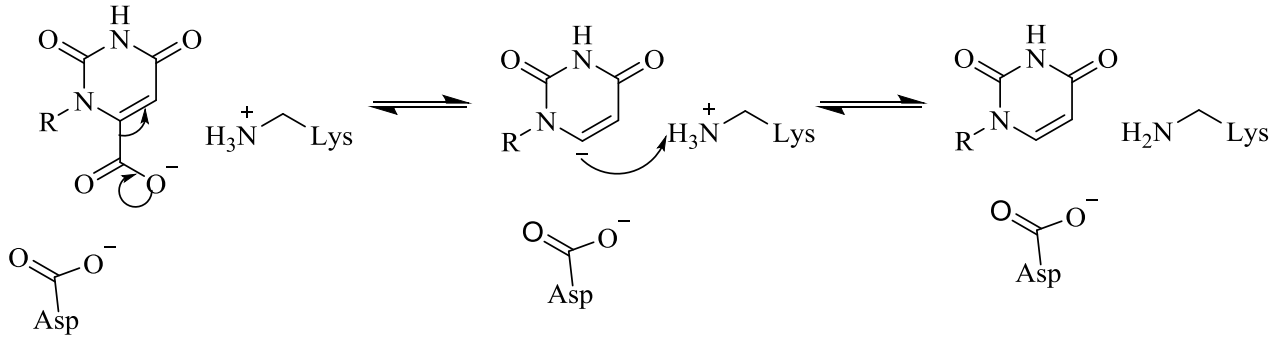

Figure 1.8 Non-oxidative decarboxylation mechanism of OMPCD

1.7. UbiD/UbiX Decarboxylase System's Pharmaceutical and Agriculture Relevance

1.7.1. UbiD/UbiX as a Target for Antibiotics

Antibiotic drugs revolutionized medicine and made our modern way of life possible. In addition to their essential clinical role, antibiotics play a role in an array of nonclinical applications including promoting livestock growth, preserving materials from contamination, and treating blight in agriculture. The successful uses of these therapeutic agents are compromised by the development of resistance to these compounds by microbes over time[66, 67].

Antibiotic resistance is an ever-increasing concern, due to the increase in drug-resistant bacteria coupled with the low rate of new antibiotic compounds being discovered. Currently, there are more than 20,000 potential resistance genes of nearly 400 different types, based on bacterial genome sequences[66]. Most classes of antibiotics were discovered in the mid to late 20^{th} century and are slowly losing their effect. Without additional research, it is likely that humanity could return to the pre-antibiotic era. Given the importance of antibiotics to our way of life, as well as the growing apprehension surrounding the threat of resistance, scientists are studying every aspect of bacteria cell processes as well as the mechanisms behind antibiotic resistance to develop new antibiotics.

There is interest in exploring the UbiD family of enzymes for its application in antimicrobial research[19]. Members of the UbiD family are found in many of the bacteria on the World Health Organization's list of the most dangerous bacteria, including *P. aeruginosa*, *Enterococcus faecium*, and *Staphylococcus aureus*[19]. UbiD catalyzes the conversion of 3-octaprenyl-4-hydroxybenzoate to 2-octaprenylphenol in the bacterial ubiquinone biosynthetic pathway[42]. Ubiquinone is essential to promote the growth of many bacteria due to its regulatory roles. For example, ubiquinone prevents the onset of anaerobic metabolism by interfering with the Arc two-component signal transduction system[68]. Also in *E. coli*, ubiquinone derivatives participate in disulfide bond formation by providing oxidizing power to the cytoplasmic membrane protein DsbB[68]. Deletion of the *ubiD* gene severely reduces ubiquinone levels (~75%) causing a severe retardation in growth rate. However, this deletion by itself is not lethal as an alternative biosynthetic pathways are present in numerous bacteria[44]. The unique ubiquinone machinery in bacteria opens the opportunity to selectively modulate the activity of UbiD to stress bacteria into a bacteriostatic state. Bacteriostatic agents limit the growth of bacteria, thus enabling the host's native defenses to kill bacteria. Bacteriostatic agents are sometimes preferred over bactericidal agents as their slower mechanism of action avoids the build-up of endotoxins that produce toxic shock syndrome which currently kills over 200,000 persons per year[69].

1.7.2. FDC1/PAD1 Decarboxylase as Agricultural Antifungal Target

Invasive, life-threatening fungal infections are a major cause of morbidity and mortality, particularly for patients with compromised immune function. Over the past 30 years, the number of immunocompromised individuals increased dramatically with the HIV epidemic as well as the increase in the incidence of cancer and practice of hematologic and solid organ

transplantation[70]. However, there are only three classes of antifungal drugs, two of which, azoles and polyenes, were introduced in clinics by 1980. These drugs are rapidly becoming outdated as more fungal strains are becoming resistant to these classes of drug molecules. Therefore it's rather sobering to consider that there is only one current class of antifungals, echinocandins, treat fungal infections[70].

Fungal infections have serious consequences. In wealthy countries, the 90-day survival following the diagnosis of candidemia varies between 55% and 70%, depending on the underlying condition of the patient. The outcomes are even worse for aspergillosis despite the availability of voriconazole, a commonly prescribed antifungal (Figure 1.9)[71]. These outcomes are even worse in developing nations. As immunosuppression therapies continue to develop in response to cancer and a host of autoimmune diseases so will the number of patients that may need antifungal therapies. As the patient count rises, fungal treatments will inevitably become ineffective, thus prompting a need for novel antifungal treatment strategies[72].

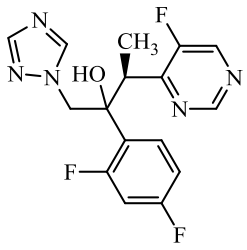

Figure 1.9 Structure of voriconazole, a commonly prescribed antifungal agent

The challenge to developing novel antifungal drugs arises from the fact that fungal pathogens are closely related to the host. Many fundamental biochemical and cell biological processes are conserved in fungi and humans[72]. Therefore, the challenge is identifying new lead molecules that disrupt processes unique to fungi. Various fungi-exclusive processes are currently being investigated as targets including the biosynthesis pathways for glycosylphosphatidylinositol and β-1,6-glucan, both of which are important for fungal cell

walls[73]. Other essential processes of fungal growth and cell viability that are being investigated include poly(A)polymerase activity, translational elongation, cAMP homeostasis, and resistance mechanisms[72, 73].

The FDC1/PAD1 decarboxylation system functions as a resistance mechanism against antifungal compounds such as ferulic acid and sorbic acid[25]. Ferulic acid received attention as an antimicrobial compound as it was found to be one of the effective components in many Chinese herbal medicines derived from plants such as *Angelica sinensis*, *Cimicifuga heraclifolia*, and *Lignsticum chuangxiong*[33]. Among 5 commonly encountered fungi, including fungi that cause interior fungal infections, ferulic acid and other cinnamic acid derivatives inhibited growth with K_i values in the μM range, demonstrating their potentials as antifungal drugs. Fortunately, the biosynthetic pathway leading to the breakdown of ferulic acid in *A. niger* and associated fungal species appears to be unique, therefore combining an FDC1 inhibitor and cinnamic acid derivatives would provide a novel antifungal therapy[33, 34].

1.7.3. FDC1/PAD1 Decarboxylase as Agricultural Antifungal Target

The potential impact of fungal blights on food business or a country have been devastating, costing hundreds of millions of dollars and causing upwards of 5000 deaths[49]. Fungi such as *Aspergillus flavus* colonize maize and other agriculture products and release aflatoxin, a poisonous carcinogen. Caffeic acid, ferulic acid, and vanillic acid inhibit the growth of these poisonous fungi by 60-100%. However, these compounds have limited effectiveness as they eventually break down into vinyl guiacol, styrene, and other decarboxylated metabolites. Ferulic acid has a low toxicity to humans (LD_{50} = 2445 mg kg^{-1}), making it an attractive food additive as a preservative[26]. However, ferulic acid and other antifungals, such as cinnamic acid, are broken down by PAD1/FDC1. Understanding the mechanism of action of the

PAD1/FDC1 decarboxylation system would lead to an understanding on how toxic fungi are able to resist these antifungal compounds, which could lead to alternative and more effective strategies at improving food security and limiting the costs of fungi-related food damage[33].

1.8. Goals of this Work

The main objectives of this project are to initiate biochemical and biophysical characterization of FDC1/PAD1 decarboxylation system, to explain how these enzymes interact, explore the substrate range and mechanism of FDC1, and to isolate mechanistic intermediates of FDC1. This project aims to provide a foundation for an understanding of the UbiD family and its relationship with the UbiX family. This goal serves two purposes. The first is to provide a platform from which enzyme engineers can apply a combination of directed evolution and metabolic engineering to produce valuable commodity chemicals in a cost-efficient and sustainable manner. The second benefit of this project is to provide some insight into how the UbiD family of enzymes work, thus providing a framework for the design novel antibiotics against bacterial and fungal species.

The research described in this thesis seeks to provide answers to these questions and others by exploring the mechanism of FDC1 and its relationship with PAD1. First, in chapter 2, the relationship between PAD1 and FDC1 was investigated through a combination of genetic engineering, membrane dialysis experiments, and UV-visible spectroscopy. The experiments show that PAD1 uses FMN to synthesize a novel, diffusible flavin cofactor that FDC1 uses to decarboxylate substrates. Next, the mechanism of FDC1 was investigated using a combination of a Hammett analysis, solvent and secondary kinetic isotope effects, and NMR exchange experiments. The secondary KIEs and Hammett analysis provided evidence that the rate-

determining step of the reaction was the decomposition of the product-PrFMN adduct. Finally, in chapter 4, the use of a substrate analog and potent inhibitor of FDC1, 2,2-fluoronitrovinylbenzene, a 1,3-dipolar cycloadduct was trapped, definitively proving that FDC1 employs a novel 1,3-dipolar cycloaddition mechanism to facilitate decarboxylation. Additionally, using bicarbonate to push the FDC1 equilibrium to favor the build-up of product-PrFMN intermediates combined with MS^2, PrFMN-styrene adducts were isolated. Lastly, mutagenesis of FDC1 was used to explore the causes of the reported changes to the PrFMN cofactor spectrum, which appeared to be due to either a lack of cofactor or the build-up of a possible phenylaldehyde-PrFMN adduct.

Chapter 2

Isofunctional Enzymes PAD1 and UbiX Catalyze the Formation of a Novel Cofactor Required by FDC1 and UbiD

The work described in this chapter has been published as Lin, F., Ferguson, K. L., Boyer, D., Lin, X., Marsh E. N. G. M. PAD1 and UbiX are Isofunctional Enzymes Catalyzing the Formation of a Novel Cofactor Required by Ferulic Acid Decarboxylase (FDC) in Yeast and 4-hydroxy-3-polyprenyl benzoic Acid Decarboxylase (UbiD) in Bacteria, *ACS Chemical Biology*, 10, 1137-1144. F. Lin constructed the relevant plasmids and performed and analyzed the results of the various dialysis assays. K.L. Ferguson & D. Boyer performed various kinetic assays and characterized the relevant gene products of the plasmids. F. Lin, K.L. Ferguson, and E.N.G. Marsh wrote the paper.

2.1 Introduction

The UbiD/UbiX decarboxylation system has interest in the search for a renewable alternative to produce commodity chemicals and as a method to arrest the resistance mechanism of fungi to breakdown antifungal compounds such as, ferulic acid[24, 34, 72]. The members of the UbiD decarboxylate a wide variety of phenylacrylic acids including anti-oxidant molecules such as ferulic acid, and *trans*-cinnamic acid. Enzyme-mediated decarboxylation is difficult because the transition state often involves is the build-up of negative charge on the α carbon. Nature has therefore evolved a variety of decarboxylases which employ a wide variety of

catalytic strategies to facilitate decarboxylation using cofactors such as pyridoxine phosphate and thiamin pyrophosphate that serve as electron sinks and Lewis acidic metal ions[11, 50, 59, 74-77]. The UbiD family of enzymes however, have long been referenced as requiring no cofactor required to do these aryl carboxylic acid decarboxylations.

Unfortunately, the presumed substrate for UbiX and UbiD, 4-hydroxy-3-octaprenylbenzoic acid, is commercially unavailable and requires an involved synthesis to synthesize. Genetic analysis established that UbiD and UbiX have two analogs in *S. cerevisiae*, FDC1 and PAD1[20, 23, 78]. Sequence comparison of these enzyme species suggests that there is a flavin binding domain in both FDC1/UbiD and PAD1/UbiX however, the role of this redox cofactor remains unexplained in the decarboxylation of phenyl acrylic acids and 4-hydroxy-3-octaprenylbenzoic acid. (Figure 2.1)

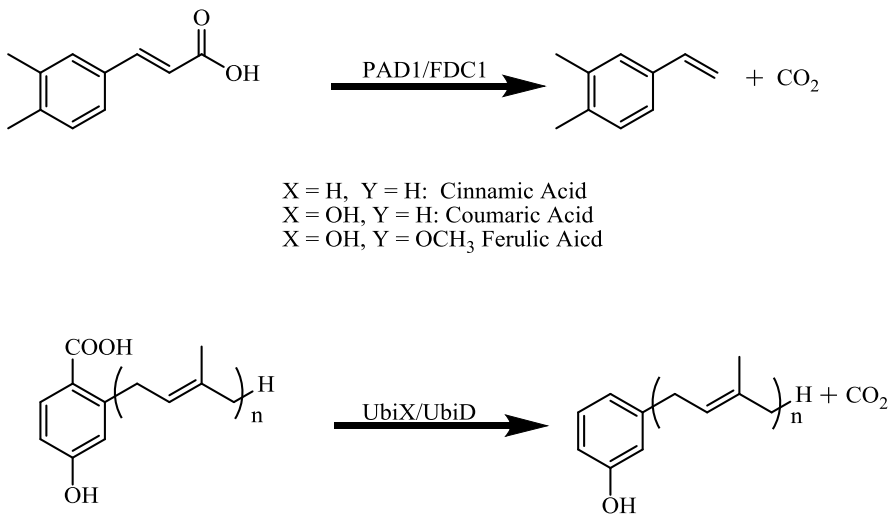

Figure 2.1 Decarboxylation of octaperenylphenolbenzoic acid by UbiD/UbiX and phenylacrylic acids by PAD1/FDC1

This chapter describes a series of characterization experiments for FDC1, PAD1, and FDC1 co-expressed with PAD1. FDC1 and PAD1 were overexpressed and purified from *E. coli*. PAD1 was determined to be a FMN containing protein, and is shown not to be a decarboxylase. Rather, PAD1 is shown to catalyze the formation of a novel diffusible cofactor, later found to be

PrFMN. The *E. coli* UbiX and UbiD are related by sequence to PAD1 and FDC1 respectively and are involved in the decarboxylation of 4-hydroxy-3-octaprenylbenzoic acid, an intermediate in ubiquinone biosynthesis. UbiX was found to also activate FDC1, suggesting that PrFMN plays a larger role in metabolism. Once holo-FDC1 was made by co-expressing PAD1 with FDC1 this resulted in significant increase in the activity of FDC1 over previously identified kinetic constants.

2.2 Materials & Methods

2.2.1 Materials

Trans-Cinnamic acid, para Coumaric Acid, Ferulic Acid, Ethyl acetate, Imidazole, Glycerol, THP, and FMN were all purchased from the Sigma Chemical company and were a biochemical grade, or HPLC reagent grade.

2.2.2 Construction of the FDC1 Expression Vector

A derivative of *E. coli* BL21 in which the *ubiX* gene was deleted by P1 phage transduction as previously described. The P1 phage lysate was prepared from the Keio single gene knockout strain of Δ*ubiX*: kan and used to transduce the *ubiX* knockout gene into *E. coli* BL21 Star (DE3) to obtain a strain designated *E. coli* BL21/Δ*ubiX*

The genes encoding FDC1 (YDR539W) from *S. cerevisiae* was synthesized commercially by GenScript U.S.A. Inc. (Piscataway, NJ, USA) and codon-optimized for expression in *E. coli*. FDC1 was then subcloned into the expression vector pET-28b utilizing the NdeI and the BamHI restriction sites to generate pFDC. pFDC introduced a vector-encoded N-terminal 6 histidine-tag to facilitate enzyme purification.

2.2.3 Construction of sctPAD1 Expression Vector

A derivative of *E. coli* BL21 in which the ubiX gene was deleted by P1 phage *trans*duction as previously described[79]. The P1 phage lysate was prepared from the Keio single gene knockout strain of Δ*ubiX*: kan and used to transduce the *ubiX* knockout gene into *E. coli* BL21 Star (DE3) to obtain a strain designated *E. coli* BL21/Δ*ubiX*

The genes encoding PAD1 (YDR538W) from *S. cerevisiae* was synthesized commercially by GenScript U.S.A. Inc. (Piscataway, NJ, USA) and codon-optimized for expression in *E. coli*. PAD1 was then subcloned into the expression vector pET-28b utilizing the NdeI and the BamHI restriction sites to generate pPAD1. The pPAD1 plasmid has a vector-encoded N-terminal 6 histidine-tag to facilitate enzyme purification.

A truncated gene was constructed by PCR to delete the N-terminal mitochondrial targeting peptide sequence (residues 1-58) using the following oligonucleotides as the forward (5'-ATTCCATGGCAAACGTATTGTGGTTGCGAT-3') and reverse primer (5'-AGTGGATCCTTATTTTTGCGAT-3') using Ppad1 as the template sequence. After amplification, the PCR product was digested with NcoI and BamHI. The resulting plasmid, ptPAD1 no his lacks an N-terminal His tag.

2.2.4. Co-expression of scFDC1 and tPAD1 and the Purification of scFDC1

The co-expression of *tpad1* and *fdc1* the two genes were introduced in tandem into pET28b and expressed from a single vector encoded promoter. The *tpad1* gene was amplified by PCR using the forward primer (5'-ATTCCATGGGCAAACGTATTGTGGTTGCGAT-3') and reverse primer (5'-AGTGGATCCTTATTTTGATTTGATACCTTCCC-3') using Ppad1 as the template. After

amplification, the PCR product was digested with NcoI and BamHI and ligated with PEt28bb linearized with NcoI and BamHI. The resulting plasmid, ptPAD1 no-His lacks an encoded N-terminal His tag. The *fdc1* gene was introduced behind the *tpad1* gene, and the stop codon deleted to allow for the incorporation of a C-terminal vector encoded six-histidine tag. This genetic construct was accomplished by PCR using the forward primer (5'-ATTGAGCTCAAGTATAAGAAGGAGATATATCATGCGCAAACTGAACCCGG-3') which introduced a ribosome binding sequence, and the reverse primer (5'-AATGTCGACTTTGTAACCGTAGCGTTTCCAGTTTTCATT-3') and using Pfdc as the template. The PCR product was digested with SacI and SalI and ligated with ptPAD1nohis cut with Sac1 and Sal1 to produce ptPAD1_FDC1, which was *trans*formed into *E. coli* BL21 (DE3) to co-express both *tpad1* and *fdc1* genes.

2.2.5. Assay of Styrene by Gas Chromatography

Assays of FDC1 activity were carried out in PBS buffer, pH 8.0 with a total volume of 500 µL using a saturating concentration of cinnamic acid, 6.7 mM, as the substrate; the concentration of FDC was typically 1.0 µM. Assays utilizing tPAD1 typically included this enzyme at 10 µM concentrations. The assay mixtures were incubated at 32 ºC for varying lengths of time. After which the products of the reaction were extracted by the addition of 500 µL of EtOAc and the concentration of styrene was determined by GC-MS

The GC-MS analysis was performed using a Shimadzu QP-2010S GC0MS instrument equipped with a quadrupole mass detector and a BD-5 column (Restek, 30m x 0.25mm x 0.25µm). The flow rate of the helium carrier gas is constant at 1 mL/min, and the inlet temperature was maintained at 200 ºC. The interface temperature was maintained at 250 ºC.

Injections (10 µL) of EtOAc was held initially at 40 ºC for 3.5 minutes and then gradually increased to 90 ºC at 14 ºC/min then gradually increased from 90 ºC to 315 ºC at a rate of 20 ºC/min, and then finally maintained at 315 ºC for 1 min. Chromatographic data were analyzed by GC-MS PostRun analysis software. Enzymatic conversion of the cinnamic acid to styrene was quantified using a calibration plot of styrene standards of known concentration.

2.2.6. Determination of the U.V.-Visible of Holo-FDC1

High activity preparations of FDC1, that is, enzyme prepared from *E. coli* strains co-expressing tPAD1 and FDC1, were examined using an 8543 Hewlett Packard spectrophotometer. A typical spectrum included 80 µM FDC1 in a 100 mM pH 7 sodium phosphate buffer at room temperature. The data was acquired using the Olis Works UV-Vis spectrum software.

2.2.7. Determination of Steady-State kinetic constants of FDC1

The activity of FDC was determined with 8543 Hewlett Packard spectrophotometer. High activity preparations of FDC that is, enzyme prepared from *E. coli* strains co-expressing tPAD1, the decarboxylation of substrates could be followed by the decrease in absorbance of the UV-active substrates. Typical assays were performed in 100 mM potassium phosphate buffer, pH 7.0, at room temperature (RT) and contained 200-500 nM FDC. The substrate concentration ranged between 0.05 -1.5 mM; at higher concentrations, the absorbance of the substrate became too high. Decarboxylase activity was followed by monitoring the decrease in absorbance at 304 nm for cinnamic acid $\varepsilon^o = 1140\ M^{-1}\ cm^{-1}$; 334 nm for para-coumaric acid $\varepsilon^o = 988\ M^{-1}\ cm^{-1}$; and 344 nm for derelict acid $\varepsilon^o = 1330\ M^{-1}\ cm^{-1}$. Velocity data (equation 1) were fitted to the Michaelis-Menten equation (2) using Origin Software.

Equation 1 $$\text{specfic activity} = \frac{(\frac{dA}{dt})}{\varepsilon_{wavelength} * [E]}$$

Equation 2 $$v = \frac{k_{cat}[S][E]}{K_M + [S]}$$

2.2.8. LC-MS of Denatured scFDC1

The molecular weights of the FDC1 and tPAD1 proteins and their associated small molecules were determined using an Agilent 6520 LC-accurate-mass Q-TOF MS system. The protein was passed through a PD-10 desalting column (GE Healthcare) and acidified with 0.1% formic acid. Samples (5 µL) were injected onto a Poroshell 300SB-C8 column equilibrated with 0.1% formic acid and 5% acetonitrile. Proteins were eluted for 5 min with 95% water: 5% acetonitrile followed by an increasing gradient of acetonitrile to 100% over the course of 7 min at a flow rate of 0.5 mL/min. Eluting proteins were detected at 280 nm. Mass data were obtained using intact protein mode and analyzed using Agilent MassHunter Qualitative Analysis software. The raw data was deconvoluted concerning maximum entropy. For small molecule analysis, proteins were precipitated with an equal volume of 1:1 dichloromethane/methanol in glass tubes and the organic solvent removed under a stream of dry nitrogen. The sample (20 µL) then was injected onto a Zorbax 300SB-C18 column equilibrated with 0.1% formic acid and 5% acetonitrile, followed by a 2 min washing with 95% water/5% acetonitrile. Then, the gradient of acetonitrile was increased to 100% over 10 min at a flow rate of 0.4 mL/min. Mass data were obtained using small molecular mode and analyzed using Agilent Mass Hunter Qualitative Analysis software. Automatic MS^2 acquisition obtained MS/MS data. A continuous scan event consisting of one full MS scan (50-2000 m/z) followed by three data-dependent MS^2 were

carried out. The three most intense ions from the initial MS scan were selected individually for collision-induced dissociation at 50 eV

2.3 Results

2.3.1. Properties of S. *cerevisiae* FDC1 Recombinantly Expressed in *E. coli*

FDC containing an N-terminal 6-histidine tag was successfully overexpressed in *E. coli*. BL21, homogenized and purified by standard methods using a nickel-NTA column (Figure 2.2). The molecular weight of the FDC1 determined by LC-ESI-MS was 57898.15 Daltons, which is in excellent agreement with the predicted mass of 57897.8 Daltons (Protein mass calculator). Analysis of FDC1 by native gel electrophoresis (Figure 2.2) indicated that the protein migrated

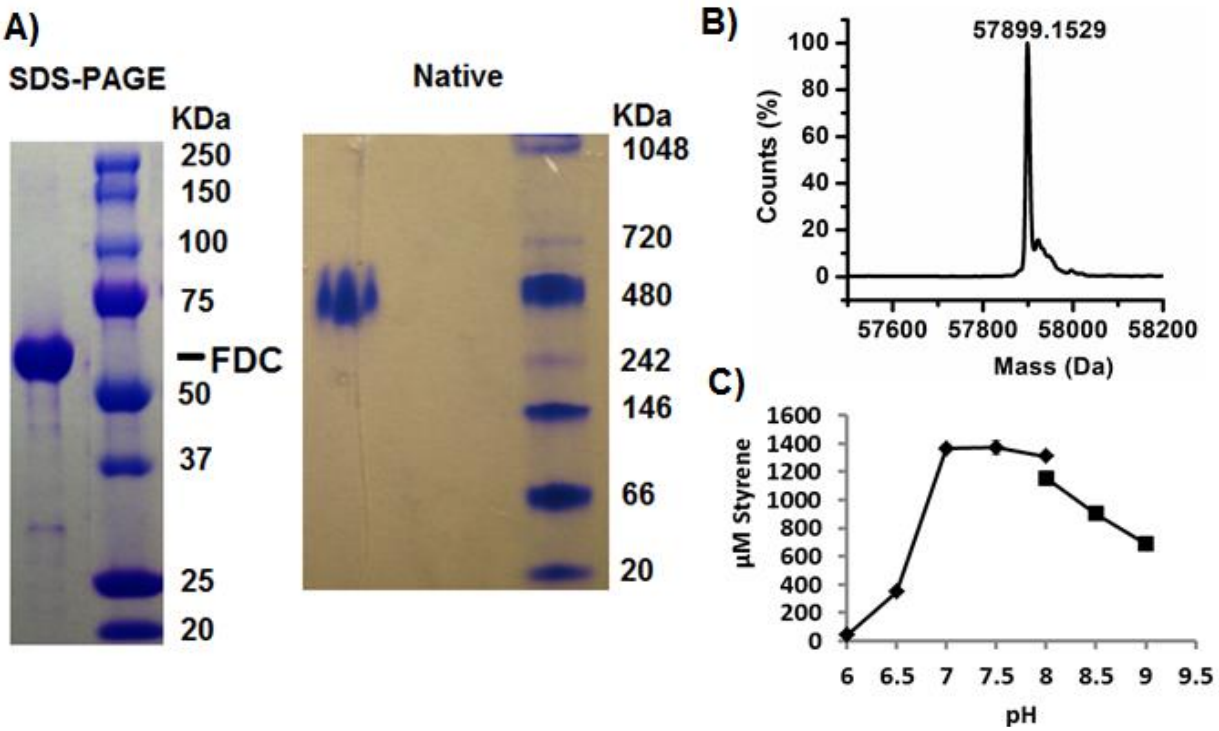

Figure 2.2. Purification and initial characterization of FDC. (A) SDS-PAGE and native PAGE analysis of purified FDC. (B) LC-ESI-MS analysis of purified FDC. (C) pH dependence of FDC1 decarboxylase yield

with an apparent molecular weight of ~480 kDa suggesting that FDC1 adopts an oligomeric structure in solution. Interestingly, FDC1 purified from *E. coli* exhibited activity in the absence

of its genetic partner PAD1, which is consistent with previous studies that found styrene produced from engineered *E. coli* cells did not require the introduction of the PAD1 gene. The enzyme activity of the PAD1/FDC1 dual enzyme system was optimal between pH 7.0 and 8.0 (Figure 2.2.).

The specific activity of the dual enzyme assay determined by GC-MS was found to be 0.54 µM styrene min^{-1} mg^{-1} enzyme. Unexpectedly, it was found that dialyzing FDC1 against phosphate buffer (membrane cutoff =3.5 kDa) for 24 hrs resulted in the almost complete loss of activity (Figure 2.3), suggesting that FDC1 activity required a low molecular weight cofactor for activity. Consistent with this, the addition of a cell-free lysate of *E. coli* BL21 was able to completely rescue activity. (Figure 2.3) However, FDC1 was unable to be reconstituted if the

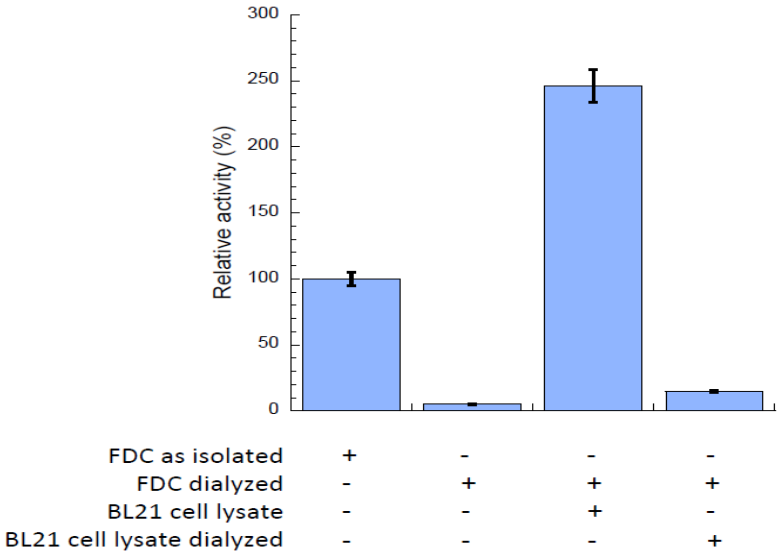

Figure 2.3. Effect of dialysis and addition of *E. coli* BL21 cell lysate on FDC1 activity. The activity of FDC1 as purified from *E. coli* BL21 is arbitrarily assigned as 100% and corresponds to specific activity of 0.54 µmol styrene*$min^{-1}$$mg^{-1}$enzyme

cell-free lysate was first dialyzed against buffer through a 3.5 kDa cutoff membrane. Attempts to activate FDC using common commercial biochemical cofactors such as thiamine

pyrophosphate, pyridoxal phosphate, nucleotides, NADH, NADPH, FMN, and FAD and various metal ions were unsuccessful.

2.3.2. *E. coli* UbiX is isofunctional with PAD1

Both FDC1 and PAD1 are reported to be essential for the decarboxylation of phenylacrylic acid in vivo in *S. cerevisiae*; therefore, it was considered whether the homologous *E. coli* protein, UbiX, was a substitute for the function of PAD1 in *E. coli*. To study this, the *ubix* gene was removed in *E. coli* BL21 to create an *E. coli* BL21/Δ*ubix* knockout strain. Expression and purification of FDC1 from the Δ*ubix* strain resulted in protein completely lacking in decarboxylase activity, and cell lysates prepared from this strain were unable to reactivate dialyzed FDC1. However, the inactive enzyme could be activated from lysates prepared from either wild-type *E. coli* BL21 or by lysates prepared from *E. coli* BL21/Δ*ubix* when purified PAD1 (lacking the N-terminal mitochondrial targeting sequence) was also added. These observations suggested that PAD1 and UbiX might function to synthesize a low molecular weight cofactor necessary for the activity of FDC1[24, 42].

2.3.3. Expression and Characterization of tPAD1 in *E. coli*.

Initial attempts to express the full-length PAD1 in *E. coli* resulted in poor levels of expression and the recombinant protein lacked the expected FMN cofactor. However, deletion of the first 58 residues, which appear to encode a mitochondrial targeting sequence, resulted in the expression of a soluble protein that could be purified by standard methods, utilizing N-terminal encoded 6-His tag affinity chromatography on a nickel-NTA column (Figure 2.4). The truncated form of PAD1 is designated tPAD1. The molecular weight of the protein determined

by LC-ESI-MS was 21808.6 Da (Figure 2.4). In excellent agreement with the predicted molecular weight of 21808.4 Da. The molecular weight of the protein was estimated as ~300 kDa by gel filtration chromatography, indicating that tPAD1 was an oligomeric protein solution.

Purified tPAD1 was yellow, and the UV-Vis spectrum exhibited maxima at 384 and 458 nm, characteristics of a protein with oxidized FMN bound to the protein. FMN was confirmed to be bound to the protein by LC-ESI-MS (Figure 2.4). Interesting, the absorption maximum at 385 nm is more intense than that at 458 nm, (Figure 2.4) whereas for FMN_{OX} the opposite is true.

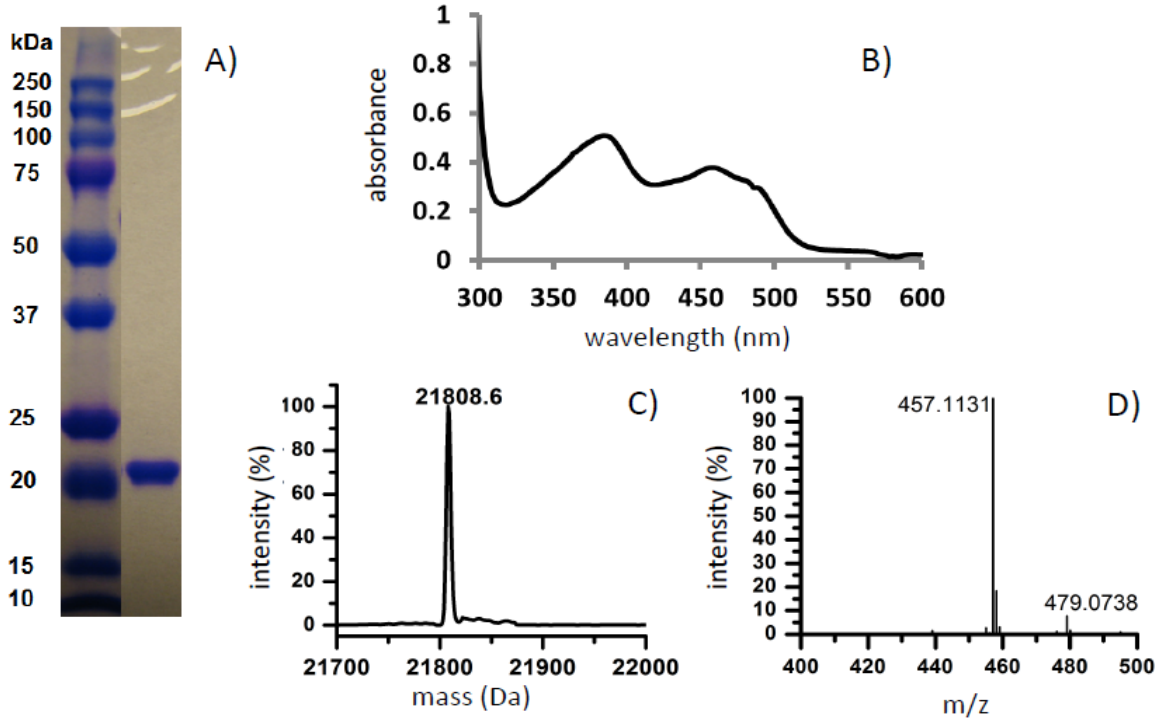

Figure 2.4 Purification and initial characterization of PAD1. (A) SDS-PAGE analysis of purified tPAD1. (B) ESI-MS of purified tPAD1. (C) UV-visible spectrum of tPAD1 indicative of bound flavin cofactor(s). LS-MS of flavin cofactor isolated from tPAD1, demonstrating, the protein contains FMN.

This experiment suggested that tPAD1 may contain another chromophore, although LC-ESI-MS identified no other known chromophore. tPAD1 was unable to catalyze the conversion of the TCA to styrene by itself. This demonstrated that contrary to initial genetic analyses, and shows the tPAD1 enzyme is not an isofunctional enzyme with FDC1.

The crystal structures of *E. coli* O157: H7 Pad1p and *P. aeroginosa* UbiX have been determined, revealing them to be dodecameric proteins containing FMN[20]. This is consistent with our characterization of PAD1 as an FMN-containing protein that exists as large oligomers in solution and suggests a common structure and function for these proteins. Interestingly, Pad1p and UbiX are structurally related to the family of flavin-dependent peptidyl cysteine decarboxylates. These include EpiD and MrsD, for which structures have been determined, that are involved in the biosynthesis of the lantibiotic peptides and mersacidin, respectively, and Dpf that catalyzes the decarboxylation of 4'-phosphate-N-pantothenol cysteine to 4'-phosphate-N-pantethine in coenzyme A biosynthesis[47,59]. However, there is currently no evidence to support either Pad1p or Pad1 functions as cysteine decarboxylases. Instead, as discussed below, our results suggest these enzymes are more likely involved in catalyzing the formation of a modified form of FMN.

2.3.4. Role of tPAD1 in the Activation of FDC1

An experiment was performed to examine whether direct interaction between FDC1 and PAD1 is necessary for the activation of FDC1. A dialysis cell was set up in which 1 µM apo-FDC1 was introduced on one side of a 3.5 kDa cutoff dialysis membrane in a buffer containing 6.7 mM cinnamic acid. On the other side of the membrane purified tPAD1 and cell lysate, or just *E. coli* BL21 DE3 cell lysate or BL21 DE3 star Δ*ubiX* cell lysate was introduced on one side of a 3.5 kDa membrane. At various times, the reaction was analyzed for the production of styrene by GC-MS (Figure 2.5). Whereas *E. coli* Δ*ubiX* cell lysate was unable to activate FDC1, the addition of 10 µM purified tPAD1 to the lysate resulted in the activation of FDC1, indicating that tPAD1 catalyzes the conversion of a small molecule in the cell lysate to

the cofactor for FDC1. Interestingly, the experiment, purified tPAD1 alone was effective at activating FDC1 in the absence of cell lysate, suggesting that during purification some of the cofactors remained bound and subsequently diffused from the enzyme. The activation of FDC1 is not due to FMN diffusing from tPAD1, as FMN itself doesn't activate FDC1. We were not able to detect the presence of the cofactor by LC-ESI-MS in samples of tPAD1. The reason for this is unclear. It is possible that this reflects the low occupancy of the cofactor in the active site of tPAD1, as a high concentration of tPAD1 relative to FDC was used in the dialysis experiment.

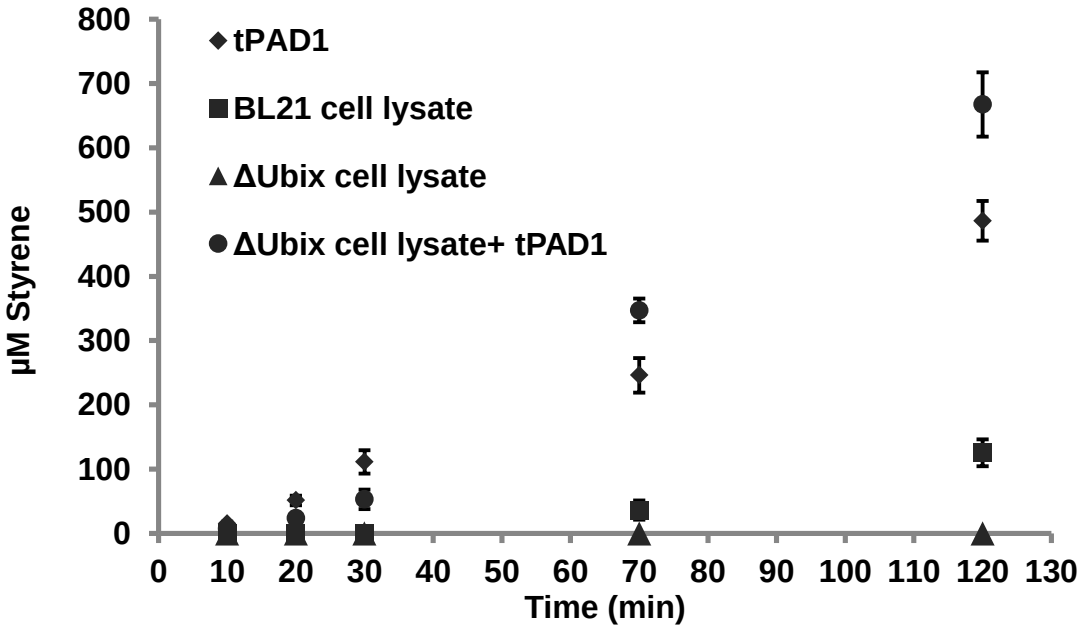

Figure 2.5 Styrene yield by a dialysis experiment where apo-FDC1 was incubated with tPAD1, BL21 DE3 cell lysate, ΔUbiX cell lysate and ΔUbiX cell lysate + tPAD1

2.3.5. Initial characterization of the FDC1 cofactor

The experiments described suggested that only a small fraction of FDC1 isolated from *E. coli* BL21 contained the cofactor. Therefore, we attempted to increase the occupancy of FDC by co-expressing FDC1 with tPAD1 lacking a His tag in *E. coli* BL21 cells. The specific activity of FDC1 purified from these enzymes was much higher: 292.4 µM styrene/(min^{-1}*mg^{-1}) enzyme which was 8 fold higher than that of preparations of FDC1 from *E. coli* lacking tPAD1.

Furthermore, the increased cofactor content resulted in an enzyme preparation that was visibly a pale-yellow color. The UV-Visible spectrum of the FDC1-bound chromophore exhibited an absorbance maximum at 342 nm characteristic of a reduced flavin (Figure 2.5)[80, 81]. However, whereas reduced flavins are readily reoxidized under the aerobic condition in which the protein was handled, the chromophore associated with FDC1 was stable, and its spectrum remained unchanged when it was released from the protein preparation by denaturation with 1:1

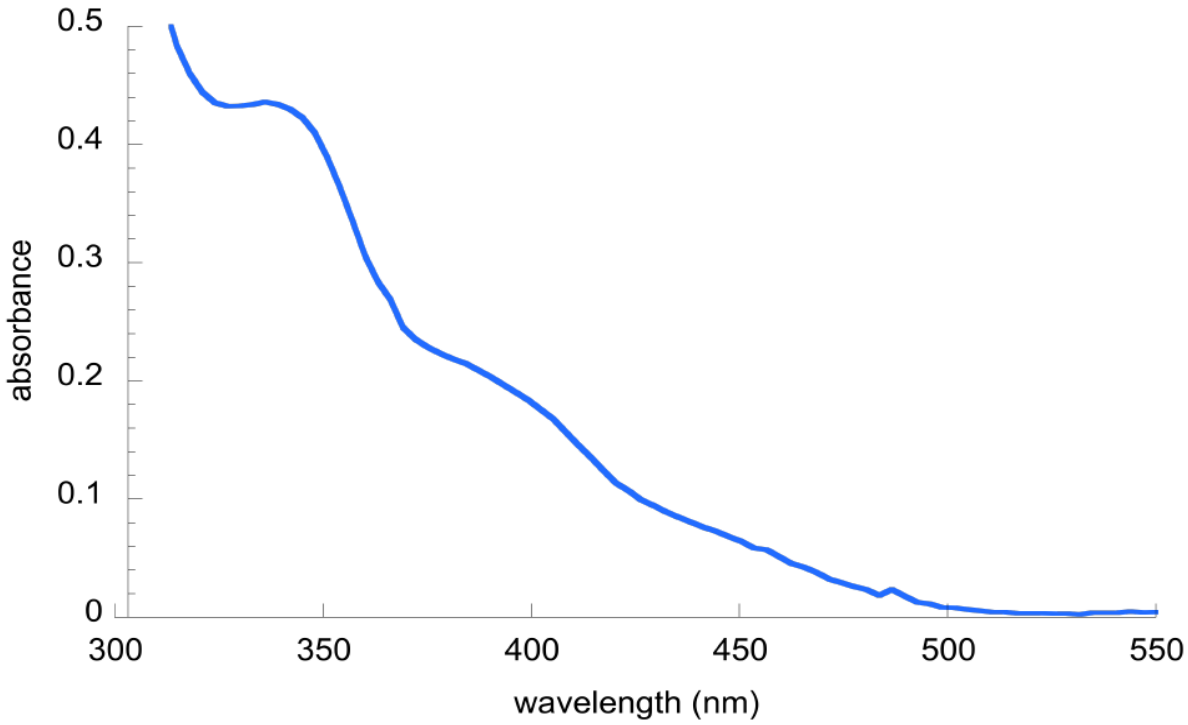

Figure 2.6 U.V.-visible spectrum of holo-FDC1. The spectrum is suggestive of a reduced flavin-like chromophore

dichloromethane/methanol. A preparation of the cofactor, obtained by precipitation of the protein with 1:1 dichloromethane/methanol, followed by removal of the organic solvent was capable of activating apo FDC1; thereby confirming that the pale-yellow chromophore associated with FDC1 is indeed responsible for the activity of the enzyme.

The protein-free cofactor was further subjected to LC-ESI-MS^2 analysis. The major species in the primary MS spectrum (Figure 2.6) was characterized a $(M+H)^+/z$ = 661.22 and

$(M+H)^+/z$ = 625.2054 that probably represents the loss of one and two water molecules respectively from the parent ion. From this, a molecular weight of the cofactor was hypothesized to be 660.2212. The experimentally determined weight, together with the intensity of the natural abundance ^{13}C peak, is consistent with a molecule possessing between 27-32 carbon atoms. I cautiously note that I cannot definitively rule out, given its labile nature, that this species might represent a fragment of the cofactor. The major species was subjected to mass fragmentation and attempts were made to match the resulting MS^2 data with various databases of small molecules including Chemical Entities of Biological Interest (ChEBI) metabolomics database, SciFinder (Chemical Abstracts Service) database, and the METLIN metabolomics database[82]. However, no convincing matches to compounds in these databases were found. Further attempts to determine the identity of the FDC1 cofactor were hindered by the small amounts of material available and the instability of the molecule, which appears to react upon release from the enzyme. Although the cofactor retained remained intact under the mildly acid conditions used in the LC analysis (0.1% formic acid), more strongly acidic (0.1 M HCl for 1 hr) or basic (0.1 M NaOH for 1 hr) conditions followed by neutralization, resulted in the disappearence of the cofactor. LC-MS analysis of acid-treated samples revealed a complex mixture of products that could not be interpreted. However, LC-MS analysis of base-treated samples revealed, among other fragments, the presence of a peak with $(M+H)^+/z$ = 457.1 Da corresponding to FMN, providing further evidence that the cofactor comprises a modified form of FMN.

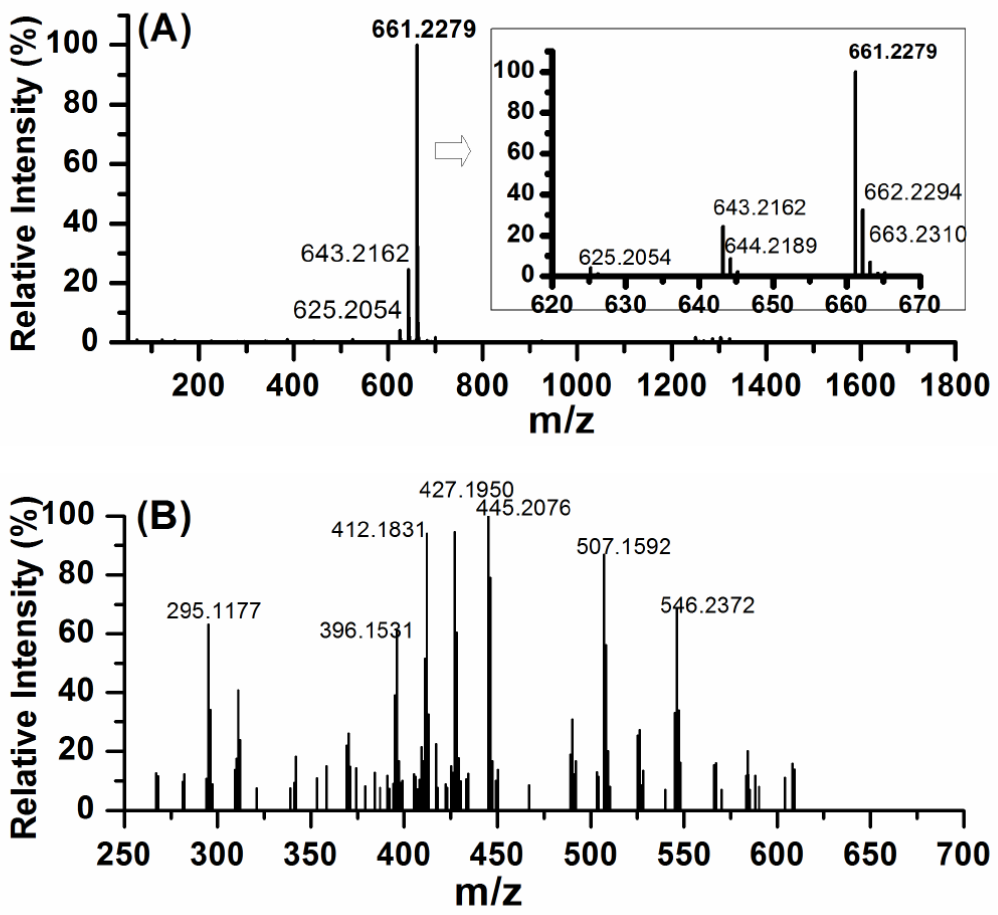

Figure 2.7 High resolution of ESI-MS spectrum of the novel cofactor for FDC. (B) High resolution ESI-MS of the highest molecular weight peak with (m+1)/z = 661.2279

Interestingly, the structures of *E. coli* UbiD, a homologous enzyme to FDC1, and an UbiD-like protein from *P. aeruginosa* have been solved; however, no cofactors are present in the crystal structure. Although the *E. coli* enzyme is a hexamer whereas the *P. aeruginosa* enzyme is dimeric, they adopt very similar tertiary structures, and it is likely that FDC adopts a similar tertiary structure[18, 19]. The UbiD enzymes comprise three domains, and it is particularly intriguing that the central domain possesses a split β-barrel fold characteristic of flavin reductases. The structures reveal a large cleft in the putative FMN or a modified FMN

derivative. I speculate that under the conditions used to express these enzymes for crystallographic analysis, endogenous UbiX could not synthesize sufficient cofactor to saturate UbiD or that the cofactor may be lost or degraded during purification. The unavailability of the native substrate of these bacterial enzymes, 4-hydroxy-3-octaprenylbenzoic acid, prevented their assay too determine whether these enzymes were indeed active enzymes.

Based on the U.V.-visible spectrum and its molecular weight, together with the fact that PAD1 contains FMN and that FDC1 resembles other flavin-binding enzymes, I propose that the novel cofactor is likely a modified form of reduced FMN. The fact that the cofactor can be stable to air suggests that it is modified at N5, as alkylation on nitrogen would stabilize the reduced flavin ring against oxidation. It was later revealed that the structure of the cofactor that involves is a reduced prenylated flavin, which would result in this new cofactor having a significantly larger mass than FMN, the cofactor would be oxygen stable, and would have spectral characteristics reticent of reduced FMN.

2.3.6. Steady state kinetic properties of FDC1

The significant improvement in the activity of FDC1 resulting from its co-expression with tPAD1 allowed the decarboxylation of ferulic acid to be followed spectrophotometer geometrically by the decrease in absorbance at 304 nm. Although this limited the upper concentration range of substrate that could be studied before the substrate absorbance became too high, this assay, being far less cumbersome than the GC-MS-based assay, made is feasible to determine cat and K_M for cinnamic acid and the structurally related compounds ferulic acid (*trans*-(4-hydroxy-3-methoxyphenyl)-acrylic acid and p-coumaric acid (*trans*-(4-

hydroxyphenyl)-acrylic acid). The kinetic constants for these substrates, at pH 7.0 and 25 ºC in 100 mM potassium phosphate buffer, are given in table 1.

Table 2.1 Steady State Kinetic Parameters for FDC1

Substrate	$k_{cat\ [65]}$ (s^{-1})	K_M (µM)	k_{cat}/K_M ($s^{-1}M^{-1}$)
trans-Cinnamic Acid	4.6 ± 0.2	180 ± 24	25500 ± 3500
trans-Ferulic Acid	3.8 ± 0.3	180 ± 41	21000 ± 4500
trans-Coumaric Acid	1.5 ± 0.1	110 ± 26	13600 ± 880

[a] $k_{cat\ [65]}$ values were calculated based on the concentration of FDC protein. As discussed in the text the true k_{cat} is likely significantly higher due to incomplete cofactor occupancy

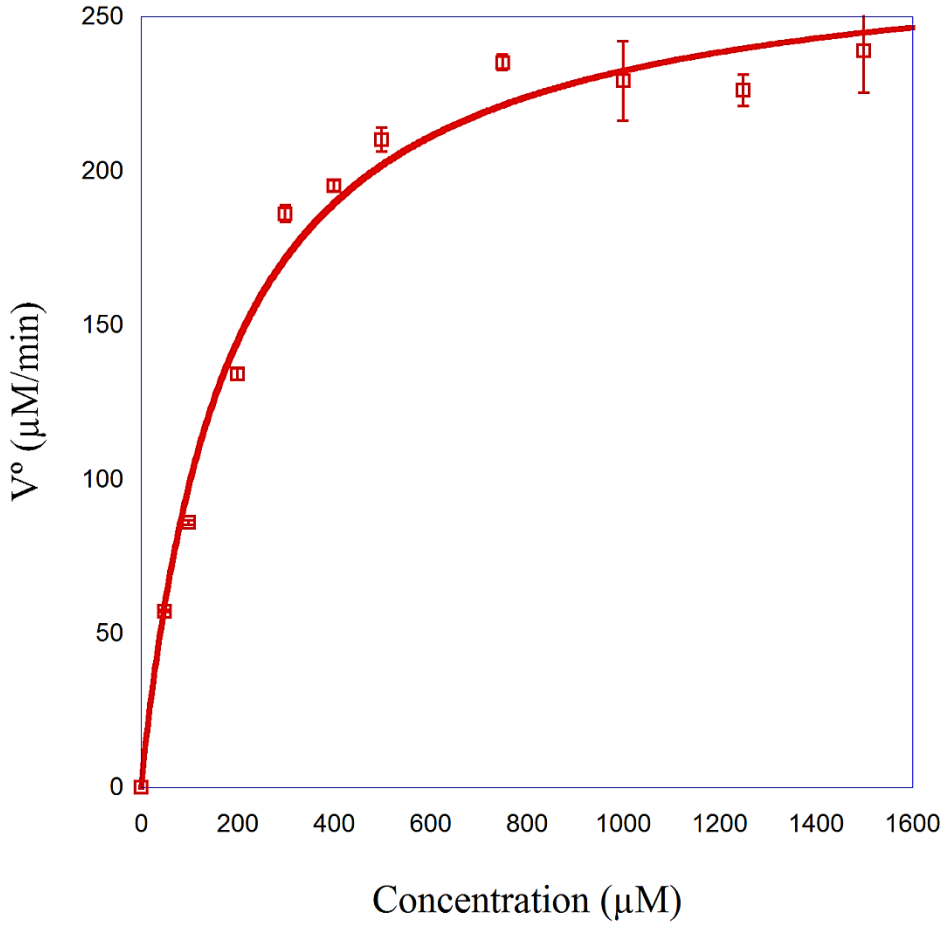

Figure 2.8 Michaelis-Menten plot of trans-cinnamic acid.

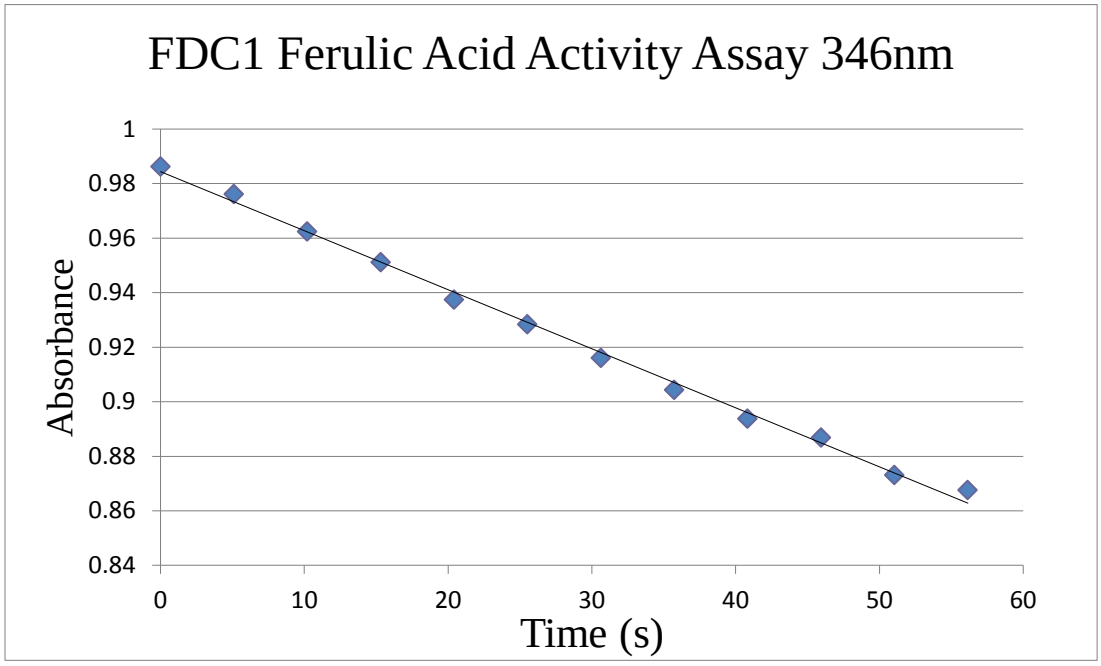

Figure 2.9 Representative FDC1 assay invoving the decarboxylation of ferulic acid monitored at 346nm

Trans-cinnamic acid proved to be the most active substrate, additionally FDC1 decarboxylated additional phenylacrylic acid substrates including ferulic and coumaric acids, only slightly less efficiently. FDC1's ability to decarboxylate a wide variety of substrates suggests that it may be active with a wider range of substituted phenyl acrylic acid derivatives, which may lend it to industrial uses. Although co-expression of FDC1 with tPAD1 results in a large increase in enzyme activity, it appears that the cofactor occupancy is still low if the extinction coefficient for the FDC1 cofactor is similar to reduced FMN. Therefore, the true k_{cat} values for FDC1 acting on these substrates may be higher than the values reported here.

I note that ferulic acid decarboxylases, also described as phenolic acid decarboxylates, have been described from a wide variety of species including, *Pseudomonas flourscences* and *B. subtillis*. However, these enzymes require no organic cofactors and are dimers of subunit Mr = 20 kDa. They catalyze the decarboxylation of phenolic acids, such as

coumaric and ferulic acids, through a mechanism involving deprotonation of the phenolic group which is required to generate a quinone intermediate. However, they do not catalyze the decarboxylation of cinnamic acid, in which the phenyl ring is inactivated. The two classes of FDC enzymes are therefore mechanistically quite distinct from each other[30].

2.4 Conclusions

The function of PAD1 and FDC1 as enzymes involved in the detoxification of aromatic carboxylic acids was first elucidated through genetic analysis of yeast mutants deficient in the metabolism of cinnamic acids and its derivatives[24]. Homologues of these genes are present in a range of other microbes including bacteria and some fungi. Although sequence similarities with better-characterized enzymes from other organisms allowed some predictions as to the structure and cofactor requirements of these enzymes to be made, the function of PAD1, which is widely distributed in microbes, is to make a PrFMN cofactor. Members of the UbiD family of enzymes utilize PrFMN to facilitate aromatic decarboxylation[48, 54, 57, 83-86]. *E. coli* strains solely overexpressing PAD1 genes, and homologs of PAD1 are unable to decarboxylate phenyl acrylic acid derivatives from the enterohemorrhagic *E. coli* strain O157: H7 bacteria strain, which exhibits no decarboxylase activity with a variety of phenyl acrylic acid derivatives. These observations make it apparent that PAD1 is miss-named as it's not a phenylacrylic acid decarboxylase; however, PAD1 transfers a DMAPP molecule onto reduced FMN to make reduced PrFMN that is up taken by FDC1 and oxidized[48, 54, 57, 83-86].

The experiments reported here constituted the first time PAD1 and FDC1 were biochemically characterized, with the functions of PAD1 and FDC1 elucidated. PAD1 synthesizes a novel cofactor required by FDC1 for decarboxylase activity. The liability of the

cofactor thus far has prevented the immediate identification of the cofactor; however, based on its UV-visible spectrum, its molecular weight, and the resemblance of PAD1 and FDC1 to other flavin-binding enzymes, I propose that the cofactor is likely a new, modified form of reduced FMN. These initial results were confirmed when FDC1 from *A. niger* were crystallized with newly elucidated cofactor PrFMN. The mechanism by the cofactor facilitates the decarboxylation of cinnamic acid was proposed to involve a novel 1,3 dipolar cycloaddition mechanism, as this type of decarboxylation reaction lacked any obvious precedent in flavin-protein chemistry[60, 79-81, 87].

PAD1 and FDC1 share sequence similarities with the *E. coli* enzymes UbiX and UbiD, which are involved in the decarboxylation of 4-hydroxy-3-octaprenylbenzoic acid, an early step ubiquinone biosynthesis. The experiments above show that UbiX can replace PAD1 in activating FDC1 and it was previously shown that PAD1 restores ubiquinone biosynthesis in a ΔubiX *E. coli* strain. Therefore, UbiX and PAD1 appear to be isofunctional enzymes. The evidence strongly implies that UbiD is, in fact, the 4-hydroxy-3-octaprenylbenzoic acid decarboxylase and that it uses the same cofactor as FDC1. The existence of Pad1p, distinct from UbiX, in some *E. coli* strains, is intriguing as it suggests there are a variety of roles for PrFMN.

Chapter 3

Uncovering the Mechanism of FDC1 through a Linear Free Energy Analysis, and Solvent and Secondary Isotope Effects

The work described in this chapter has been published as Ferguson, KL., Arunrattanamook, N., Marsh, E. N. G. (2016) Mechanism of the Novel Prenylated Flavin-Containing Enzyme Ferulic Acid Decarboxylase Probed by Isotope Effects and Linear Free-Energy Relationship. Biochemistry, 55, 2857-2863. N. Arunrattanamook and K.L. Ferguson collaborated on the Hammett Analysis. K.L. Ferguson performed and analyzed the entirety of the isotope effect experiments. K.L. Ferguson synthesized and analyzed the isotopically labeled singly labeled deuterated cinnamic acid. K.L. Ferguson performed and analyzed the results of the NMR deuterium exchange experiment. K.L. Ferguson, N. Arunrattanamook, E.N.G. Marsh wrote the paper.

3.1 Introduction

UbiX and UbiD family of enzymatic decarboxylase attracted interest for their potential industrial application to produce high value, optically pure chemicals under mild conditions in environmentally friendly bioprocesses and their potential as an antifungal and antibiotic

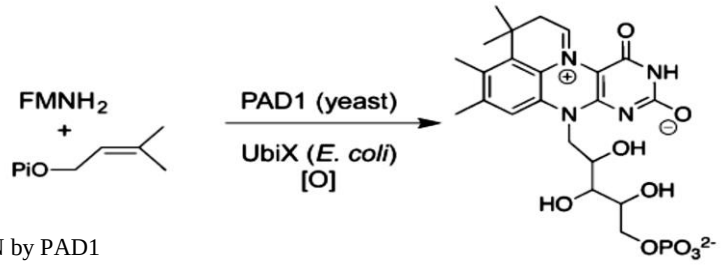

Figure 3.1 Synthesis of PrFMN by PAD1

formulation. Recent studies on FDC1 and UbiD enzymes established the presence of a new flavin derived cofactor, prenylated Flavin, and that these PrFMN decarboxylases decarboxylate β, γ-unsaturated carboxylic acids through a unique 1,3 dipolar cycloaddition mechanism.

The *ubiX* and *ubiD* and the related *pad1* and *fdc1* genes have been shown to encode proteins responsible for non-oxidative reversible decarboxylation of aromatic substrates. These genes are widely distributed in archaea, yeast, and fungal genomes as means to breakdown xenotoxins whereas Ubix and UbiD play a key role in the prokaryotic ubiquinone biosynthetic pathway. The genomic analysis led to the suggestion that *ubiX* and *ubiD* and the related *pad1* and *fdc1* genes encode redundant decarboxylases. However the last chapter provided evidence that these enzymes do not encode redundant decarboxylases, but instead, UbiX and Pad1 are responsible for synthesizing PrFMN (Figure 3.1). Recent crystal structures of PAD1reveals how DMAP and oxidized FMN bind; a crystal structure of E49Q mutant was able to trap an intermediate which DMAP reacted with reduced FMN. The reaction ultimately results in reduced PrFMN although the mechanism by which the reduced PrFMN oxidizes to form the imminium form of the cofactor whether enzymatic or spontaneous remains uncertain. FDC and UbiD both utilize the imminium form of the cofactor to facilitate the decarboxylation a range of aromatic carboxylic acids[51, 88]. Crystal structures of *A. niger*, *S. cerevisiae*, and *Candida dubliniensis* revealed various PrFMN cofactor species including the ketamine form, hydroxylated imminium PrFMN and oxidized imminium PrFMN. To observe which of these species is the active cofactor, and to gain insights into the catalytic mechanism, *A. niger* FDC1 crystals were soaked with a range of *trans*-cinnamic acid derivatives and related compounds. Phenylpyruvate produced an alpha-tethered keto-enol tautomerized adduct. The crystal structure containing the phenylaldehyde adduct combined with DFT calculations of potential FDC1

intermediates resulted in a proposed mechanism (Figure 3.2) involving a novel 1,3-dipolar cycloaddition. The azomethine ylide of PrFMN is proposed to form a 1,3 dipolar cycloaddition

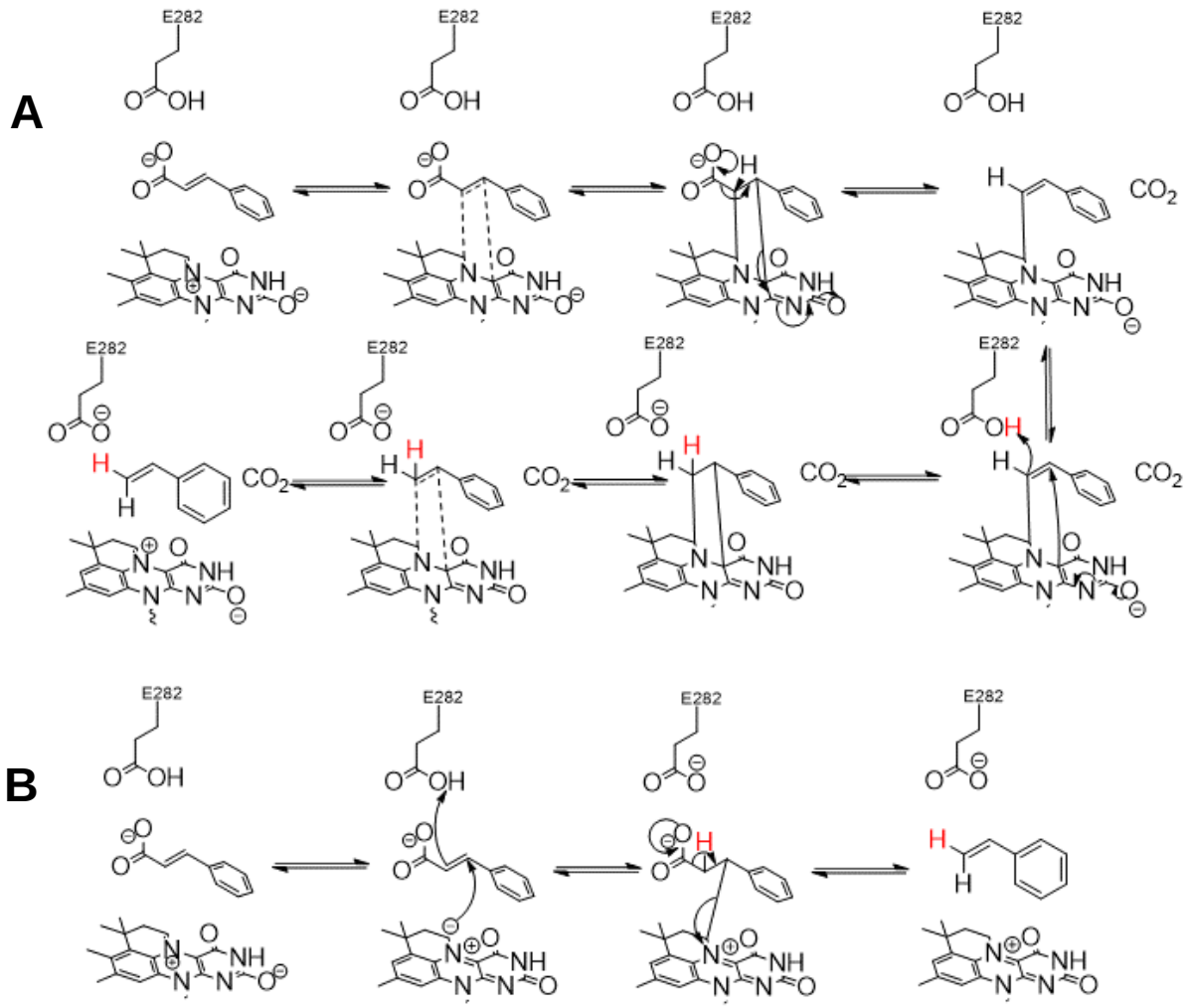

Figure 3.2 (A) Proposed mechanism for the *A. niger* FDC1-catalyzed decarboxylation of phenylacrylic acid involving a 1,3-dipolar cycloaddition to the PrFMN cofactor (B) Proposed mechanism for the *A. niger* FDC1-catalyzed decarboxylation of phenylacrylic acid involving a Michael addition-elimination reaction[51,56]

with a α, β -unsaturated bond of the phenylacrylic acid. This is followed by a Grob-type fragmentation, after which glutamic acid 282 protonates the alpha tethered intermediate which results in a second 1,3 dipolar cycloaddition mechanism. This results in a product-PrFMN adduct which then undergoes ring collapse to release the vinyl benzene derivatives and the PrFMN.

The mechanism of FDC1 is of considerable interest because thermal pericyclic reactions are infrequent in enzymes, and 1,3-dipolar cycloadditions are unprecedented. Based on the crystallographic evidence and the computational simulations the 1,3 dipolar cycloaddition mechanism is preferred over an alternative mechanism involving a Michael addition of PrFMN to the double bond of the phenyl acrylic acid followed by decarboxylation and elimination of the cofactor (Figure 3.2). In this chapter, I investigate the mechanism using a combination solvent isotope effects, secondary isotope effects, NMR proton exchange experiments, and a linear free-energy analysis to probe the enzymatic processes of the newly discovered PrFMN decarboxylase.

3.2 Materials and Methods

3.2.1 Materials

trans-cinnamic acid, styrene, *para*-coumaric acid, 4-methoxycinnamic acid, 4-fluorocinnamic acid, 4-formylcinnamic acid, 4-bromocinnamic acid, 4-chlorocinnamic acid and 4-methylcinnamic acid were purchased from Acros Organic. *Trans*-cinnamic acid, 3-nitrocinnamic acid, and 3-methoxycinnamic acid were obtained from Sigma Aldrich Co. 4-cyanocinnamic acid was purchased from Matrix scientific. 4-aminocinnamic acid and 4-nitrocinnamic acid were purchased from Tokyo Chemical Industries. 4-(2-carboxy-vinyl)-benzoic acid methyl ester was purchased from Santa Cruz Biotechnology. All other chemicals were purchased from Sigma Aldrich Co.

d_7-*trans*-cinnamic acid and 3-d_1-*trans*-cinnamic acid were purchased from Sigma-Aldrich, 2-d_1-*trans*-cinnamic acid was synthesized by reaction of benzaldehyde with d_6-acetic anhydride using standard literature procedures.

Holo-FDC1 was recombinantly expressed in *E. coli* and purified as described previously.

3.2.2. Determination of k_{cat}/K_M by U.V.-Visible Spectroscopy

Assays of FDC1 activity were routinely performed in 100 mM phosphate buffer (pH 7.4) at 25 ºC. Stock solutions of the substrates were prepared in DMSO. Assays contained substrates at various initial concentrations between 10 and 50 µM. Reactions were initiated by the addition of FDC1 to a final level between 50 and 500 nM depending on the activity of the enzyme with a substrate. The kinetics of the substrates was monitored spectrophotometrically, using an 8543 Hewlett Packard spectrophotometer, by monitoring depletion of the substrates.

3.2.3. Determination of the Extinction Coefficient of Each Substrate

A 1mM stock solution of each substrate was made up in 100 mM pH 7.5 phosphate buffer. A calibration curve was constructed using five concentrations between 5 µM and 100 µM using the 8543 Hewlett-Packard spectrophotometer. The wavelengths used to watch the enzyme activity, and extinction coefficients of the various substrates are given in Table 3.1

Table 3.1 Assay wavelengths and extinction coefficients for phenylacrylic acid derivatives used in this study.

Substituent	Assay wavelength (nm)	ε substrate (M^{-1} cm^{-1})	ε product (M^{-1} cm^{-1})
p-NH_2-	292	17900	1840
p-HO-	294	16900	7930
pCH_3O-	290	18900	5410
pCH_3-	280	19000	N/A
p-H-	276	17900	N/A
p-F-	276	14300	948
m-CH_3O-	276	14300	N/A
p-Cl-	280	21200	1810
p-Br-	278	22000	2630
p-CH_3OOC-	300	19000	N/A
m-NO_2-	280	14800	7240
p-CN-	284	26600	7230
p-CHO-	304	24800	N/A
p-NO_2-	314	18000	9760

3.2.4. Synthesis of β Deuterated *trans*-Cinnamic Acid

0.84g(0.0082 mol) Potassium acetate (Fisher) was weighed out into a three-necked round-bottomed flask. The flask was then heated in an oil bath to 170-190 ^{o}C while under dried nitrogen. Passing dry nitrogen and warming the round bottom flask served to remove any moisture from the base and the vessel.

2.5 mL (0.0094 mol) Benzaldehyde (Sigma-Aldrich) was dried over molecular sieves (Sigma) and introduced into the two-necked round-bottomed flask via a glass syringe. The flask also equipped with a drying tube (Dririte), and reflux condenser. A stir bar was introduced.

5.0g (0.049 mol) Acetic anhydride d_6 (Sigma-Aldrich) was introduced into the flask via a glass syringe. The drying tube was removed after five minutes, and dried nitrogen flowed through the apparatus.

The reaction proceeded for 14 hrs at between 165 - 200 ^{o}C. After the reaction progressed for one hour TLC (alumina plate eluted with 60/40 EtOAc/Hexane) showed the presence of TCA (co-spotted with standard). After 14 hrs a solid reddish-brown solid oil was present in the flask. To this extract the TCA from the reddish-brown oil approx. 50.0mL MeOD was added with 3 g of activated carbon. This solution was heated to boiling briefly and gravity filtered while hot. The resulting clear solution was pD adjusted to pD 2 using concentrated DCl, which resulted in a white precipitate formed, which was then filtered. The charcoal cake residue in the filter was washed with more MeOD. After a few washes, the filtrate started becoming yellowish colored. The decolorization of the crude material indicated that the impurity was removed by the charcoal. Any colored filtrates were treated separately from the clear filtrates. These subsequent washes were pD adjusted and filtered as well. The crude d_1-TCA (0.60 g) was recrystallized by adding approx. 10mL D_2O to the crude in a 150mL beaker, and heating to near boiling. This was followed by dropwise addition of MeOD until everything was dissolved. The beaker was allowed to cool to room temperature. The white translucent plate-like crystals formed immediately and were filtered and 1:1 mixture of D_2O and MeOD. ^{1}HNMR confirmed the alpha-deuterated TCA (94-95% deuterated) as evidenced by a very diminished doublet at 6.5ppm (protonated alpha proton) relative to the beta proton at 7.8ppm. Yield was found to be 16%[89].

3.2.5. Preparation of the Deuterated Buffers

100 mM solutions buffers at various pHs were used to study the FDC activity as followed: pH 4.0-6.5, 100mM sodium citrate; pH 6.5-8, 100 mM sodium phosphate; pH 8.0-9.0, 100mM Tris Chloride. The buffer salts were dissolved in 99.8% D_2O and lyophilized, three times, to produce deuterated buffers. The pD of the buffers were either raised or lowered using DCl and NaOD. Mixed D_2O / H_2O buffers were prepared at various mole fractions by combining deuterated and proteated buffers to the desired ratios, differences in molar volumes between H_2O and D_2O were accounted for using the values of 18.126 mL/mol and 18.058 mL/mol respectively. The mole fraction of D_2O in each assay was re-calculated to account for the isotopic purity of D_2O. The enzyme was buffer exchanged in the D_2O buffer and the mixed D_2O / H_2O buffers. pL was correct using equation 2 where χ is the mole fraction of D_2O[90].

Equation 3 $$pL = pH_{obs} + 0.311x + 0.0766x^2 + 0.00009$$

3.2.6. Deuterium Exchange Using ^{1}H NMR

Carbon dioxide was removed from the deuterated citrate buffer by first bubbling argon through a sodium hydroxide solution, and then carbon dioxide was thoroughly removed from the deuterated citrate solution. Samples were prepared by buffer-exchanging the protein solution three times by repeatedly concentrating the protein in a 30kDa amicon filter and then diluting the protein solution in the deuterated citrate buffer pD 6.5. Proton exchange was monitored using ^{1}H NMR at 400 MHz with 1-s pulses at a 60º angle at 22 ^{o}C and following the disappearance of the styrene resonance at 5.2 ppm. The reaction buffer was compromised with 100mM potassium citrate in D_2O (pD = 6.5) 10 µM FDC, 10mM $KHCO_3$, and 2.5 mM styrene[91].

3.2.7 GC-MS Experimental Protocol for Constructing a Yield-Based Proton Inventory

To measure the intrinsic solvent deuterium isotope effect on styrene formation, the reactions were performed in buffers containing various mole fractions of D_2O. The protein was exchanged into the various buffers before the addition of the substrate to reduce the H_2O contribution as much as possible from the enzyme stock solution. To quantify the amount of H-styrene and D-styrene the reactions were quenched by the addition of 500 µL of ethyl acetate and the styrene was extracted after 2 minutes. The products of the reaction were then loaded on a Shimadzu QP-2010 GC-MS system equipped with a DB-5 column (30 m x 0.25 mm x 0.25 µm). The flow rate of the helium carrier gas is constant at 1 mL/min the inlet temperature was maintained at 200ºC. The interface temperature was maintained at 250 ^{o}C. Injections (8 µL) of the ethyl acetate extracted were made in splitless mode. The oven temperature was held initially at 40 ^{o}C for 3.5 min, gradually increased to 90 ^{o}C at 14 ^{o}C /min, then gradually increased from 90 ^{o}C to 315 ^{o}C at 20 ^{o}C /min, and finally maintained at 315 ^{o}C for 1 min. GC-MS PostRun analysis software analyzed chromatographic data. The styrene peak was resolved at the 7.6-minute mark of the run. D-styrene intensity was corrected by removing the intrinsic ^{13}C styrene contribution[90].

3.2.8. U.V.-Visible Protocol for the Determination of Secondary Kinetic Isotope Effects

Secondary KIEs were established at 280 nm, by monitoring the disappearance of TCA, each experiment was repeated 9 times to achieved to achieve the desired degree of precision. Secondary KIEs were established at a substrate concentration of 50 µM and enzyme concentrations of 50 nM so that the measurements represent the KIE on V_{max}/K_M. Experiments were performed at a pD and pH of 6.5, where the activity of the enzyme is independent of pH.

3.2.9 Curve Fitting

Plots of kinetic data were generated, and curve fitting performed using the Origin Program (OriginLab). The data for the description of FDC activity were fit to Eq. 4 which describes the relationship between the change in absorbance and the change in concentration of a substrate at a given time point. The data for the description of mole fraction of styrene yields with respect to the mole fraction of the solvent were fit to equation 5. Data describing $\log(k_{cat}/K_M)$ activity with respect to σ - was fit to equation 6. pK_a values of FDC1 were determined using equation 7.

Equation 4

$$V = \frac{\left(\frac{\Delta Abs}{dt}\right)}{\left(\varepsilon_{wavelength(substrate)} * [E]\right)}$$

Equation 5

$$\chi_{products} = SIE_{obs}\left(\frac{1}{\chi_{solvent}} - 1\right)$$

Equation 6

$$\rho = \sigma \log\left(\frac{\left(\frac{k_{cat}}{K_M}\right)_X}{\left(\frac{k_{cat}}{K_M}\right)_H}\right.$$

Equation 7

$$k_{cat} = \frac{Vmax}{(1 + 10^{pK_{a1} - pH} + 10^{pH - pK_{a2}})}$$

3.3 Results

3.3.1 Linear Free Energy Analysis

Linear free-energy relationships provide a powerful tool with which to interrogate reaction mechanisms. Hammett analysis is rarely used in enzymology due to the narrow substrate range of most enzymes, although, for more promiscuous enzymes, linear free energy analysis proves to be highly informative[92, 93]. Interpretation of LFERs is often complicated by additional considerations such as differences in hydrophobicity or Vander der Waal's radius.

Thus single parameter linear free energy analysis is seldom possible to analyze the relationship between an enzyme and its substrates. The broad substrate range of FDC1 makes it an excellent candidate to conduct a Hammett analysis of its decarboxylation mechanism[27]. The kinetics of decarboxylation were studied for a series of 14 para- and meta-substituted phenylacrylic acids and related to a series of parameters including; σ, σ -, σ +, and hydrophobicity.

The Hammett analysis suggests that among the substrates examined the most kinetically significant attribute was the negative electronic substituent parameter. σ – which is generally associated with phenols, anilines, and other groups with loosely held lone pair electrons conjugated with a substituent capable of accepting a lone pair of electrons via resonance. The most widely accepted systems for defining σ – is aniline, due to the ability of the lone pair of electrons to readily delocalize and reform the immine resonance structure. In the mechanisms presented a σ – would be appropriate with a lone pair of electrons is reacting from either the amine group, in the case of the 1,3 dipolar cycloaddition mechanism or having the electrons from the carboxylate group moving to fill the electron hole that would exist after the gamma-carbon PrFMN bond breaks pushing electrons back onto the PrFMN[92]. Interestingly and unexpectedly, for a decarboxylation reaction, ρ is negative (ρ = -0.39)(figure 3.3). This points to a few things, first a chemical step in the reaction as the rate-determining step, rather than a substrate-binding or product release step, in which case the ρ would be expected to be close to zero. Secondly, the negative rho value is consistent with a buildup of positive charge in the rate determining transition state, unlike most decarboxylation reactions where the decarboxylation would result in buildup of negative charge leading to a positive ρ value. Therefore, it seems unlikely, regardless of the precise details of the mechanism, that the decarboxylation step is rate-determining[94].

Table 3.2 k_{cat}/K_M values measured for FDC-catalyzed decarboxylation of various phenylacrylic acid derivatives

Substituent	σ^-	k_{cat}/K_M ($M^{-1} s^{-1}$)	$\log(k_{cat}/K_M)$
p-NH_2-	-0.66	12400 ±674	4.09 ± 0.023
p-HO-	-0.37	4550 ± 247	3.66 ± 0.023
pCH_3O-	-0.27	28100 ± 1800	4.45 ± 0.027
pCH_3-	-0.17	27000 ± 1600	4.43 ± 0.025
p-H-	0	24500 ±1450	4.39 ± 0.023
p-F-	0.02	27500 ±1760	4.44 ± 0.027
m-CH_3O-	0.12	27000 ± 2000	4.44 ± 0.031
p-Cl-	0.23	19700 ± 1210	4.29 ± 0.026
p-Br-	0.26	21400 ± 1320	4.33 ± 0.026
p-CH_3OOC-	0.66	11500 ± 322	4.06 ± 0.012
m-NO_2-	0.71	14300 ± 1020	4.16 ± 0.030
p-CN-	0.88	12800 ± 884	4.11 ± 0.029
p-CHO-	1.13	8690 ± 305	3.88 ± 0.015
p-NO_2-	1.25	8690 ± 162	3.94 ± 0.008

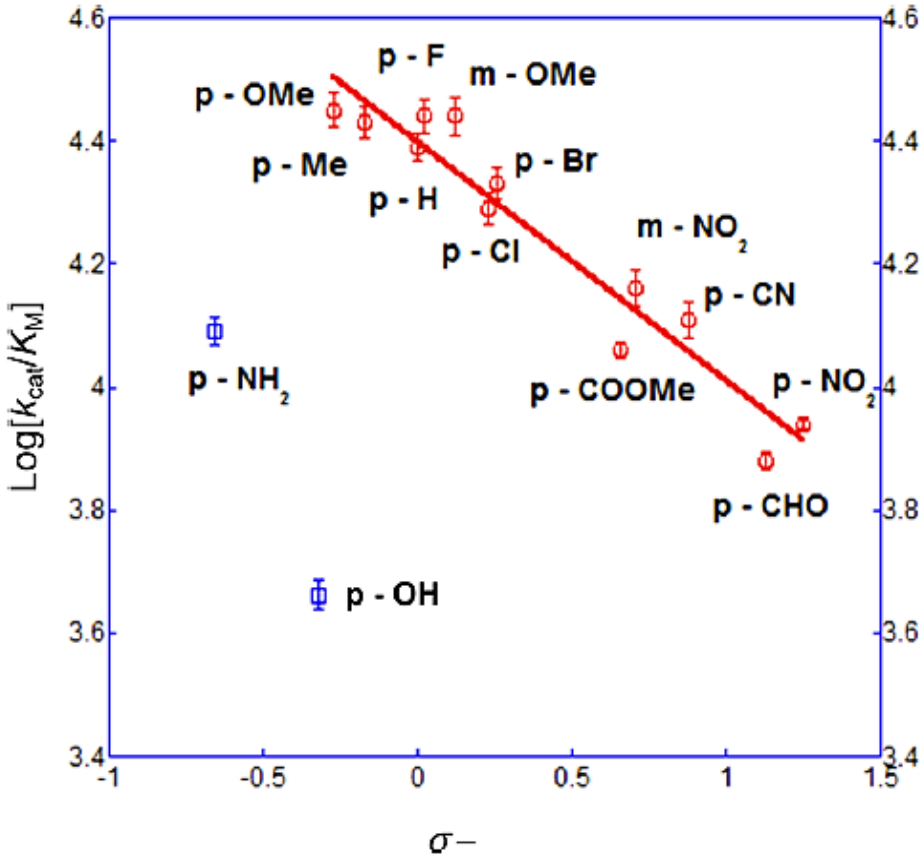

Figure 3.3 Hammett analysis of FDC1-catalyzed decarboxylation of 12 different para- and meta- substituted phenylacrylic acids

3.3.2 pH dependence and solvent isotope effects

Initial characterization by ^{1}H NMR of the styrene produced in the FDC1 reaction established that the solvent proton is incorporated *trans* to the phenyl ring of styrene, as evidenced by the disappearance of the signal at 5.2 ppm when the reaction was performed in D_2O (Figure 3.5). Therefore, decarboxylation occurs with the retention of configuration at C_α, which is in accord with the geometry of the active site and the proposed role of Glu285 acting as the proton donor[51].

Because pH may influence solvent isotope effects, I first investigated the activity of FDC1 as a function of pH and pD. Under V_{max} conditions, the enzyme exhibits a bell-shaped pH

dependence, typical of many enzymes, with an activity maximum at pH 6.5. the acidic limb is characterized by pKa = 5.3 ± 0.1, and the basic limb is characterized by a pKa = 8.0 ± 0.1. the enzyme activity determined in deuterated buffers was found to be very similar, although the pKa of the acidic limb was shifted to a lower value (pKa = 5.0 ± 0.1) (Figure 3.5). Using the pH & pD curve the solvent isotope effect on Vmax was found to be close to unity (^{D}Vmax = 0.95 ± 0.05; n = 5), indicating that proton transfer to the product is not a kinetically significant step in the determination of k_{cat}[90, 95].

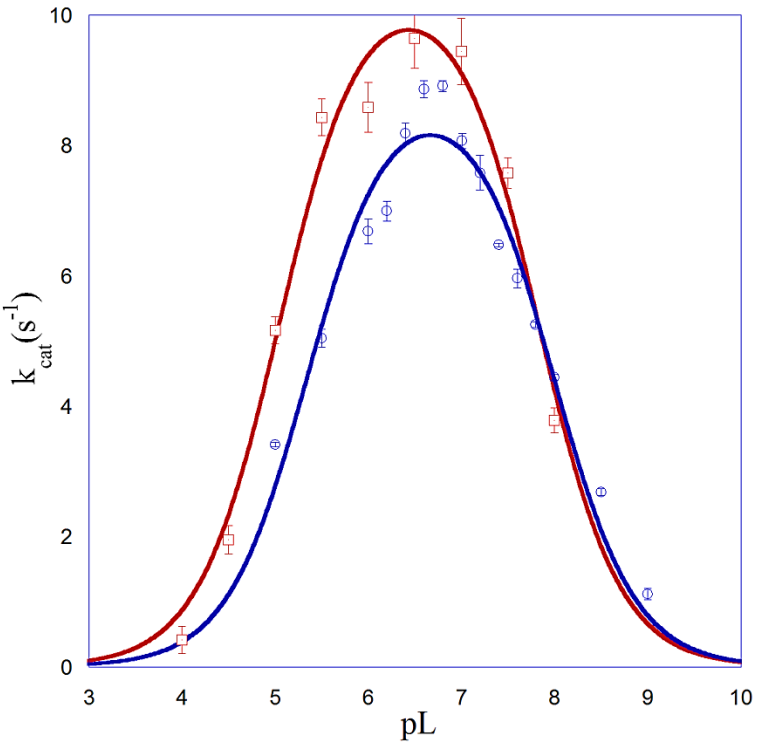

Figure 3.4 pL-rate profile for decarboxylation of trans-cinnamic acid by FDC in H_2O (blue) and D_2O (red) buffers kinetic data was fit to equation 7

To investigate the protonation step in more detail, I conducted a proton inventory analysis, which enabled measurements on the solvent KIE on V_{max}/K_M). Reaction mixtures were set up at pL 6.5 in buffers containing 0.1 mole fraction increments of deuterium (χD_2O). The styrene produced by the reaction was isolated, and the mole fraction of deuterated styrene ($\chi_{styrene}$) was determined by GC-MS. While $^{D}V/K_{solvent}$ was determined to be $^{D}V/K_{solvent}$ = ~3.3± 0.09, this was determined by fitting the proton inventory to equation 2[90, 96, 97].

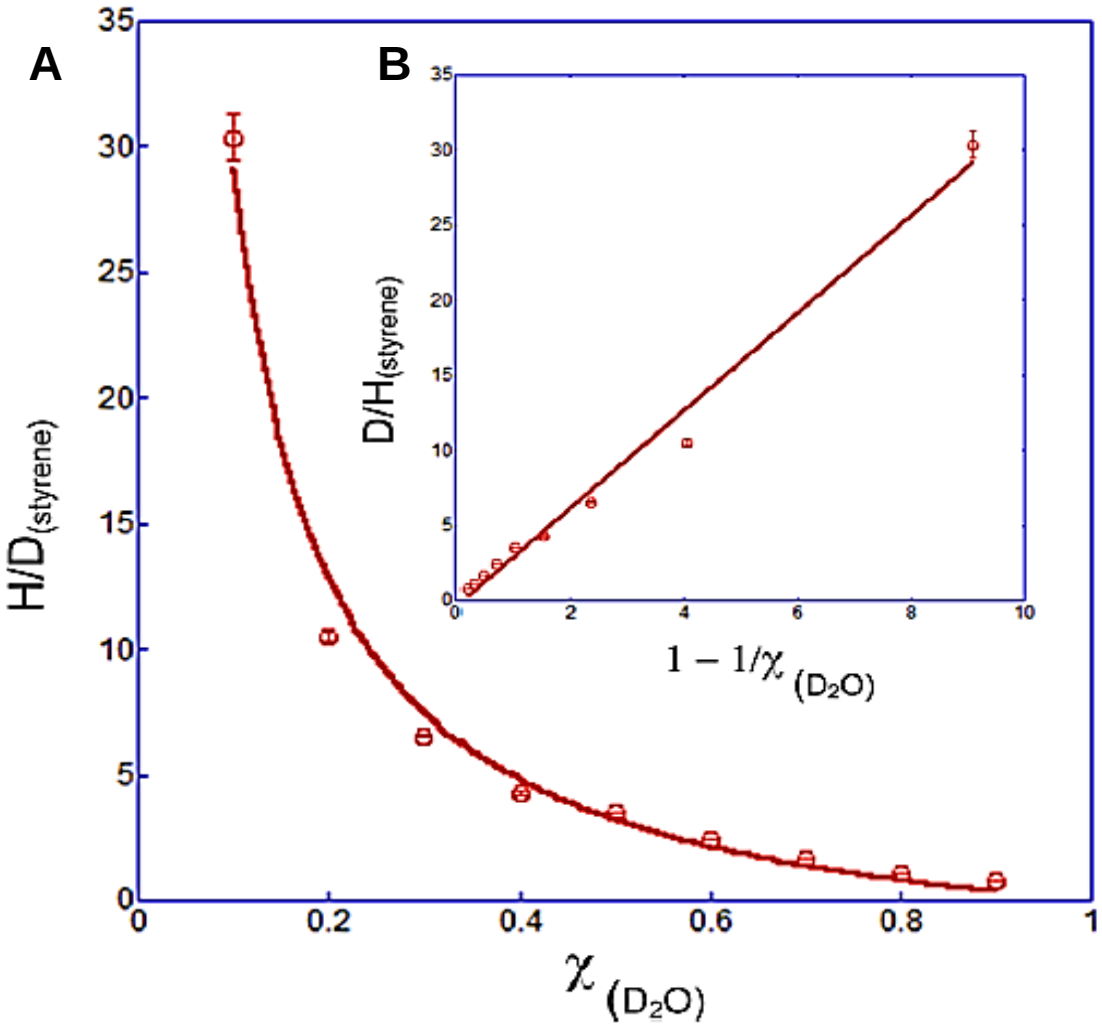

Figure 3.5 (A) Proton inventory for FDC. The mole fraction of D_2O in the solvent is plotted against the ratio of protonated to deuterated styrene. the solid red line represents the best fit to deuterated styrene. The solid red line represents the best fit to equation 2. (B) A linearized plot of the data. The data was fit to equation 4

From this analysis, a substantial solvent KIE on V_{max}/K_m is evident, with $^{D}(V/K)_{solvent}$ = 3.33 ± 0.09. I note that the equation above assumes that only a single proton is in motion in the transition state; the high fidelity of the fit suggests that this assumption is valid. The φ_{obs} , which is the inverse of the $^{D}(V/K)_{solvent}$ is 0.300 which too low for an equilibrium isotope effect with a single proton in motion, indicating that this isotope effect observed is likely a kinetic primary solvent isotope effect[96]. KIEs on V_{max} are observed only if the isotopically sensitive step is rate-determining under saturating substrate conditions, whereas the KIE on V_{max}/K_m represents the KIE determined at low substrate concentrations and reflected all steps up to and including the first irreversible step. The data, therefore, indicates that the steps that control V_{max}/K_m and V_{max} are different[96]. These results are an indication that protonation of the product is associated with a significant energetic barrier that occurs before the first irreversible rate-determining step of the reaction[96, 97]. As discussed below, these steps are likely associated with the resolution of the PrFMN-product adduct. This energetic barrier is unlikely the rate determining step that limits k_{cat}, as this would be inconsistent with the fact that the solvent KIE on V_{max} is unity and that secondary KIEs are normal rather than exhibiting an inverse KIE.

3.3.3 Secondary Kinetic Isotope Effects.

Secondary kinetic isotope effects report on changes in the hybridization of bonds adjacent to the site of the reaction and may be either normal or inverse. They are particularly informative for an examination of changes in the geometry of carbon atoms: the transition from tetrahedral to planar geometry is associated with a normal secondary KIE, whereas the transition from planar to tetrahedral geometry is associated with an inverse secondary KIE. To investigate the mechanism of the FDC1 reaction, secondary deuterium KIEs were measured at both the β -

and γ -positions of phenylacrylic acid in both D_2O and H_2O buffers (the commercially available γ -deuterated phenyl acrylic acid was also deuterated on the phenyl ring; the remote isotope was assumed not to influence the KIE at the γ -position). KIEs were determined at 25 ºC in 100 mM sodium citrate buffer (pL = 6.5) by a direct comparison of reaction rates at low substrate concentrations relative to K_M so that the measurements represent KIEs on V_{max}/K_M(Table 3.3)[97].

In H_2O, no apparent 2º KIE was observed at the β -position, whereas at the γ -position a large, normal 2º KIE was measured ($2^{o D}V/K$ γ H_2O = 1.10 ± 0.03; n = 9). In contrast, in D_2O the apparent 2º KIE at the β -position became significantly ($2^{o\ D}V/K_{\alpha}$ = 1.12 ± 0.03; n = 9). When the KIE were measured in deuterium oxide, the 2º KIE at the β-position was suppressed and was unity within error. When deuterated phenylacrylic acid was the substrate, large 2º KIE were measured in both H_2O and D_2O. The fact that these KIEs are normal indicates that they both arise from the rehybridization of the β and γ -carbons from tetrahedral to planar geometry during the reaction[74, 96, 97].

The secondary KIEs measured for FDC1 provide further evidence that a chemical step, rather than a substrate bidding or product release step, is rate determining. Normal 2º KIEs are observed α- and β-position of phenyl acrylate, although they are solvent dependent which complicates their interpretation. Normal 2º isotope effects are indicative of a change of geometry at the carbon atoms from tetrahedral to planar, which supports the formation of the styrene bond in the final cyclo-elimination reactions. The change in the apparent 2º KIEs observed when the reaction is performed in D_2O is unusual but may be explained by the fact that, when the β -carbon undergoes rehybridization, it contains additional deuterium from the solvent.

This will introduce a cryptic 2 º KIE at a carbon that could mask the 2º KIE at the β-carbon. Along those same lines, this additional deuterium atom would explain the further increase in 2º KIE when the β, γ -deuterated substrates are used. This normal solvent selective 2 KIE further suggests that the 1,3 cyclo-elimination reaction occurs in a concerted but asynchronous reaction.

Table 3.3 Summary of secondary kinetic isotope effects measured for the FDC1-catalyzed decarboxylation of deuterated phenylacrylic acids in H_2O and D_2O

Deuterium position	2^o $^DV/K$ (H_2O)	2^o $^DV/K$ (D_2O)
C- β	0.99 ± 0.02	1.12 ± 0.030
C- γ	1.10 ± 0.016	1.01 ± 0.027
C- β and C- γ	1.15 ± 0.017	1.32 ± 0.035

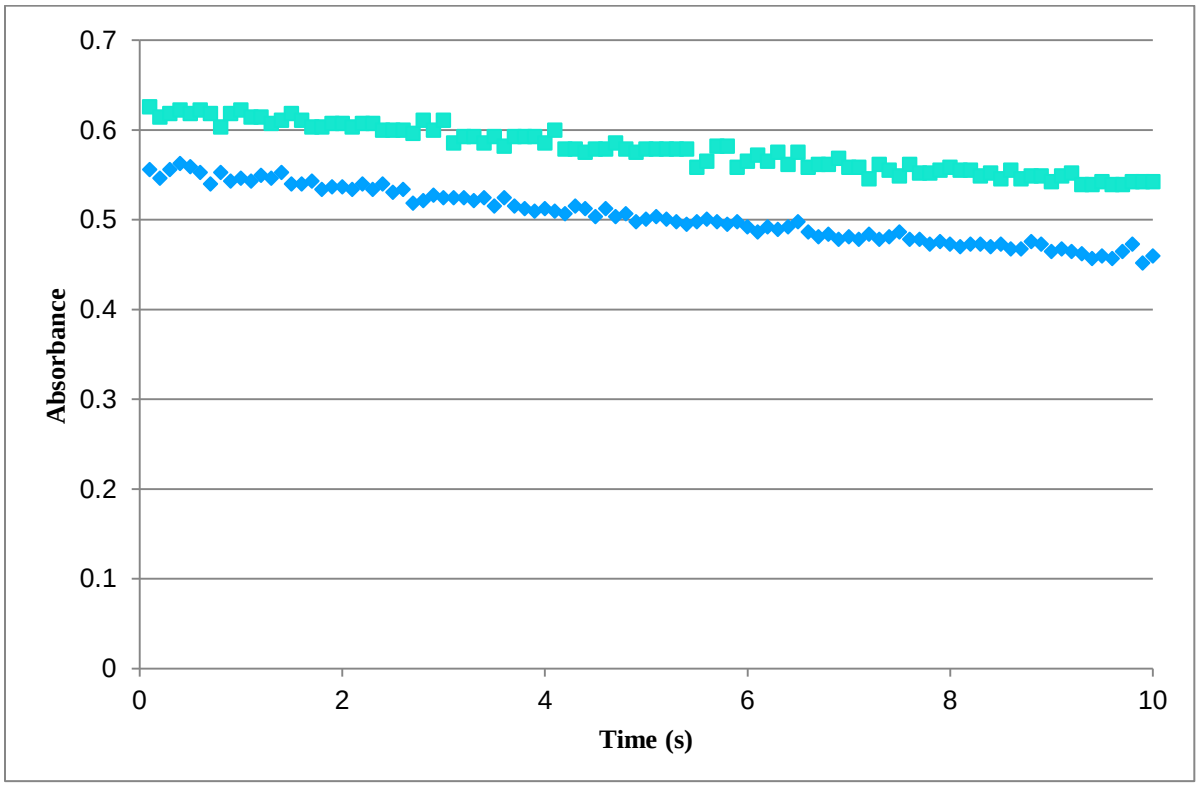

Figure 3.6 Representative curves for the secondary isotope effect assay with the teal squares being deuterated β, γ Cinnamic acid with blue diamonds representing TCA

3.3.4. Deuterium Exchange into Styrene.

The decarboxylation catalyzed by FDC1 can be driven in the reverse direction in the presence of styrene and a high concentration of bicarbonate. I used the reversibility of the reaction to examine the requirements for proton transfer between Glu285 and the substrate. Reaction mixtures were set up in citrate-buffered D_2O solutions containing 2 mM styrene that were either purged of dissolved CO_2 or supplemented with 20 mM $KHCO_3$. We monitored the exchange of deuterium into styrene using ^1H NMR by following the disappearance of the resonance at 5.20 ppm. The stereospecificity with which deuterium is incorporated in styrene is consistent with the α-carbon of the substrate. If the α-carbon was free to rotate about the Cα-Cβ bond that would have resulted in scrambling in the isotope. The experiment resulted in a sole simplification of the signal at 5.75 ppm due to the cis-C1 hydrogen from a doublet of doublets to a doublet together with a slight upfield isotope induced chemical shift.

In carbonate deficient systems, little to no exchange of the deuterium was observed (Figure 3.6), whereas the addition of potassium bicarbonate resulted in deuterium exchange into styrene occurring at a rapid rate with an apparent rate constant app of ~1.5 min^{-1}. This result demonstrates that CO_2 must be present in the active site for protonation/deprotonation of the styrene-PrFMN adduct to occur. This implies that the dissociation of CO_2 does not occur until after the product is protonated when the reaction proceeds in the decarboxylation direction.

The deuterium exchange into styrene occurred quite rapidly with an apparent rate constant app of 1.5 min^{-1}. This incorporation of deuterium exchange occurred much more rapidly than the rate of carboxylation, as previously, of which takes multiple hours to undergo one turnover.

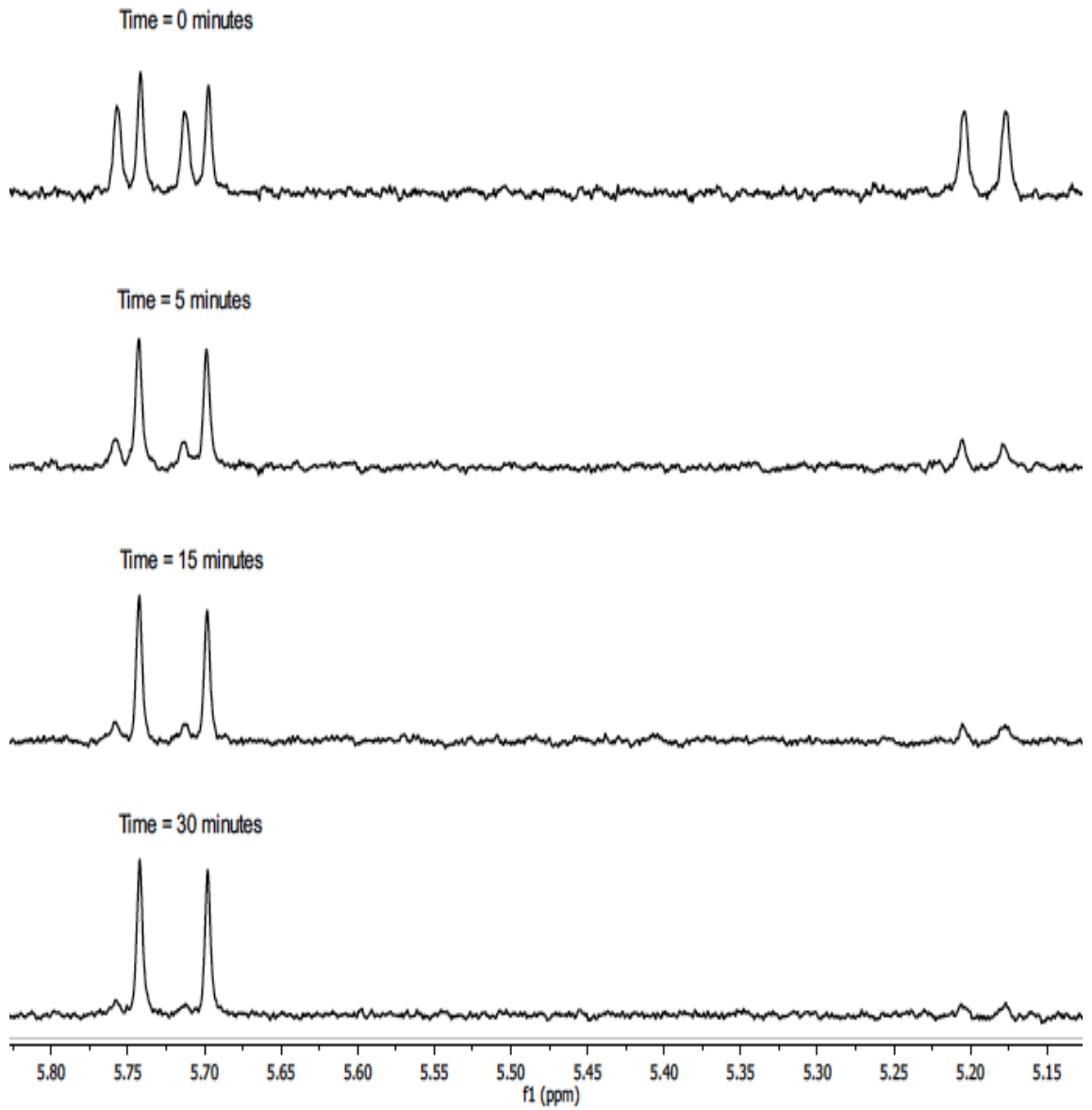

Time = 30 minutes No HCO_3^-

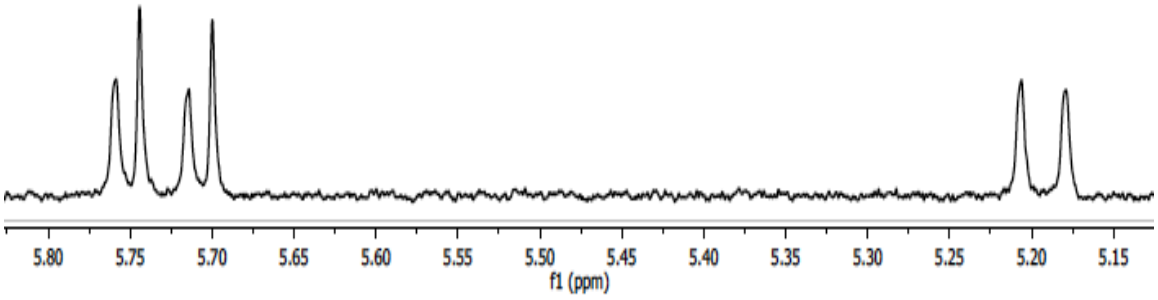

Figure 3.7 FDC-catalyzes deuterium exchanged into styrene in the presence of HCO_3^-. ^{1}H NMR spectra were recorded at 500 MHz at between 0 and 30 minutes after addition of FDC1. The bottom spectrum was recorded under the same conditions in the absence of HCO_3^-.

3.4. Conclusion

The novel isopentenyl modification of FMN converts a cofactor generally associated with redox reactions into one that supports decarboxylation. The proposed mechanism involving a 1,3-dipolar cyclo-addition of PrFMN with phenylacrylic acid seems plausible, as the prenylation of the flavin introduces functionality into the cofactor which is expected to have a ylide character similar to that of an azomethine ylide (Figure 3.8). The kinetic experiments described in this chapter provide some insight into the reaction mechanism and the rate determining step of the reaction. The results do not definitively rule out the previously considered mechanism which a Michael addition of PrFMN to phenylacrylic acid facilitates decarboxylation.

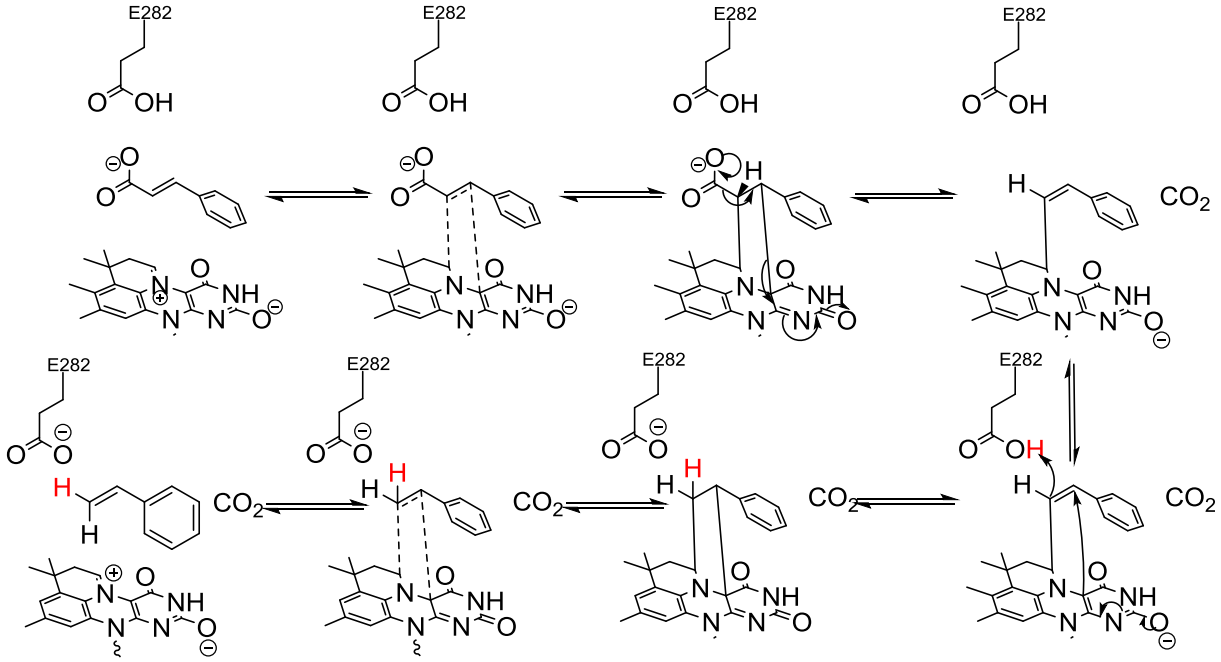

Figure 3.8 Proposed mechanism for the FDC-catalyzed decarboxylation of phenylacrylic acid involving a 1,3 dipolar cycloaddition to the PrFMN cofactor

In light of the experiments presented above, the proposed Michael addition mechanism is less likely. The normal 2º KIE indicates the rate-determining step would show that rehybridization of the β, γ bonds which would accompany decarboxylation would be rate limiting. These results

are inconsistent with the negative ρ found in the Hammett analysis which suggests that decarboxylation is rate limiting.

These results are mostly consistent with the proposed 1,3-dipolar cycloaddition mechanism. However there are some key differences between the previously proposed mechanism and the mechanism supported by these experiments[51]. First the carbon dioxide does not seem to leave the active site during the course of the reaction, secondly the resolution of the PrFMN-product adduct seems to occur in an asymmetric manner, which is contrary to the previously described mechanism. The Hammett analysis and the secondary isotope effect suggest that the rate-determining step in the 1,3 dipolar cycloaddition mechanism is the resolution of the product-PrFMN adduct through a cyclo-elimination reaction. This step would result in a build-up in positive charge in the rate-determining transition state as well as the rehybridization of α, β carbon of styrene from tetrahedral to planer geometry. However, no direct evidence exists for the formation of these intermediates. The substrate reactivity patterns and the kinetic analysis presented here are possibly useful in guiding efforts to engineer FDC1 towards alternative substrates and greater catalytic efficiency.

Chapter 4

Mass spectrometry, Mutants, and U.V.-Visible spectrometry Analysis of Mechanistically Relevant Intermediates Using a Substrate Analog and Styrene

The work described in this chapter has been partly published as Ferguson, K.L., Eschweiler, J., Rutolo, B., Marsh, E. N. G. (2017) Evidence for the 1,3-Dipolar Cycloaddition Mechanism in the decarboxylation of Phenylacrylic Acids Catalyzed by Ferulic Acid Decarboxylase. Journal of the American Chemical Society, 139, 10972-10975. K.L. Ferguson designed and performed experiments relating to the inhibition of FDC1 by FNVB, and analyzed the results. K.L. Ferguson and J. Eschweiler designed and analyzed the results of the Native Mass Spectrometry experiments. J. Eschweiler solely performed all mass spectrometry experiments and provided computational support for the data provided. K.L. Ferguson, J. Eschweiler, B. Ruotolo, and E.N.G. Marsh wrote the manuscript.

4.1 Introduction

The mechanism by which FDC1 catalyzes the decarboxylation of phenylacrylic acids remains unsettled. Based on the crystal structure of FDC1 reacted with phenylpyruvate, as well as the data described in the previous chapters, it is proposed that the decarboxylation of phenylacrylic acids involves a novel 1,3 dipolar cycloaddition mechanism. Decarboxylation then occurs by a Grob-type elimination of carbon dioxide in which the flavin acts as an electron sink (Figure 4.1). Protonation of this intermediate by active site glutamate residue yields a

styrene-PrFMN adduct that then undergoes a cyclo-elimination to release the product and reform the PrFMN[48, 83-86].

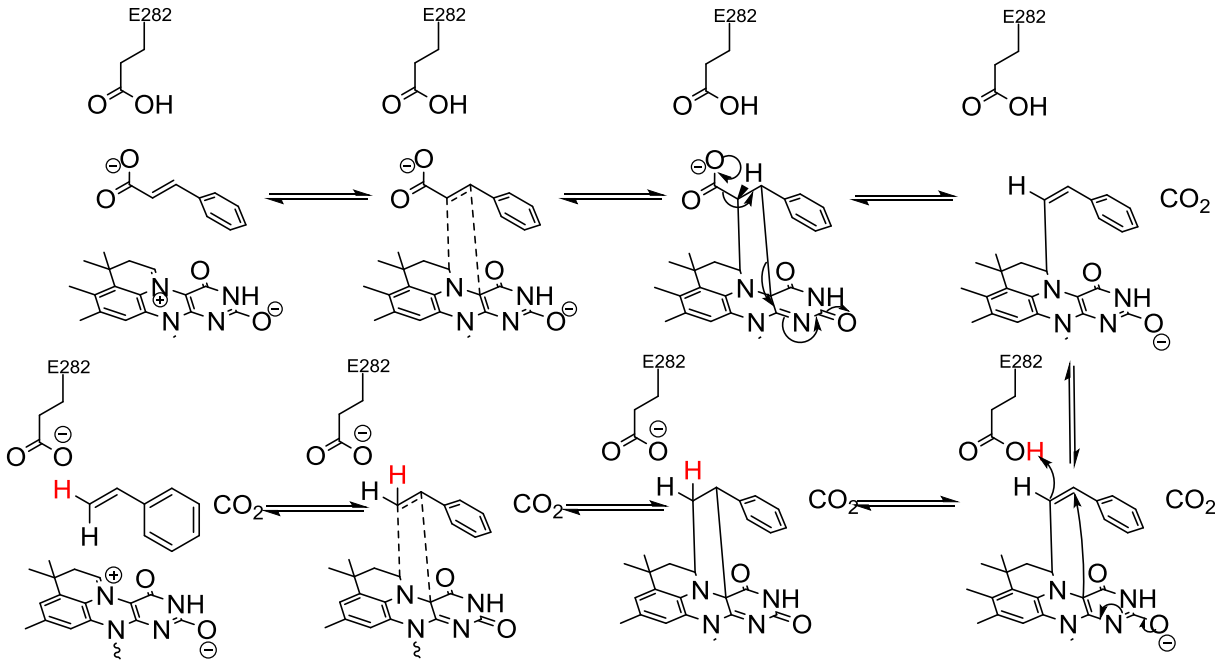

Figure 4.1 Proposed mechanism for the FDC-catalyzed decarboxylation of phenylacrylic acid involving a 1,3 dipolar cycloaddition to the PrFMN cofactor

The basis for this 1,3-dipolar cycloaddition mechanism is the azomethiline ylide functionality that the PrFMN contains, as nitrogen ylides are well known to undergo 1,3 dipolar cycloaddition reactions; however, ylides are also intrinsically nucleophilic[98, 99]. The cycloaddition mechanism of ylides are well known and well characterized in synthetic chemistry[98, 99]. The reaction is dominated by the interaction of the highest occupied molecular orbital (HOMO) of the ylide and the lowest unoccupied molecular orbital of the dienophile. It is possible to react FDC with a substrate analog with a low energy LUMO that would undergo a pericyclic reaction and form a stable intermediate that would allow for characterization[100].

Substrate analogs that function as mechanism based inhibitor of enzymes have proven to be a potent tool to uncover intermediates in enzyme reactions[101]. (Z)-2-Fluoro-2-nitro-

vinylbenzene (FNVB) was a promising candidate, as the nitro group, a strong electron-withdrawing group, and an excellent isostere for a carboxylate group, and fluorine is also electronegative group and a good isostere for hydrogen[101-104].

Another method to trap mechanistically relevant intermediates is to utilize low activity mutants of an enzyme that accumulate mechanistic intermediates. Several low activity mutants of the FDC1 homolog in *A. niger*, already were analyzed about their activity. R173A, E277Q, and E282Q were all previously found to be inactive. These inactive mutants have analogous residues in FDC1 in *S. cerevisiae* at Glu285, Glu 279, and Arg175. Previous work hypothesizes that the Glu282 is responsible for the protonation of the intermediate complex (Figure 4.1) that leads to the generation of styrene and the reformation of the PrFMN cofactor. No explanation was offered for the other two mutants being inactive, other than to suggest that these mutants change the U.V.-visible spectrum of the enzyme and thus may affect either the local cofactor environment, the relative concentration of the cofactor, or how the cofactor matures[80]. Mutating Glu285 to alanine would possibly arrest the reaction before the protonation step, thereby allow for isolation and characterization of the initial 1,3 dipolar cycloadduct by tandem mass spectrometry and monitoring its formation by spectroscopy[51, 86].

FDC1 is well characterized as a reversible decarboxylase that readily complexes with styrene with a high concentration of bicarbonate. Previously described work in chapter 2 suggests that the proton exchange in the reverse reaction occurs with a rate of 1.4 min^{-1}. Thus if PrFMN readily forms the product-PrFMN adduct with a high concentration of bicarbonate making it possible to isolate and characterize these adducts by tandem mass spectrometry. FDC1 reacted with styrene and its d_7-styrene analog and employing tandem mass spectrometry it might be possible to isolate a PrFMN-product intermediate.

In this chapter, I describe a series experiments monitoring the interaction of the PrFMN and the proposed FNVB substrate analog. Also, I collaborated with the Ruotolo lab here at the University of Michigan to probe FDC1 by native MS and to look for covalently modified PrFMN adducts including; Styrene-PrFMN, d_7-Styrene-PrFMN, FNVB-PrFMN. Finally, I performed mutagenesis on the Glu285 and Arg175 to slow the protonation step of the forward reaction and explore why these mutations limit the reactivity of the enzyme.

4.2. Materials and Methods

4.2.1. Materials

Trans-cinnamic acid was purchased from Across Organic, and 2-fluoro-2-nitro-vinylbenzene was purchased from Spirochem, Zurich. All other reagents were purchased from Sigma Aldrich Co and were of the highest grade commercially available. WT FDC1 from *S. cerevisiae* was purified as previously described in chapter 2 section 2.2.2 Invitrogen provided XL10-gold cells. His-Trap HP (5 mL) Ni-affinity column was obtained from GE Healthcare. The QuikChange lighting kit and all materials associated materials were obtained from Agilent.

4.2.2. Site-directed Mutagenesis

E285A, E285Q, R175A, and R175K primers were designed using the QuikChange Primer Design tool, courtesy of Agilent and ordered from IDT technologies. PCR reactions for the mutants were then performed according to the QuikChange Lightning Site-Directed Mutagenesis Kit. The reaction mixtures contain 5 µL 10x reaction buffer, 100 ng of the dsDNA template, 1 µL of dNTP mix, 1.5 µL of quick solution reagent, 125 ng of the forward and reverse primer, and finally enough nuclease-free water to increase the reaction volume to 50

µL. The initiation of the PCR reaction followed the addition of µL of the QuikChange Lighting Enzyme.

A three-step PCR was run with an initial denaturing step at 95 ºC for two minutes, followed by 18 cycles of 95 ºC for 20 seconds, 60 ºC for 10 seconds, and then an elongation step of 68 ºC for 5 minutes. The final elongation step consisted of holding the PCR reaction at 68 ºC for 5 minutes. The parent plasmid template in the PCR mixture was then digested with 1 µL of DpnI, 1x NEB cutsmart buffer, and enough DNAse free water to bring the total reaction volume to 50 µL at 37 ºC for 2 hrs. The mutant plasmid chemical competent XL-10 gold cells.

The XL-10 gold cells were pre-chilled into 1.5-mL polypropylene round-bottom tube on ice. 100 µL of cells was placed into the pre-chilled tubes, and 4 µL of beta-mercaptoethanol mix provided by the XL-10 gold kit were aliquoted into the cells. The cells were incubated on ice for 10 minutes; the cells were swirled gently every 2 minutes. 2 µL of the DNA mixture was added to the chilled cells. The DNA and cells were incubated then incubated on ice for 30 minutes. The cells were then heat-pulsed in the tubes in a 42 ºC water bath for 30 seconds. The cells were then allowed to rest on ice for 2 minutes. 450 µL of SOC media was then added to the cells, and the cells could rest in an incubator at 37 ºC for 1 hr with gentle rocking. The cells were then plated on kanamycin resistant agar. Colonies were picked for overnight growth, and their DNA was purified and verified by sequencing. Alignments to identify successful mutant were performed with Codon Aligner. Mutant plasmids were then transformed into BL21(DE3) star cell lines for protein expression.

The BL21 (DE3) star OneShot cells were thawed gently on ice per *trans*formation. 250 ng of DNA was added to 50 µL of cells and allowed to incubate on ice for 30 minutes gently agitating the solution every 2 minutes. The cells were then heat shocked for

30 seconds in a 42 ºC water bath for 30 seconds. 450 µL of SOC media was then added to the cells, and the cells could rest in an incubator at 37 ºC for 1 hr with gentle rocking. The mutant cells were then plated on kanamycin resistant agar plates.

4.2.3. U.V.-Visible Assay between FDC1 & FDC1 Mutants and FNVB

The reaction of FDC1 with 2-fluoro-2-nitrovinylbezene (FNVB) was performed in 100 mM citrate buffer (pH 6.25) containing 10% glycerol at 25 ºC. A stock solution of FNVB (Spirochem, Zurich) was prepared in DMSO and diluted into the reaction buffer at various initial concentrations between 5 and 25 µM. Reactions were initiated by addition of FDC1 to a final concentration 5 µM. The reaction was followed spectrophotometrically by monitoring the decrease in absorbance at 326 nm assuming an extinction coefficient of 13,700 $M^{-1}cm^{-1}$. Typically, measurements were made over a period of 10 minutes with time points being taken every 10 seconds. Assays were done in triplicate to establish statistical significance.

4.2.4. U.V.-Visible Time Course Assay of the Reaction between FNVB and WT FDC1

Assays were performed on a Hewlett Packard 8542 spectrophotometer. The reaction of FDC1 with 2-fluoro-2-nitrovinylbezene (FNVB) was performed in 100 mM citrate buffer (pH 6.25) containing 10 % glycerol at 25 ºC. A stock solution of FNVB (Spirochem, Zurich) was prepared in DMSO and diluted into the reaction buffer at various initial concentrations between 5 and 25 µM. Reactions were initiated by addition of FDC1 to a final concentration 5 µM. The reaction was followed spectrophotometerometrically by monitoring the decrease in absorbance at 326 nm assuming an extinction coefficient of 13,700 $M^{-1}cm^{-1}$. Typically, measurements were

made over a period of 2 minutes with points taken every 4 seconds. Assays were done in triplicate to establish statistical significance

4.2.5. Mass Spectrometry of FDC1

100 µL samples containing FDC, 50 µM were reacted with FNVB, 50 µM, as described above for 10 min. Samples were buffer exchanged into 500 mM ammonium acetate buffer, pH 6.9 using two Micro Bio-Spin Columns (Bio-Rad, Hercules, CA). The final concentration of the buffer exchanged protein was 5-10 µM. Samples were analyzed under native MS conditions using a Synapt G2 ion mobility mass spectrometry platform (Waters Inc, Milford MA). The FDC1-FNVB native protein complex the capillary voltage was set to 1.5kV.

4.2.6. MS^2 Analysis of FDC1

Apo-FDC, holo-FDC, and FNVB incubated FDC were ionized using nanoelectrospray ionization. The initial instruments settings were set to minimize ion activation, thereby maintaining non-covalent interactions such that no significant signals were observed for free FMN-related peaks. The capillary voltage was set to 1.5 kV, and the sampling and extraction cones were set to 30 V and 0 V, respectively with the trap collision energy at 20 V.

For collision-induced dissociation experiments, the trap collision energy was raised to 100 V to dissociate the noncovalently-bound species including; FMN, PrFMN, and the FNVB-PrFMN adduct, giving rise to a series derived peaks at low m/z. Spectra were processed in Masslynx (Waters Inc, Milford MA).

4.2.7. Mass Spectrometry Analysis of R175A, R175K, E285A, E285Q Mutants

100 µL samples containing FDC1, 50 µM were reacted with FNVB, 50 µM, as described above for 10 min. Samples were buffer exchanged into 200 mM ammonium acetate buffer, pH 6 using two Micro Bio-Spin Columns (Bio-Rad, Hercules, CA) except the R175K mutant which was exchanged into a 200 mM ammonium acetate buffer, pH 8. The final concentration of the buffer exchanged protein was 5-10 µM. Samples were analyzed under native MS conditions using a Synapt G2 ion mobility mass spectrometry platform (Waters Inc, Milford MA). The FDC1-FNVB native protein complex the capillary voltage was set to 1.5 kV.

4.2.8. MS^2 Analysis of R175A, R175K, E285A, E285Q Mutants

R175A, R175K, E285A, E285Q FDC1 were ionized using nanoelectrospray ionization. The initial instruments settings were set to minimize ion activation, thereby maintaining non-covalent interactions such that no significant signals were observed for free FMN-related peaks. The capillary voltage was set to 1.5 kV, and the sampling and extraction cones were set to 30 V and 0 V, respectively with the trap collision energy at 20 V.

For collision-induced dissociation experiments, the trap collision energy was raised to 100 V to dissociate the noncovalently-bound species including; FMN, PrFMN, and the many other adducts, giving rise to a series derived peaks at low m/z. Spectra were processed in Masslynx (Waters Inc, Milford MA).

4.2.9. MS^2Analysis of Styrene-PrFMN Adduct

100 µL samples are containing FDC, 100 µM were reacted with styrene, and 200m M NH_4OAc pH 6.5, 100 µM, and 10 mM NH_4HCO_3 as described above for 10 min.

Samples were buffer exchanged into 200mM ammonium acetate buffer, pH 6.9 using two Micro Bio-Spin Columns (Bio-Rad, Hercules, CA). The final concentration of the buffer exchanged protein was 25 µM.

The FDC1 with the Styrene-PrFMN adduct was ionized using nanoelectrospray ionization. The initial instruments settings were set to minimize ion activation, thereby maintaining non-covalent interactions such that no significant signals were observed for free FMN-related peaks. The capillary voltage was set to 1.5kV, and the sampling and extraction cones were set to 30V and 0V, respectively with the trap collision energy at 20 V. For CID experiments, the trap collision energy was raised to 100 V to dissociate the noncovalently-bound FNVB-PrFMN adduct, giving rise to a series of Styrene-PrFMN derived peaks at low m/z. Spectra were processed in Masslynx (Waters Inc, Milford MA)[54].

4.3. Results

4.3.1. Mass Spectra Analysis of holo-FDC1, apo-FDC1, and FNVB Bound FDC1

Native mass spectra are shown in Figure 4.2, of apo-FDC1, holo-FDC1, and FNVB incubated FDC1 electron sprayed under physiological-pH conditions (500 mM ammonium acetate, pH 6.9). FDC1 is a dimer species. FDC1 in the apo form presents a variety of charge states ranging from $[2M+19H]^{19+}$ to $[2M+24H]^{24+}$, with the $[2M+21H]^{21+}$ being the most intense mass charge peak. FDC1 in the holo form and with FNVB bound exhibits narrower range of charges from $[2M+19H]^{19+}$ to $[2M+22H]^{22+}$. However, for holo-FDC the most intense peak is +20 species, bound enzymes however exhibit the most intense charge peak at +21. This data is consistent with all other previous MS investigations of FDC1[55].

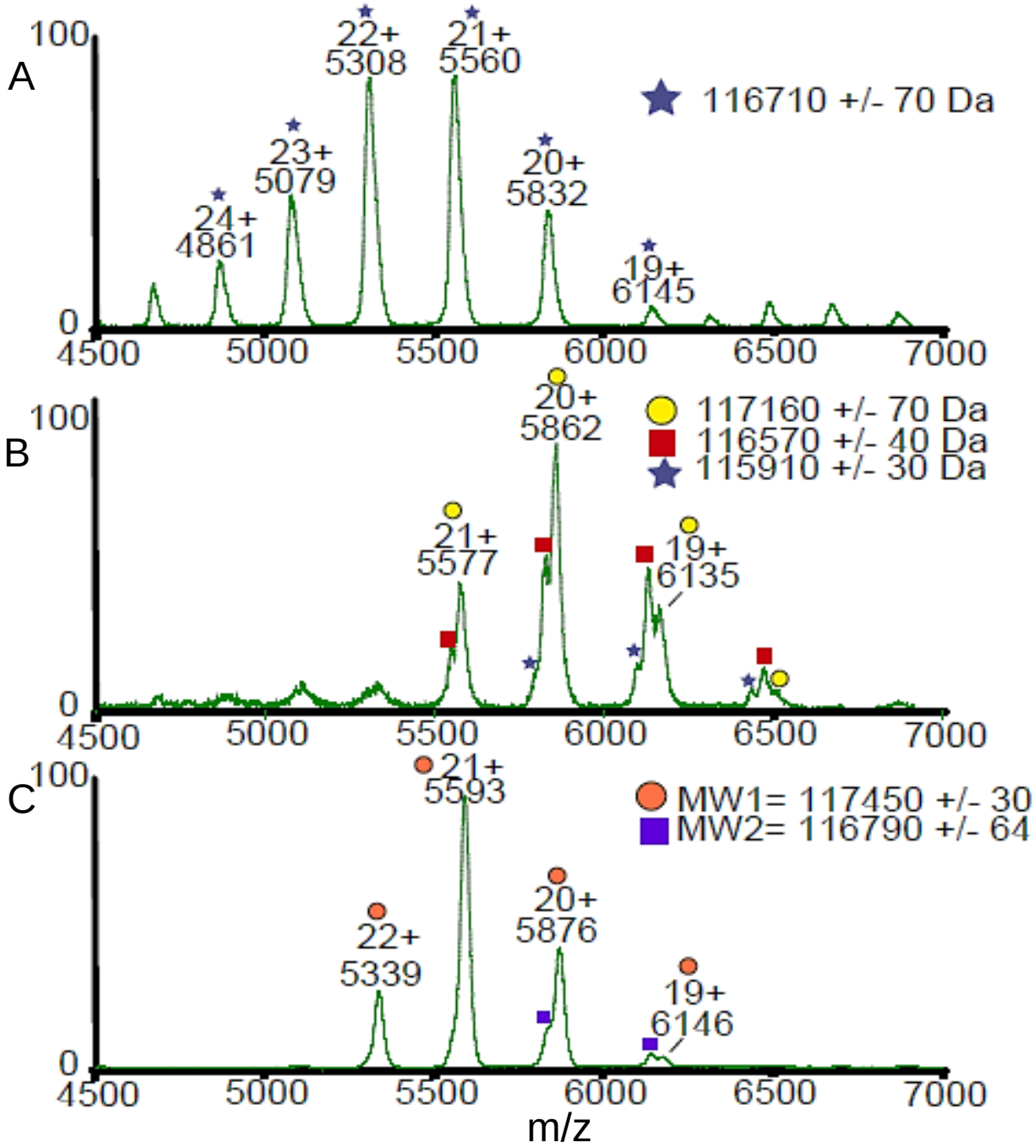

Figure 4.2 (A) Native mass spectrum of the apo-FDC1. (B) Native mass spectrum of the holo-FDC1. (C) Native mass spectrum of holo-FDC1 incubated with FNVB

The holo-FDC1 spectrum in Figure 4.2 arises predominantly form protein dimers with two non-covalently bound cofactors, with approximately a third of the total ion intensity attributed to the protein with one non-covalently bound cofactor and just a small amount of protein, is observed without any cofactor. In contrast upon the addition of the FNVB, the apo-protein is essentially absent, and the doubly occupied accounts almost all of protein species observed.

The mass of the inhibitor bound FDC1 is larger than the mass of the doubly bound holo-FDC1 by 290 daltons, which is 44 daltons lower than that of the mass that would result from 2 inhibitor molecules being directly bound to holo-FDC1. The mass difference between the singly inhibitor bound and doubly inhibitor bound holo-FDC1 is 660 daltons, which is 32 daltons less than the predicted mass of the PrFMN-Inhibitor complex of 692 daltons.

4.3.2 MS^2 Analysis of holo-FDC1, apo-FDC1, and FNVB Bound holo-FDC1

Native tandem mass spectrometry of apo-FDC1, holo-FDC1, and inhibitor-bound holo-FDC1 allowed for the dissociation of non-covalently bound species from the enzyme. Apo-FDC1 exhibited a dominant peak at m/z 457.143 $[M+H]^+$, representing FMN which has been shown to bind to FDC1 lacking the PrFMN cofactor species. The holo-FDC1 exhibits a dominant peak at 525.17 $[M+H]^+$ as well as a peak at 563.17 due to the potassium adduct $[M+K]^+$. The potassium adduct may form the potassium ion found to be in the active site of FDC1, as the buffers all lack potassium, indicating that the PrFMN is indeed dissociating from the active site of FDC1. The inhibitor FDC1 complex exhibits several unique peaks in addition to the familiar m/z peaks of 525.175 and 563.17. The unique m/z peak of 730.167 is the ion with the highest intensity and corresponds the mass of the inhibitor-PrFMN cycloadduct complexed to a potassium ion. The other unique mass ion peaks at 683.189 and 645.227 are either likely

breakdown products associated with the inhibitor-PrFMN cycloadduct complex or small mass peaks intrinsic to the protein. The 645.227 and 683.189 peaks could match the previously described phenylaldehyde-PrFMN protonium adduct and the corresponding potassium adduct[51].

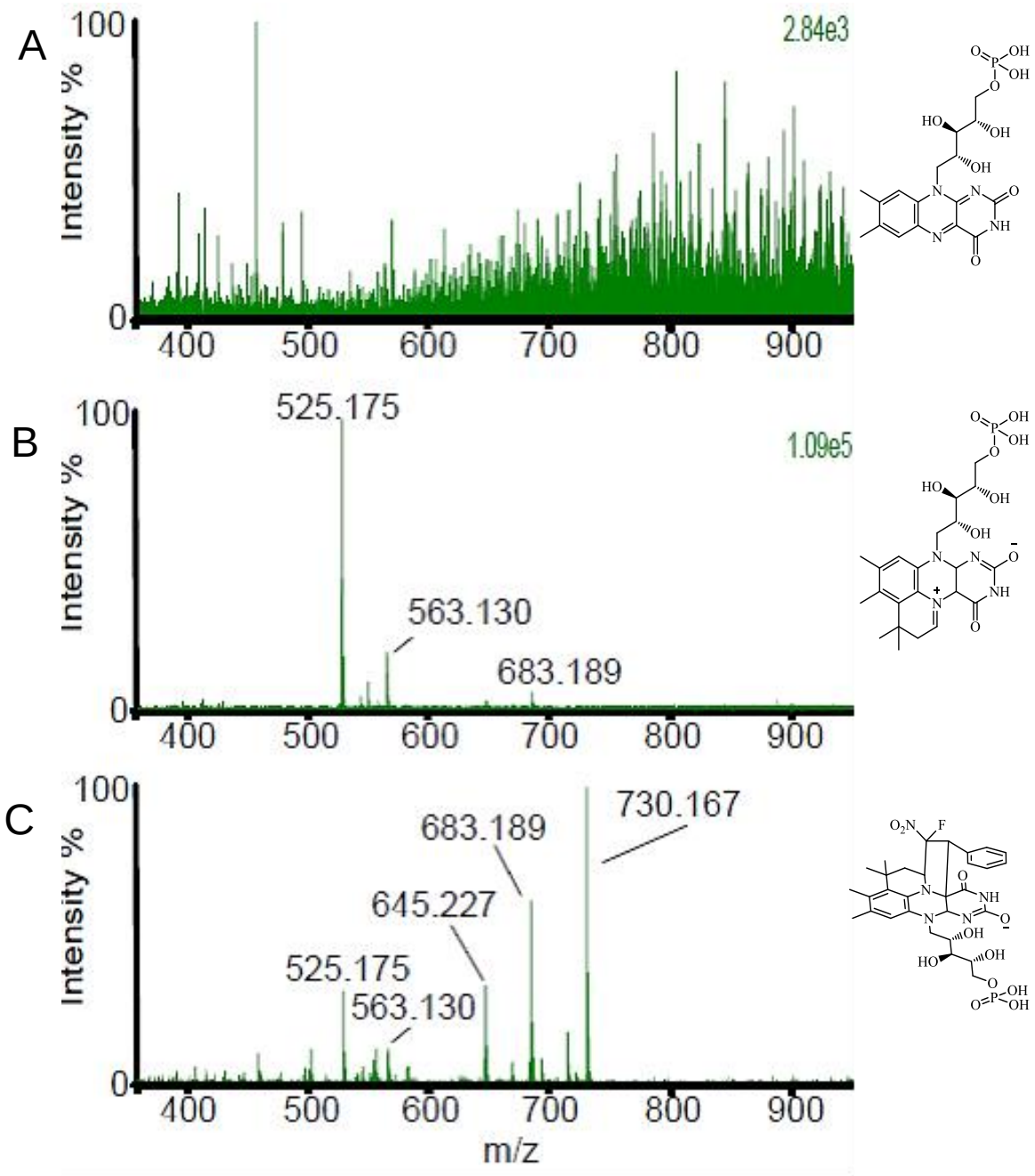

Figure 4.3 (A) Tandem mass spectrum of apo-FDC1 (B) tandem mass spectrum of holo-FDC1 (C) tandem mass spectrum of holo-FDC1 incubated with FNVB

4.3.3 MS^2Analysis of holo-FDC1 Reacted with Bicarbonate and H_8 & D_8 Styrene

The reversible nature of FDC1 along with the gentle nature of tandem mass spectrometry allowed for the identification of product-PrFMN adducts formed during the reverse reaction. The styrene-incubated FDC1 exhibited unique peaks which represent the PrFMN-styrene complex with a mass of 629.258 $[M+H]^+$ and 667.218 $[M+K]^+$. The d_8 styrene exhibited unique peaks which represent the d8-PrFMN-Styrene complex with a mass of 636.271 $[M+H]^+$ and 674.247 $[M+K]^+$ which represents a 7-dalton shift. The terminal *trans*-hydrogen of styrene was previously shown to readily exchange with the surrounding solvent, which explains why there is only a 7 Da shift instead of the expected 8 Da shift.

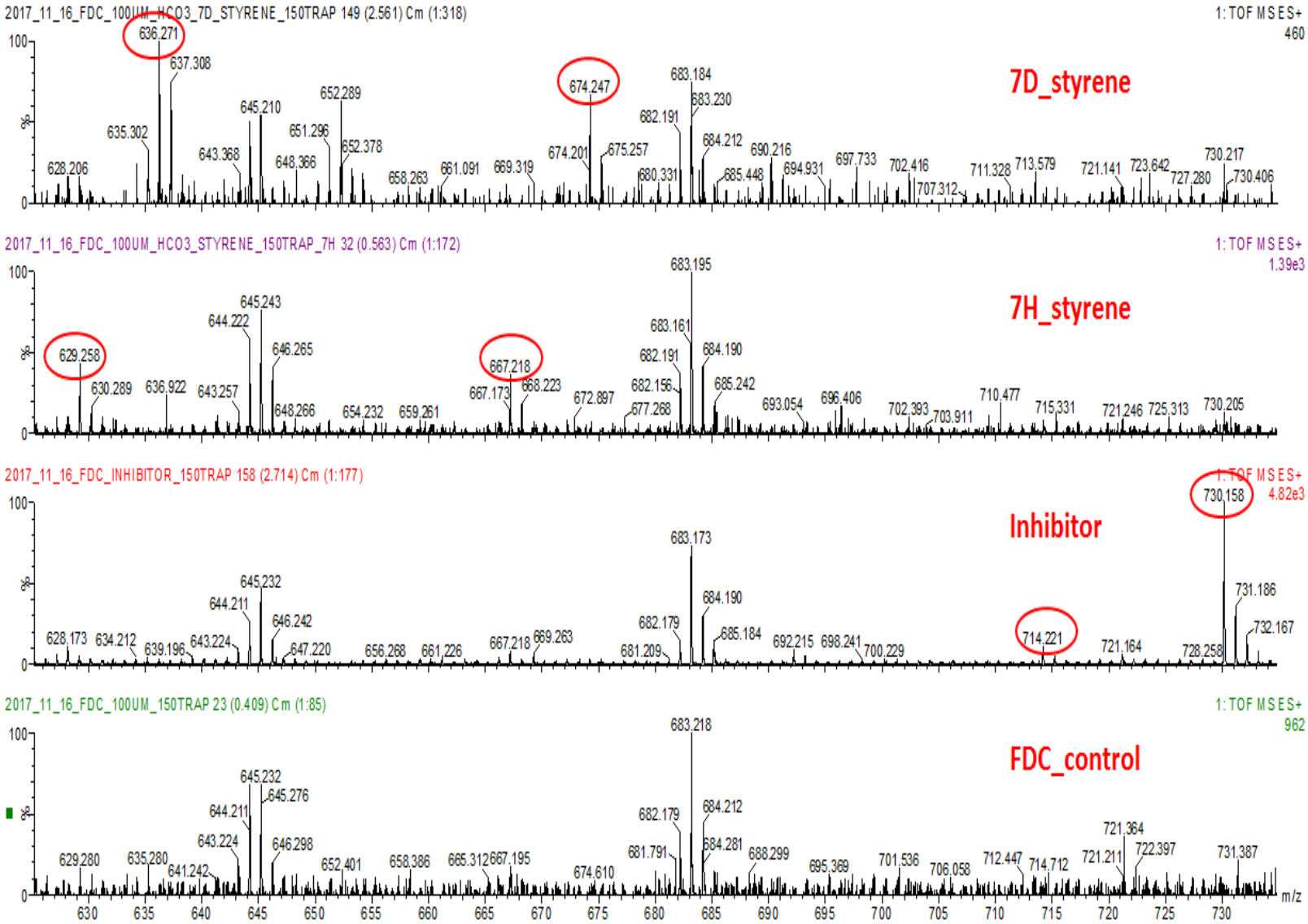

Figure 4.4 MS^2 of FDC1 incubated with d8-styrene, styrene, FDC1 incubated FNVB, holo-FDC1

4.3.4 U.V.-Visible Analysis of holo-FDC1 Reacted with FNVB

When holo-FDC1 reacts with FNVB the U. V. –visible spectrum exhibits a decrease in absorbance at 326 nm while generating a new absorbance band centered on 425 nm. The decrease in the absorption occurring at 326 nm is characteristic of disruption of the extended pi-system that is characteristic of FNVB. Additionally, a new weaker absorption band centered at 440 nm appears[54, 80, 105-107].

Flavins possess rich and informative electronic spectra that are indicative of both redox and protonation states and are sensitive to changes in the substitution pattern of the isoalloxazine ring system[105]. U.V.-Visible spectra have been characterized for both C4α, N5-dialkyl flavins and N5-alkyl flavinium cations, which correspond to the reaction of FNVB with PrFMN by either cyclo-addition or Michael addition mechanisms. C4α, N5-dialkyl flavins have a characteristic absorbance at ~400 nm that is sensitive to the electronic properties of other substituents on the complex. In contrast, the N5-alkyl flavinium cation is characterized by strong absorption bands at 350 and 550 nm. The spectrum of the PrFMN-FNVB product, with its broad absorbance band at 425 nm, is indicative of the formation of a cycloadduct, rather than a Michael addition adduct.

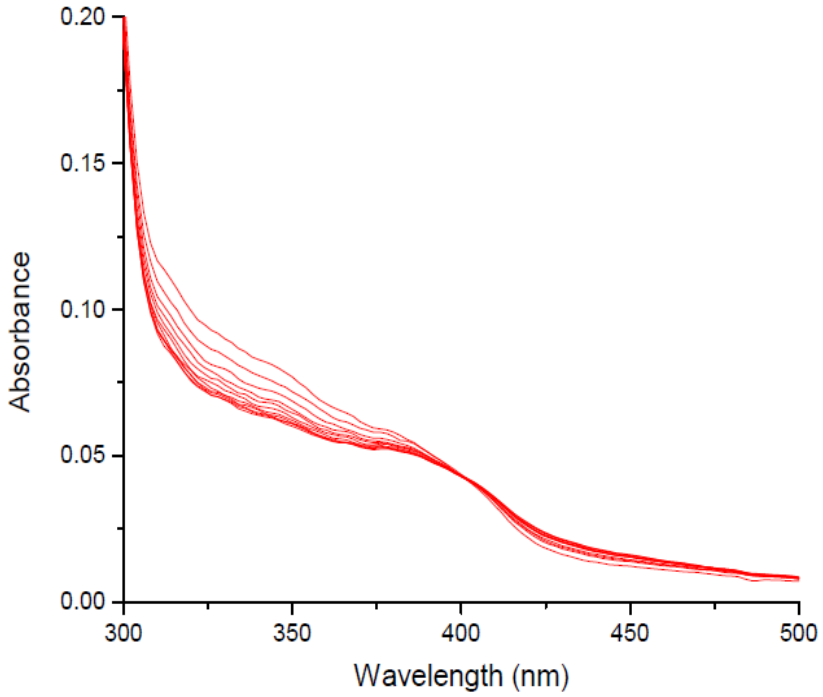

Figure 4.5 FDC1 incubated with FNVB over the course of 2 minutes

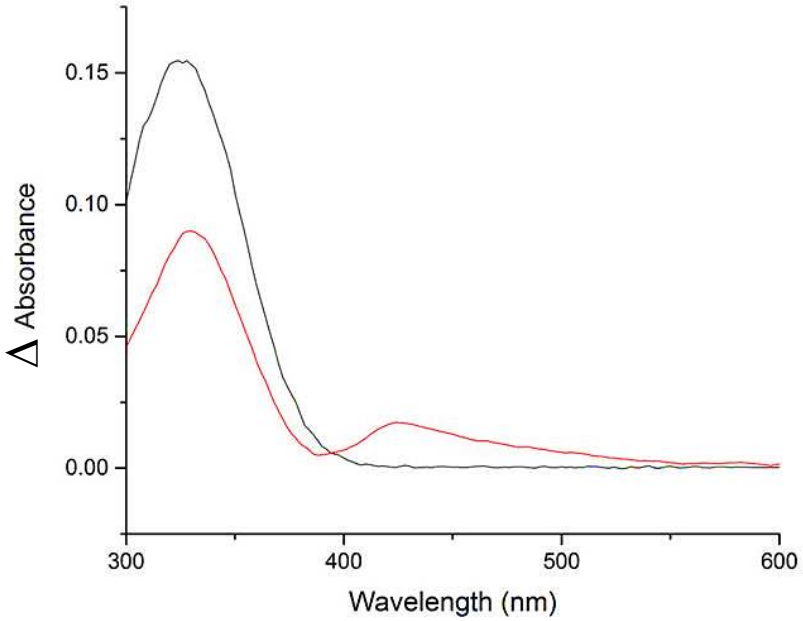

Figure 4.6 Time dependent difference spectra between FDC1 incubated with FNVB and FDC1 at spectra time equals 0 and time equals 2 minutes

4.3.5. Inhibition Rate of Holo-FDC1 Reacted with FNVB

FNVB was reacted with 5 µM of FDC1 and the decrease at 326 nm was fit to a first-order kinetic model, as this reaction results in a dead end enzyme-inhibitor complex. The reaction rate was 0.64 ± 0.04 min^{-1}. FNVB was shown to be a potent inhibitor, as the reaction rate was independent of FNVB concentration within the ability to measure the reaction. These observations indicate that the observed rate constant represents the true rate constant of a chemical step representing the reaction between FNVB and PrFMN rather than FNVB binding to the enzyme.

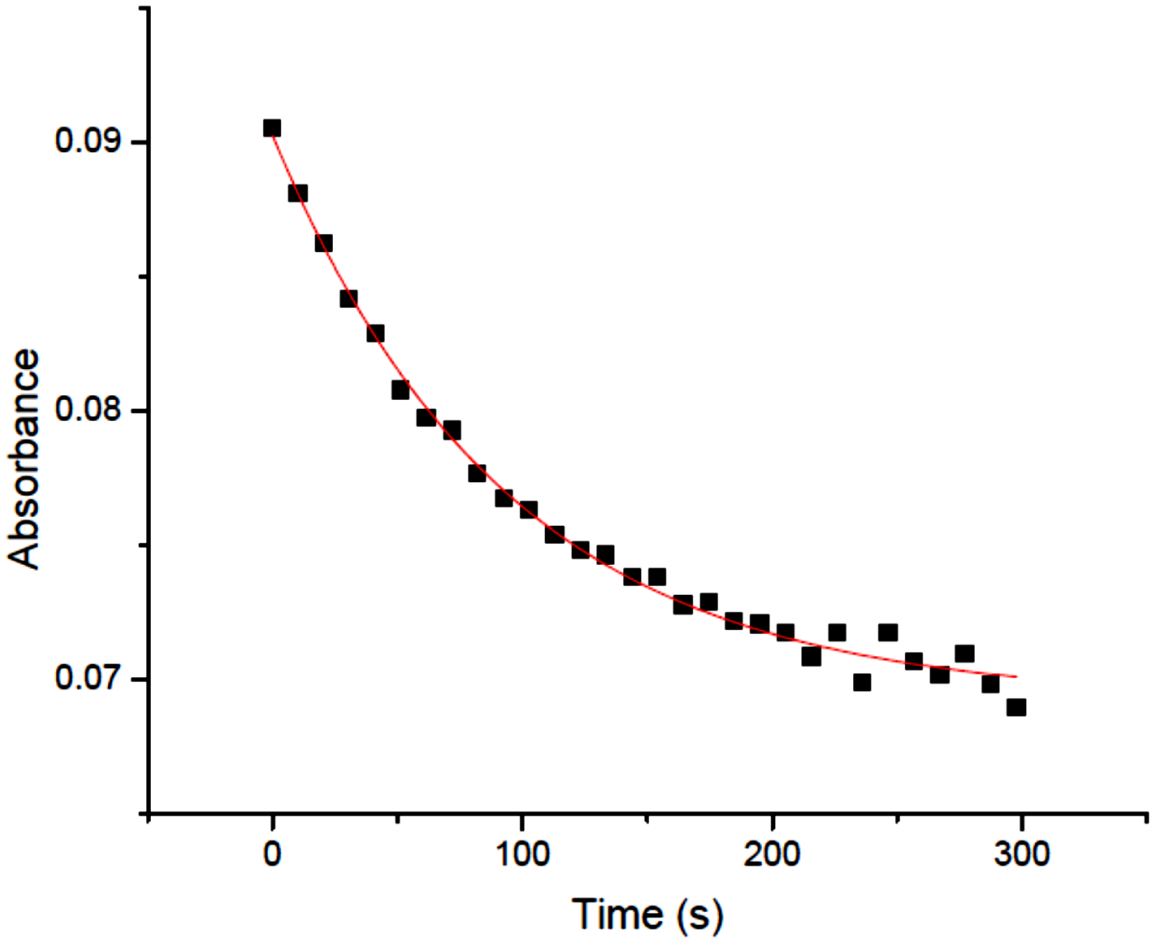

Figure 4.7 Time dependent spectrum of FDC1 incubated with FNVB at 325nm

4.3.6 Mutagenesis

Based on the analysis of the crystal structure and previous mutagenesis work [51, 57] two amino acids in the active site were chosen to be mutated: E285 and R175. E285 has previously been proposed as general acid in the FDC1 catalytic cycle, and thus mutating out E285 should slow the reaction, hopefully revealing mechanistic intermediates before the protonation step through either U.V.-Visible spectroscopy or tandem mass spectrometry. The other candidate was R175, as previously established alanine scanning mutagenesis suggested that this residue was responsible for both cofactor binding and maturation[57]. These mutants exhibited considerably less activity, together with altered U.V.-visible spectra, and new tandem mass spectrum peaks compared to the wildtype enzyme.

4.3.7. Spectroscopic Characteristics of the R175A, R175K, E285A, E285Q Mutants

These amino acids have previously been described, but there was only limited information on how these mutations affect the spectra of the PrFMN[51]. The R175A and R175K mutants both exhibited weak spectral features[51]. One explanation for this is that Arg175 is responsible for binding the cofactor to FDC1, thus mutating Arg175 to alanine or a more flexible lysine prevents the cofactor to binding. A second hypothesis postulated by Bailey et al. 2017 is that arginine 175 plays a role in the oxidative maturation of the reduced PrFMN to the active immine oxidized PrFMN[57].

4.3.8. Activity of the R175A, R175K, E285A, E285Q Mutants with TCA and FNVB

Active site mutants R175A, R175K, E285A, E285Q, exhibited a considerable decrease in activity. E285A and E285Q exhibited no discernable activity. This reduction in activity is

consistent with previous results that postulate that the replacement of the E285 with an alanine or a glutamine mutation removes the general acid responsible for the protonation of the product [57]. The E285A did not bind FNVB, which readily outcompetes the native substrate to bind and inactivate FDC. One possibility is that on the E285 residue plays a role in stabilizing the interaction between the PrFMN and the inhibitor. E285Q did not exhibit any activity with the native substrate. The E285Q mutant interaction with the inhibitor was nonexistent at pH 6.5. This could be due to a change in the charge state of the active site compared to the wild type. To probe whether or not the change in the charge state of the active site affects the binding of the inhibitor the experiment was repeated at pH 10. At pH 10 the inhibitor did bind to the PrFMN as noted by the decrease in the absorbance maxima of the inhibitor at 350 nm signifying that active site cannot be positively charged, otherwise the substrate will not bind.

The R175A and R175K mutants exhibited considerably reduced activity, as determined by GC-MS and UV-Vis with a k_{ca} value of 0.84 μM^{-1} min^{-1}, which resulted in a 99.9% reduction in activity. This reduction in activity has been attributed to the R175A and R175K variants being unable to oxidize the PrFMN to the iminium form of the cofactor, regardless of the evidence that the oxidation or PrFMN can occur independently of FDC1 [57, 108]. In light of this and additional tandem MS experiments noted below, an alternative explanation is that the R175 amino acid is directly involved in the binding of PrFMN, thus mutating R175 results in the K_d of PrFMN becoming too large to get high incorporation of PrFMN into FDC1.

4.3.9. MS^2 analysis of the R175A, R175K, E285A, E285Q mutants

10 µM solutions of each mutant were subjected to native mass spectrometry and tandem mass spectrometry as described earlier. The mutants' protein spectra all

exhibited similar characteristics to the wildtype FDC spectra such as presenting as a dimeric protein with the most abundant charge state being +20. However, there was considerable variation in the mass spectra of the cofactor of the mass spectrum of the mutant enzyme versus the wildtype tandem mass spectrum.

Both the R175A and R175K cofactors exhibit m/z values of 525.15, 547.14, and 563.15 which corresponds to the [PrFMN+H], [PrFMN+Na], and [PrFMN+K] adducts which are all present in wild type FDC. However, new peaks of higher intensity were observed with m/z = 645.24, 667.206, and 683.17 which seems to mirror the proton, sodium, and potassium adducts that readily couple with PrFMN(Figure 4.8). Analysis of the amount of PrFMN bound to the R175A mutant indicates that mutation of R175 to alanine dramatically lowers the amount of PrFMN bound to the protein (Figure 4.9).

The cofactor spectra of the E285A and E285Q mutants were similar to those of the arginine mutants. The E285A mutant exhibited m/z peaks 645.24, 667.206, and 683.17 which represent a X+H, X+Na, and X+K adduct. The E285Q tandem mass spec experiment was perfomred in pH 8 buffer; unknown peaks by 1 Da indicating that these species bound to the protein are pH sensitive, and that consistent choice of buffer conditions is needed to make reliable experimental observations.

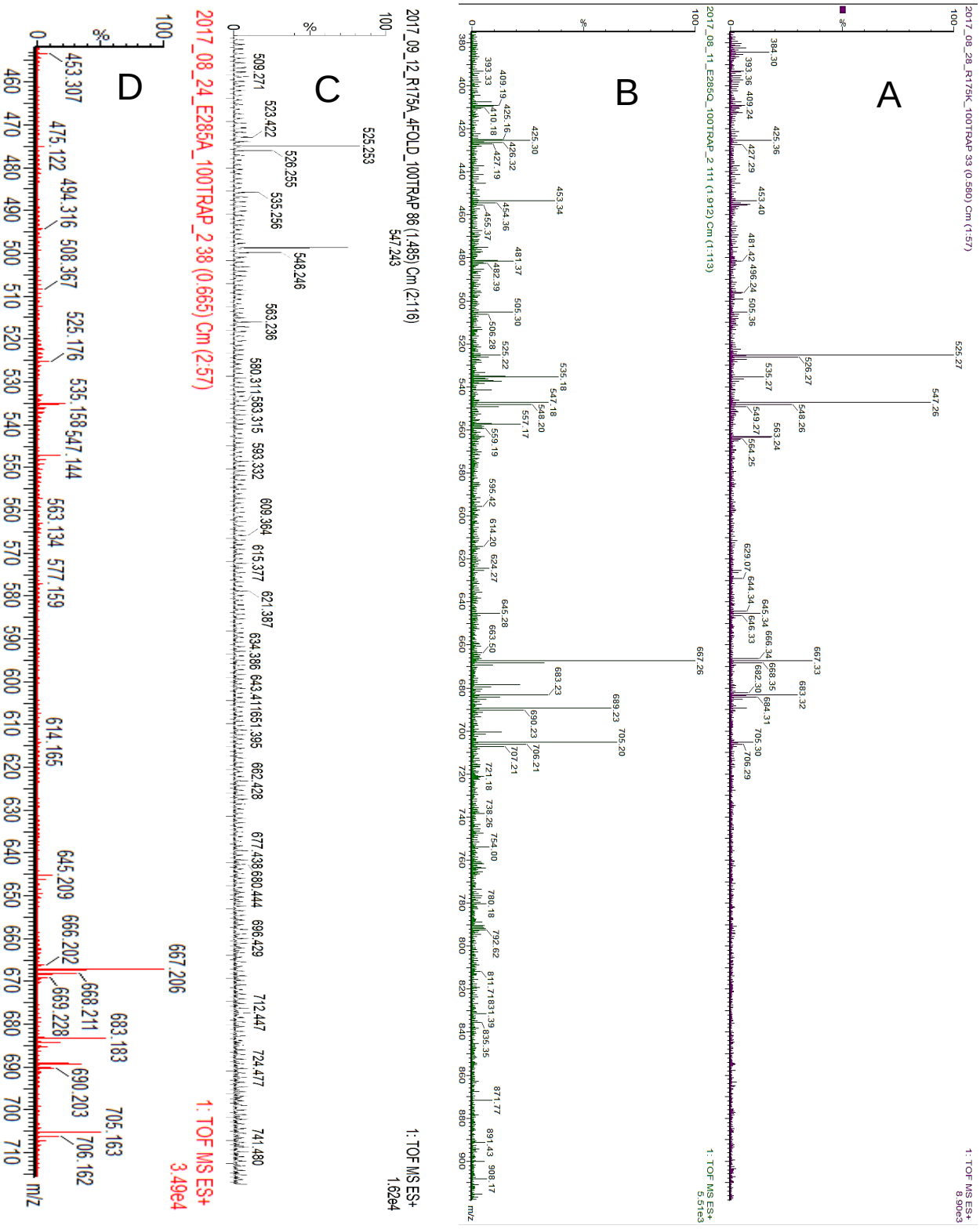

Figure 4.8 (A) MS^2 of the R175K mutant (B) MS^2 of the E285Q mutant (C) MS^2 of the R175A mutant (D) MS^2 of the E285A mutant

A PrFMN Concentration Relative to the Wildtype FDC1

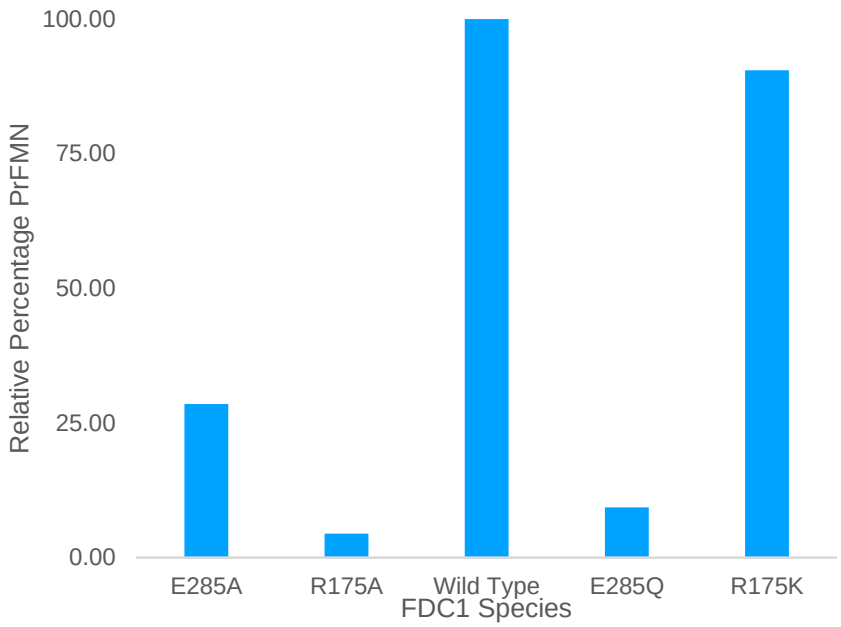

B 645 Peak Concentration Relative to the Wildtype FDC1

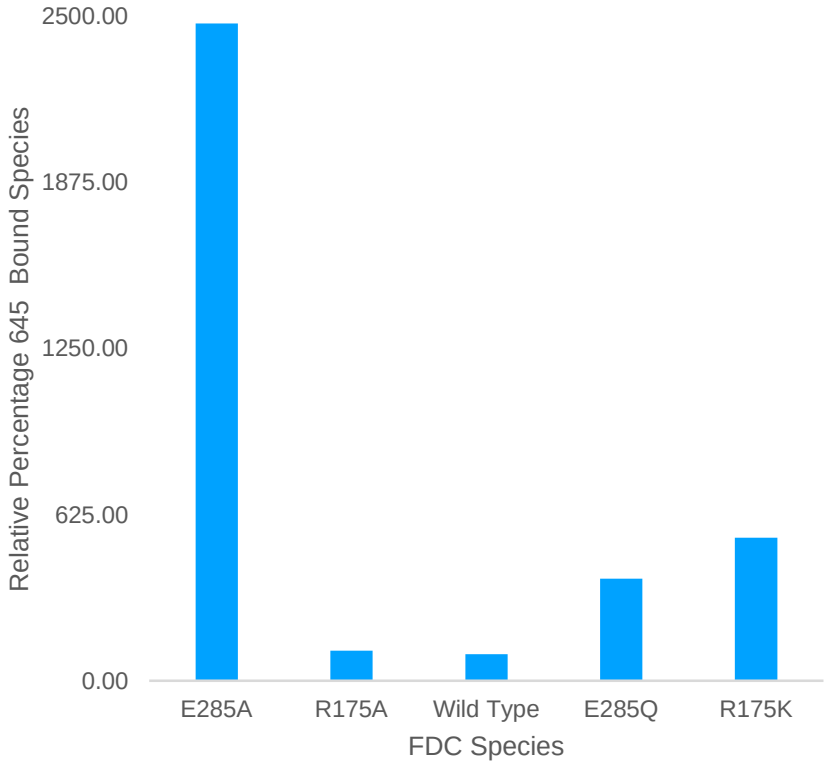

Figure 4.9 (A) Relative mass peak of 525.17 PrFMN peak with the intensity of the normalized WT peak set to 100 percent (B) The mysterious 645 Da peak relative to the wildtype FDC1 with the intensity of the WT peak set to 100 percent

4.4 Conclusion

Before this study, direct spectrophotometric and mass spectrometry evidence for the existence of these proposed 1,3-dipolarcycloadducts was based on tendancy of azomethiline yilides to react by a 1,3-dipolar cycloaddition mechanism, as well as plant enzymes' tendancy to undergo 1,3-dipolar cycloaddition reactions. These results provide the first direct experimental evidence that this novel and structurally complex flavin-derived cofactor is reactive towards 1,3-dipolar cycloaddition chemistry. There is a distinct red-shift that results from complexing the inhibitor FNVB with PrFMN results in a new local maximum at 450 nm. This type of spectrophotometric shift is characteristic of from a neutral, dialkylated flavin molecule, which has been shown with synthesized flavin derivatives. These results are consistent with the mass spectrometry evidence where FDC1 incubated with FNVB forms a potassium adduct with a 1,3 dipolar cycloadduct between the FNVB and the PrFMN. Also, when styrene and bicarbonate were incubated together with FDC1 the styrene-PrFMN adduct could be detected by mass spectrometry.

The mutagenesis experiments presented above may provide some insight into the role of two residues critical to the activity of FDC1. The R175 residue and the analogous R172 residue of FDC from *A. niger* were previously described by Bailey et al. 2017 as being critical to the oxidative maturation of the PrFMN cofactor, regardless of the previously reported work by Arunrattanamook 2017 that the cofactor of *S. cerevisiae* can oxidatively mature independent of the FDC1[108]. Comparing the mass spectrometry data for the wild-type FDC and the R175 mutant instead suggest that the R175 mutant doesn't bind PrFMN as tightly as the wild-type enzyme. All the mutants, but especially the E285 mutants, showed several unknown higher molecular weight adducts that are bound to the enzyme. These unknown species could be the

reason the enzyme spectra of these mutants are different from the wild-type enzyme. It is possible that these unknown spectra are either phenyl aldehyde PrFMN adduct

The results presented here provide direct evidence to supports the Grob-Type decarboxylation mechanism in FDC1 that is facilitated by the formation of a pentacyclic prFRMN substrate adduct through cycloaddition, and the formation of a pentacyclic PrFMN substrate adduct through cyclo-addition. Furthermore, the mass spectra data suggests that there could be some higher molecular weight species bound to FDC1 instead of the PrFMN. Future experiments should focus on trying to fragment these higher molecular weight adducts to try to gain some structural insight into what these higher molecular weight adducts are. Furthermore, introducing double mutants into the active site and observing the change in the distribution of these protein bound small molecules could elucidate whether these small molecules are PrFMN adducts such as the phenylaldehyde-PrFMN adduct or some form of proto-cofactor.

Chapter 5 Conclusions and Future Directions

5.1. Overview

Investigations into ferulic acid decarboxylase from *S. cerevisiae* were motivated by the potential fo this enzyme to provide a sustainable route to produce heavily utilized and valuable compounds including; styrene, vinyl guiacol, 1,3 pentadiene. UbiD from *P. aeruginosa* and FDC1 from *A. niger* were identified as potential targets for antibiotic development. UbiD plays a vital role in the synthesis of ubiquinone, which is essential for aerobic growth, and ubiquinone derivatives which serve as a vital signaling molecules in bacteria. FDC1 from *A. niger* was identified as an antifungal target for its broad representation among fungi and its role as breaking down established antifungal compounds such as cinnamic acid and ferulic acid[77]. The FDC1/PAD1 decarboxylase system from *S. cerevisiae* was originally identified as a potential candidate for the sustainable production of plastic monomers and biofuels based on its ability to readily decarboxylate cinnamic acid as well as sorbic acid[54]. For either of these goals to be achieved, additional biochemical characterization of the system was needed, which has been the subject of this dissertation[52-54].

5.1.1. The Relationship between FDC1 & PAD1

Both FDC1 and PAD1 or UbiX are necessary for phenylacrylic acid decarboxylation activity. tPAD1 and FDC1 were independently expressed and purified FDC1 exhibited an initial activity of 0.54 μmol/(min*mg enzyme), however when FDC1 was dialyzed FDC1 lost its associated activity. However, upon the addition of *E. coli* BL21 cell lysate to FDC1, the activity was restored, thus suggesting that FDC1 required a small molecular partner present in the cell

lysate. UbiX, a PAD1 analog endogenous to *E. coli* was suspected to PAD1's function in activating FDC. This relationship was confirmed when a Δ*ubiX E. coli* Bl21 lysate failed to reactivate FDC, implying that UbiX was isofunctional with PAD1 as both were able to reconstitute FDC1. To answer the question whether PAD1/UbiX directly interacted with FDC1 and 6.7 mM of cinnamic acid, and tPAD1 with Δubix BL21DE cell lysate were placed opposite a 3kDa membrane to see whether PAD1 produced a small molecule from the BL21 cell lysate which would then be uptaken by apo-FDC1 to facilitate the decarboxylation of cinnamic acid. Apo-FDC was reactivated under these conditions, showing that FDC1 is directly responsible for the decarboxylation activity, whereas PAD1/UbiX is responsible for the production of the recently identified, oxygen stable PrFMN cofactor.

5.1.2. Mechanistic Study of the New PrFMN Decarboxylation Mechanism

Following the establishment of the relationship between FDC1 and tPAD1, crystal structures of both UbiX from *P. aeruginosa* and FDC1 from *S. cerevisiae* were reported. The discovery of the PrFMN, with its novel isopentenyl modification, raised questions as to how it functioned in the decarboxylation mechanism. With the crystal structures, two mechanisms were proposed a 1,3 dipolar -cycloaddition mechanism, a mechanism never seen before in biochemistry, and a more conventional Michael addition mechanism. Potential mechanisms were investigated using isotope effects, NMR analysis, and a Hammett analysis. The Hammett analysis with σ- correlation with which provided strong evidence that the rate determining step is chemical in nature. The negative rho value ($\rho = -0.39$) for the Hammett plot indicated that the rate determining step involved a build-up of positive charge in the transition state, an observation that suggested that decarboxylation is not the rate determining step, because decarboxylation

reactions typically result in a build-up of negative charge. The secondary deuterium isotope at the α or β carbons is normal, which suggests that the rate determining step involves the rehybridization of these bonds from an sp^3 to an sp^2. Also, the secondary isotope effects are solvent dependent suggesting that the rehybrization of these carbon centers occur asynchronously. These effects suggest the Michael addition mechanism as unlikely, as these results suggest that the rate determining steps is chemical in nature, and Hammett analysis suggests that decarboxylation is not the rate determining therefore either formation the michael adduct would be rate determining, or the break of the PrFMN-Michael complex would determine the rate of the reaction. The normal isotope effects suggest that the formation of the Michael complex, would not be the rds. as that would result in inverse secondary KIE. These results would lead to the breaking of the PrFMN-Michaelis complex as rate determining and the solvent isotope effects suggest that the breaking of this bond would have to precede decarboxylation due to the large KIE on (V/K) and computational studies suggest that this is energetically unfavorable, and thus the Michael addition-elimination mechanism seems unlikely[84]. The evidence therefore suggests that the presented 1,3 dipolar cycl-addition mechanism is a likely candidate for the enzymatic mechanism. However, the NMR deuterium exchange experiment suggests that carbon dioxide does not immediately diffuse from the enzyme because for protonation to occur carbon dioxide needs to be bound to the enzyme.

5.1.3. Trapping Mechanistic Intermediates

Following the initial mechanistic investigation, substrate analogs and mutants were employed in an attempt to trap the putative cyclo-adduct. Alpha-fluoronitrovinylbenzene, was considered to be a good isostere for cinnamic acid with the nitro and fluoro groups activating the

double bond for cycloaddition[104]. FNVB was found to be a potent inhibitor of FDC1 1exhibiting a Ki value in the nanomolar range. FNVB reacted with FDC1 to produce an enzyme bound species with a new U.V.-visible spectrum, which suggested that the substrate analog formed a complex with the PrFMN. FDC1 was briefly incubated with FNVB for and then subjected to tandem mass spectrometry to identify small molecules bound directly to the enzyme. Incubation with FNVB resulted in a new peak of mass 731.2 daltons which was found to represent PrFMN - FNVB cycloadduct complexed with a potassium ion. Slow mutants of FDC1, were exploited to isolate and characterize either the product-PrFMN adduct or the substrate-PrFMN complex. Styrene-PrFMN and d_7-styrene-PrFMN complexes were readily isolated by mass spectrometry. The mutants revealed a change in the distribution of bound species to FDC. The 667 mass peak increased in intensity in the E285 mutants, while the 525 mass peak decreased significantly. The R175 mutants appeared to bind PrFMN significantly less tightly 525 simply, but this mutation did not alter the relative intensity of the 667 peak.

5.2 Future Directions

5.2.1. Transient Kinetics and Future Isotope Effect Measurements

Further experiments are necessary to address some interesting features that FDC1 exhibits. With the identification of a distinct spectrophotometric shift that results from the formation of PrFMN dialkyl adducts it is possible to develop an assay to monitor the reaction between the PrFMN and the substrates. Transient kinetics can be employed and by using the diverse operating conditions of FDC1 to determine the rates of formation of these short-lived PrFMN-substrate and PrFMN-product intermediates for non-ideal substrates including unsaturated linear substrates such as; sorbic acid and aromatic substrates such as 2-indole

carboxyalates. Determining the rates of the formation and breakdown of these adducts would allow for researchers uncover the *in vitro* energetics of these reactions and compare those experimentally determined energetics to the energetics generated *in silico* for a variety of substrate types. To accomplish this a researcher would need to select an appropriate substrate with slow, steady-state kinetics, and appropriate environmental conditions including pH and temperature controls.

Transient kinetics could probe several individual steps of the enzymatic mechanism using the same isotopically labeled substrates provided in chapter 3; these could be combined with using an isotope ratio mass spectrometry to probe the isotope effect of decarboxylation using natural abundance ^{13}C effects for a complete suite of isotope effect experiments. Given the reversible nature of reaction, stopped flow experiments and natural abundance ^{13}C isotope effect experiments can be performed on both the forward and the reverse directions for the FDC1. By combining these results with the primary solvent isotope effect established by an internal competition experiment in chapter 2 every chemical step of the reaction could be effectively probed. The Hammett analysis, and isotope effects previously established that a chemical step is rate-determining in the reaction.

5.2.2. Identifying Other Small Molecules that Potentially Bind to FDC1

An open question that needs to be further investigated is the identity of the 683, 667, and 645 mass peaks representing the protonated, sodium, and potassium adducts of a small molecule with a mass of 644 daltons. Analysis of common mass spectrometry contaminants as well as common biological metabolites yielded no explanation for the 644-Da peak. The gentle tandem mass spectrometry conditions of the experiments above provide assurances that these peaks are

small molecules that are bound to the protein rather than peptide fragments. These peaks could represent a phenylaldehyde-PrFMN adduct or some other small molecule inherent to FDC1. These peaks are present in the wild-type FDC1 in a small amount, however upon mutating the active site the relative concentration of these small molecules increases, while the PrFMN mass peaks decrease. Isolating and characterizing these intermediates may provide insight into the oxidative maturation of PrFMN if these species are indeed related to PrFMN, or provide insight to some secondary molecular species that is also intrinsically able to bind to FDC1. Either of these outcomes would contribute to the understanding of the activation pathway FDC1 needs to undergo to become active in vivo.

Active site mutants of FDC1, E285A and E285Q exhibit a high level of these peaks compared to the wild type, and a comparatively low amount of PrFMN. The E285Q mutant would be good to crystallize since glutamine is a good isostere for glutamic acid. Thus the phase information of FDC1 would change little from the previously crystalized *S. cerevisiae* crystal structure. This observation would allow for the phase information of the wild-type FDC1 to be applied to an E285Q FDC1 crystal structure. The crystallization conditions for FDC1 were previously reported, thus providing a good starting point for experimental conditions that could be used to crystalize FDC1 mutants. If these higher molecular weight species are indeed related to PrFMN, crystallographic evidence would provide the most direct answer, and should be explored.

5.2.3. Rational Engineering of FDC1

With the advances in the understanding of how FDC1 and the broader UbiD family undergo decarboxylation reactions, researchers now could begin improving the activity and broadening the substrate pool of FDC1 and, more broadly members of the UbiD family to make these enzymes more active as well as broaden the number of substrates these enzymes can decarboxylate. With the crystal structure and the mechanism of FDC1 published computational modeling combined with enzyme engineering efforts could focus on expanding the substrate pool. Manipulations of FDC could focus on the volume of the active site allowing for larger substrates, or perhaps constrain the active site to improve the activity of linear substrates such as sorbic acid, or 1,3 pentadionic acid. Some potential mutagenesis targets include mutating tryptophan in the substrate binding channel, or I330 or F440 to alter the active site space to allow for additional substrates to react or change the preferred substrate. Researchers could also engineer the PrFMN to modulate the activity of members of the UbiD family.

5.2.4. Develop Inhibitors for UbiD Family Members in Bacteria or Fungi

The work presented previously provides insight on how to inhibit FDC1, a model enzyme of the UbiD family, using a substrate analog, FNVB. This inhibitor provides a starting scaffold for the development of novel therapeutics targeting bacterial UbiD family members. The nitro group serves as an acceptable isostere for carboxylate, however this can be further explored by switching out the terminal nitro group with a sulfonate or phosphate group have been shown to be isosteres of carboxylate groups. Additionally, the Hammett analysis provides insight into how various functionalities of the ring impact the reaction, which can be exploited to develop better inhibitors. Finally, the assays presented in chapter 4 offer methods to confirm covalent

inhibition of FDC1. The assays presented as well as the confirmed inhibitor can also be used as a scaffold to develop and confirm more potent FDC1 inhibitors, which would directly target the resistance mechanism of ruminant species to naturally abundant antibiotic compounds such as ferulic, or cinnamic acid.

References

1. *World Population Prospects the 2017 Revision*. 2017, United Nations, Department of Economic and Social Affairs, Popultion Division p. 1-53.

2. Biermann, U.F., W.; Lang, S.; Lihs, W.; Machmuller, G.; Metzger, J. O.; Klaas, M. R.; Schifer, H. J.; Schneider, M. P., *New Syntheses with Oils and Fats as Renewable Raw Materials for the Chemical Industry.* Angew Chem Int Ed Engl, 2000. **39**: p. 2206-2224.

3. Corma, A.I., S.; Velty, A., *Chemical Routes for the Transformation of Biomass into Chemicals.* Chem Rev, 2007. **107**: p. 2411-2502.

4. Shin, J.H., et al., *Production of bulk chemicals via novel metabolic pathways in microorganisms.* Biotechnol Adv, 2013. **31**(6): p. 925-35.

5. Straathof, A.J., *Transformation of biomass into commodity chemicals using enzymes or cells.* Chem Rev, 2014. **114**(3): p. 1871-908.

6. Ltd., D.S.A.P., *C8: The impact of oil price on styrene price* 2013, Duncan Sheddon & Associates PTY. LTD.

7. Claypool, J.T., Raynman, D. R.., Jaroboe, L. R., Nielsen, D. R. *Technoeconomic evaluation of bio-based styrene production by engineered Escherichia coli.* J Ind Microbiol Biotechnol, 2014. **41**(8): p. 1211-6.

8. Maul, J.F., B. G.; Kontoff, J. R.; Eichenauer, H.; Ott, K., *Polystyrene and Styrene Copolymers*. 2005.

9. Donald J. Darensbourg, P.W., and Charles G. Riordan, *Mechanistic Aspects of Decarboxylation Reactions of Group 10 (PCy3)2M(H)O2CH* J Am Chem Soc, 1989. **112**(15): p. 5759-5762.

10. Kochi, R.A.S.a.J.K., *Chapter 4: Oxidative decarboxylation of acids by Pb(OAc)4*, in *Organic Reactions*. 1999, John Wiley and Sons.

11. Liu, A.Z., H., *Transition Metal-Catalyzed Nonoxidative Decarboxylation Reactions.* Biochemistry, 2006. **45**(35): p. 10407-10411.

12. Rodriguez, N. and L.J. Goossen, *Decarboxylative coupling reactions: a modern strategy for C-C-bond formation.* Chem Soc Rev, 2011. **40**(10): p. 5030-48.

13. Faber, K., *Biotransformation in Organic Chemistry*. 2011: Springer International Publishing. 439.
14. Choi, J.M., S.S. Han, and H.S. Kim, *Industrial applications of enzyme biocatalysis: Current status and future aspects.* Biotechnol Adv, 2015. **33**(7): p. 1443-54.

15. Hutchison, C.A., III, Phillips, S., Edgell, M. H., Gillam, S., Jahnke, P., and Smith, M., *Mutagenesis at a Specific Position in a DNA Sequence.* Journal of Biological Chemistry, 1978. **253**p. 6551-6560.

16. Correa, R.C., Rhoden, S. A., Mota, T. R., Azevedo, J. L., Pamphile, J. A., de Souza, C. G., Polizei Mde, L., Bracht, A., Peralta, R. M., *Endophytic fungi: expanding the arsenal of industrial enzyme producers.* J Ind Microbiol Biotechnol, 2014. **41**(10): p. 1467-78.

17. Chen, R., *Enzyme engineering: rational redesign versus directed evolution.* Trends in Biotechnology, 2001. **19**(1): p. 1-2.

18. Bhuiya, M.W., Lee, S. G., Jez, J. M., Yu, O., *Structure and Mechanism of Ferulic Acid Decarboxylase (FDC1) from Saccharomyces cerevisiae.* Appl Environ Microbiol, 2015. **81**(12): p. 4216-23.

19. Jacewicz, A., Izumi, A., Brunner, K., Schnell, R., Schneider, G., *Structural insights into the UbiD protein family from the crystal structure of PA0254 from Pseudomonas aeruginosa.* PLoS One, 2013. **8**(5): p. e63161.

20. Rangarajan, E.S., Li Y., Iannuzzi, P., Tocilj, A., Hung, L., Matte, A., Cygler, M., *Crystal structure of a dodecameric FMN-dependent UbiX-like decarboxylase (Pad1) from Escherichia coli O157: H7.* Protein Sci, 2004. **13**(11): p. 3006-16.

21. Kopec, J., R. Schnell, and G. Schneider, *Structure of PA4019, a putative aromatic acid decarboxylase from Pseudomonas aeruginosa.* Acta Crystallogr Sect F Struct Biol Cryst Commun, 2011. **67**(Pt 10): p. 1184-8.

22. McKenna, R. and D.R. Nielsen, *Styrene biosynthesis from glucose by engineered E. coli.* Metab Eng, 2011. **13**(5): p. 544-54.

23. Clausen, M., C.J.L., Megnet, R. and, P. W., *PAD1 encodes phenylacrylic acid decarboxylase which confers resistance to cinnamic acid in Saccharomyces cerevisiae.* Gene, 1994. **142**: p. 107-112.

24. Mukai, N., Masaki, K., Fujii, T., Kawamukai, M., Lefuji H., *PAD1 and FDC1 are essential for the decarboxylation of phenylacrylic acids in Saccharomyces cerevisiae.* J Biosci Bioeng, 2010. **109**(6): p. 564-9.

25. Baqueiro-Pena, I., Rodriguez-Serrano, G., Gonzalez-Zamora, E., Augur, C., Loera, O., Saucedo-Castaneda, G., *Biotransformation of ferulic acid to 4-vinylguaiacol by a wild and a diploid strain of Aspergillus niger.* Bioresour Technol, 2010. **101**(12): p. 4721-4724.

26. Nesci, A.V. and M.G. Etcheverry, *Control of Aspergillus growth and aflatoxin production using natural maize phytochemicals under different conditions of water activity.* Pest Manag Sci, 2006. **62**(8): p. 775-784.

27. Stratford, M., Plumridge, A., Pleasants, M.W., Michaela, N., Baker-Glenn, C.A.G., Pattenden, G., Archer, D.B., *Mapping the structural requirements of inducers and substrates for decarboxylation of weak acid preservatives by the food spoilage mould Aspergillus niger.* Int J Food Microbiol, 2012. **157**(3): p. 375-383.

28. In-young Lee, T.G.V., and John P. N. Rosazza, *Decarboxylation of ferulic acid to 4-vinylguaicol by Bacillus pumilus in aqueous-organic solvent two-phase systems.* Enzyme and Microbial Technology, 1998. **23**: p. 261-266.

29. Jean-Francois Cavin, V.D., and Charles Divies, *Gene Cloning, Transcriptional Analysis, Purification, and Characterization of Phenolic Acid Decarboxylase from Bacillus subtilis.* Applied and Enviromental Microbacteriology, 1998. **64**(4): p. 1466-1471.

30. Jung, D.H., Choi, W., Choi, K.Y., Jung, E., Yun, H., Kazlauskas, R.J., Kim, B.G., *Bioconversion of p-coumaric acid to p-hydroxystyrene using phenolic acid decarboxylase from B. amyloliquefaciens in biphasic reaction system.* Appl Microbiol Biotechnol, 2013. **97**(4): p. 1501-1511.

31. Lise Barthelmebs, C.D., and Jean-Francois Cavin, *Knockout of the p-Comarate Decarboxylase Gene from Lactobacillus plantarum reveals the Existence of Two Other Inducible Enzymatic Activities Invovled in Phenolic Acid metabolism.* Appl Environ Microbiol, 2000. **66**(8): p. 3368-3375.

32. Lupa, B., Lyon, D., Gibbs, M.D., Reeves, R.A., Wiegel, J., *Distribution of genes encoding the microbial non-oxidative reversible hydroxyarylic acid decarboxylases/phenol carboxylases.* Genomics, 2005. **86**(3): p. 342-351.

33. Ou, S. and K.-C. Kwok, *Ferulic acid: pharmaceutical functions, preparation and applications in foods.* Journal of the Science of Food and Agriculture, 2004. **84**(11): p. 1261-1269.

34. Lattanzio, V.D., V.; Divenere, D.; Lima, G.; and Salerne, M., *Antifungal Activity of Phenolics Against Fungi Commonly Encountered During Storage* Ital. J. Food Sci. , 1994. **1**: p. 23-30.

35. McKenna, R.T., B.; Pugh, S.; Neilsen, D., *Rational and combinatorial approaches to engineering styrene production by S. cerevisiae.* Microbial Cell Factories, 2014. **13**(123): p. 1-12.

36. Priefert, H., J. Rabenhorst, and A. Steinbüchel, *Biotechnological production of vanillin.* Applied Microbiology and Biotechnology, 2001. **56**(3-4): p. 296-314.

37. Zago, A.D., G.; Bruschi, C. V., *Cloning, Sequencing, and Expression in Escherichia coli of the Bacillus pumilus Gene for Ferulic Acid Decarboxylase.* Appl Environ Microbiol, 1995. **61**(12): p. 4484-4486.

38. Stratford, M., A. Plumridge, and D.B. Archer, *Decarboxylation of sorbic acid by spoilage yeasts is associated with the PAD1 gene.* Appl Environ Microbiol, 2007. **73**(20): p. 6534-42.

39. Rodriguez, H.L., J. M.; Curiel, J. A.; Rivas, B., Mancheno, J. M.; Munoz, R., *Characterization of the p-Coumaric Acid Decarboxylase from Lactobacillus plantarum CECT 748.* J Agric Food Chem., 2008. **56**: p. 3068-3072.

40. Rodriguez, H., Angulo, I., de Las Rivas, B., Campillo, N., Paez, J.A., Munoz, R., Macheno, J.M., *p-Coumaric acid decarboxylase from Lactobacillus plantarum: structural insights into the active site and decarboxylation catalytic mechanism.* Proteins, 2010. **78**(7): p. 1662-1676.

41. Seo, J.H., Hwang, J.Y., Seo, S.H., Kang, H., Hwang, B.Y., Kim, B.G., *Computational selection, identification and structural analysis of omega-aminotransferases with various substrate specificities from the genome sequence of Mesorhizobium loti MAFF303099.* Biosci Biotechnol Biochem, 2012. **76**(7): p. 1308-1314.

42. Zhang, H. and G.T. Javor, *Regulation of the isofunctional genes ubiD and ubiXof the ubiquinone biosynthetic pathway of Escherichia coli.* FEMS Microbiology Letters, 2003. **223**(1): p. 67-72.

43. Bentinger, M., M. Tekle, and G. Dallner, *Coenzyme Q--biosynthesis and functions.* Biochem Biophys Res Commun, 2010. **396**(1): p. 74-79.

44. Cox, G.B.Y., G. L.; McCann, L. M.; Gibson, R., *Biosynthesis of Ubiquinone in Escherichia coli K-12 Location of genes Affecting the Metabolism of 3-Octaprenyl-4-hydroxybenzoic Acid and 2-Octaprenylphenol.* Journal of Bacteriology, 1968. **99**(2): p. 450-458.

45. Leppik, R.A.Y., I. G.; Gibson, F., *Membrane-Associated Reactions in Ubiquinone Biosynthesis in Escherichia coli 3-Octaprenyl-4-hydroxybenzoate Carboxylase.* Biochimica et Biophysica Acta, 1976. **436**: p. 800-810.

46. Hiratsuka, T.F., K.; Ishikawa, J.; Yamashita, H.; Itoh, N.; Seto, H.; Dairi, T., *An Alternative Menaquinone Biosynthetic Pathway Operating in Microorganism.* Science, 2008. **321**: p. 1670-1672.

47. Michael Blaesse, T.K., Robert Huber, and Stefan Steinbacher, *Crystal structure of the peptidyl-cysteine decarboxylase EpiD complexed with a pentapeptide substrate.* The EMBO journal, 2000. **19**(23): p. 6299-6310.

48. Marshall, S.A., K.A.P. Payne, and D. Leys, *The UbiX-UbiD system: The biosynthesis and use of prenylated flavin (prFMN).* Arch Biochem Biophys, 2017. **632**: p. 209-221.

49. Hussain, M.A. and C.O. Dawson, *Economic Impact of Food Safety Outbreaks on Food Businesses.* Foods, 2013. **2**(4): p. 585-589.

50. Jordan, F. and H. Patel, *Catalysis in Enzymatic Decarboxylations: Comparison of Selected Cofactor-dependent and Cofactor-independent Examples.* ACS Catal, 2013. **3**(7): p. 1601-1617.

51. Payne, K.A., White, M.D., Fisher, K., Khara, B., Bailey, S.S., Parker, D., Rattray, N.J., Trivedi, D.K., Goodacre, R., Beveridge, R., Barran, P., Rigby, S.E., Scrutton, N.S., Hay, S., Leys, D., *New cofactor supports alpha,beta-unsaturated acid decarboxylation via 1,3-dipolar cycloaddition.* Nature, 2015. **522**(7557): p. 497-501.

52. Lin, F., Ferguson, K.L., Boyer, D.R., Lin, X.N., Marsh, E.N.G., *Isofunctional enzymes PAD1 and UbiX catalyze formation of a novel cofactor required by ferulic acid decarboxylase and 4-hydroxy-3-polyprenylbenzoic acid decarboxylase.* ACS Chem Biol, 2015. **10**(4): p. 1137-44.

53. Ferguson, K.L., N. Arunrattanamook, and E.N.G. Marsh, *Mechanism of the Novel Prenylated Flavin-Containing Enzyme Ferulic Acid Decarboxylase Probed by Isotope Effects and Linear Free-Energy Relationships.* Biochemistry, 2016. **55**(20): p. 2857-63.

54. Ferguson, K.L., Eschweiler, J.D., Ruotolo, B.T., Marsh, E.N.G., *Evidence for a 1,3-Dipolar Cyclo-addition Mechanism in the Decarboxylation of Phenylacrylic Acids Catalyzed by Ferulic Acid Decarboxylase.* J Am Chem Soc, 2017. **139**(32): p. 10972-10975.

55. Beveridge, R., Migas, L.G., Payne, K.A.P., Scrutton, N.S., Leys, D., Barran, P.E., *Mass spectrometry locates local and allosteric conformational changes that occur on cofactor binding.* Nat Commun, 2016. **7**: p. 12163.

56. Leys, D. and N.S. Scrutton, *Sweating the assets of flavin cofactors: new insight of chemical versatility from knowledge of structure and mechanism.* Curr Opin Struct Biol, 2016. **41**: p. 19-26.

57. Bailey, S.S., Payne, K.A.P., Fisher, K., Marshall, S.A., Cliff, M.J., Spiess, R., Parker, D.A., Rigby, S.E.J., Leys, D., *The role of conserved residues in Fdc decarboxylase in prenylated flavin mononucleotide oxidative maturation, cofactor isomerization, and catalysis.* J Biol Chem, 2018. **293**(7): p. 2272-2287.

58. Li, T.I., H.; Fu, R.; Hasegawa, Y.; Zhang, H.; Liu, A., *α-Amino-β-Carboxymuconate-ε-Semialdehyde Decarboxylase (ACMSD) Is a New Member of the Amidohydrolase Superfamily.* Biochemistry, 2006. **45**: p. 6628-6634.

59. Li, T., Huo, L., Pulley, C., Liu, A., *Decarboxylation mechanisms in biological system.* Bioorg Chem, 2012. **43**: p. 2-14.

60. Massey, V., *Activation of Molecular Oxygen by Flavins and Flavoproteins.* Journal of Biological Chemistry, 1994. **269**(36): p. 22459-22462.

61. Strauss, E., Kinsland, C., Ge, Y., McLafferty, F.W., Begley, T.P., *Phosphopantothenoylcysteine synthetase from Escherichia coli. Identification and characterization of the last unidentified coenzyme A biosynthetic enzyme in bacteria.* J Biol Chem, 2001. **276**(17): p. 13513-6.

62. Benning, M.M.H., T.; Gerlt, J. A.; Holden, H. M., *New Reactions in the Crotonase Superfamily: Structure of Methylmalonly CoA Decarboxylase from Escherichia coli.* Biochemistry, 2000. **39**: p. 4630-4639.

63. Cendron, L., Berni, R., Folli, C., Ramazzina, I., Percudani, R., Zanotti, G., *The structure of 2-oxo-4-hydroxy-4-carboxy-5-ureidoimidazoline decarboxylase provides insights into the mechanism of uric acid degradation.* J Biol Chem, 2007. **282**(25): p. 18182-18189.

64. Warshel, A.S., M.; Villa, J.; Florian, J., *Remarkable Rate Enhancement of Orotidine 5'-Monophosphate Decarboxylase Is Due to Transition-State Stabilization Rather Than to Ground-State Destabilization.* Biochemistry, 2000. **39**: p. 14728-14738.

65. Appleby, T.C.K., C.; Begley, T. P., Ealick, S., *The Crystal Structure and Mechanism of Orotidine 5'-monophosphate Decarboxylase.* PNAS, 2000: p. 2005-2010.

66. Davies, J., D. Davies, *Origins and evolution of antibiotic resistance.* Microbiol Mol Biol Rev, 2010. **74**(3): p. 417-433.

67. Kohanski, M.A., D.J. Dwyer, J.J. Collins, *How antibiotics kill bacteria: from targets to networks.* Nat Rev Microbiol, 2010. **8**(6): p. 423-435

68. Georgellis, D.K., O.; Lin, E. C. C., *Quinones as the Redox Signal for the Arc Two-Component System of Bacteria.* Science, 2001. **292**: p. 1-2

69. Pankey, G.A.S., L. D., *Clinical Relevance of Bacteriostatic versus Bactericidal Mechanisms of Action in teh Treatment of Gram-Positive Bacterial Infections.* Clinical Infectious Disease, 2004. **38**: p. 864-870.

70. Richardson, L.A., *Understanding and overcoming antibiotic resistance.* PLoS Biol, 2017. **15**(8): p. e2003775.

71. Nemeth, J., Oesch, G., Kuster, S.P., *Bacteriostatic versus bactericidal antibiotics for patients with serious bacterial infections: systematic review and meta-analysis.* J Antimicrob Chemother, 2015. **70**(2): p. 382-395.

72. Roemer, T., D.J. Krysan, *Antifungal drug development: challenges, unmet clinical needs, and new approaches.* Cold Spring Harb Perspect Med, 2014. **4**(5).

73. Poulat, C., Nivoix, Y., Launoy, A., Lutun, P., Bachellier, P., Rohr, S., Woehl, M.L., Leveque, D., Bru, V., Herbrecht, R., Gourieux, B., *Assessment of high-priced systemic antifungal prescriptions.* Med Mal Infect, 2017. **47**(6): p. 382-388.

74. Cleland, W.W., *Mechanism of Enzymatic Oxidative Decarboxylation.* Acc. Chem. Res., 1999. **32**: p. 862-868.

75. Belcher, J., McLean, K.J., Matthews, S., Woodward, L.S., Fisher, K., Rigby S.E., Nelson, D.R., Potts, D., Baynham, M.T., Parker, D.A., Leys, D., Munro, A.W., *Structure and biochemical properties of the alkene producing cytochrome P450 OleTJE (CYP152L1) from the Jeotgalicoccus sp. 8456 bacterium.* J Biol Chem, 2014. **289**(10): p. 6535-6550.

76. Kourist, R., Guterl, J.K., Miyamoto, K., Sieber, V., *Enzymatic Decarboxylation-An Emerging Reaction for Chemicals Production from Renewable Resources.* ChemCatChem, 2014. **6**(3): p. 689-701.

77. Ebenau-Jehle, C., Mergelsberg, M., Fischer, S., Bruls, T., Jehmlich, N., von Bergen, M., Boll, M., *An unusual strategy for the anoxic biodegradation of phthalate.* ISME J, 2017. **11**(1): p. 224-236.

78. Gulmezian, M., Hyman, K.R., *The role of UbiX in Escherichia coli coenzyme Q biosynthesis.* Arch Biochem Biophys, 2007. **467**(2): p. 144-153.

79. Baba, T., Ara, T., Hasegawa, M., Takai, Y., Okumura, Y., Baba, M., Datsenka, K.A., Tomita, M., Wanner, B.L., Mori, H., *Construction of Escherichia coli K-12 in-frame, single-gene knockout mutants: the Keio collection.* Mol Syst Biol, 2006. **2**: p. 2006-2008.

80. Ghisla, S.M., V.; Lhoste, J.; Mayhew, S., G., *Fluorescence and Optical Characteristics of Reduced Flavines and Flavoproteins.* Biochemistry, 1974. **13**(3): p. 589-597.

81. Andorfer, M.C., Belsare, K.D., Girlich, A.M., Lewis, J.C., *Aromatic Halogenation by Using Bifunctional Flavin Reductase-Halogenase Fusion Enzymes.* Chembiochem, 2017. **18**(21): p. 2099-2103.

82. de Matos, P., R. Alcantara, Dekker, A., Ennis, M., Hasting, J., Haug, K., Spiteri, I., Turner, S., Steinbeck, C., *Chemical Entities of Biological Interest: an update.* Nucleic Acids Res, 2010. **38**: p. D249-D254.

83. Lan, C.L., Chen, S.L., *The Decarboxylation of alpha,beta-Unsaturated Acid Catalyzed by Prenylated FMN-Dependent Ferulic Acid Decarboxylase and the Enzyme Inhibition.* J Org Chem, 2016. **81**(19): p. 9289-9295.

84. Tian, G., Y. Liu, *Mechanistic insights into the catalytic reaction of ferulic acid decarboxylase from Aspergillus niger: a QM/MM study*. Phys Chem Chem Phys, 2017. **19**(11): p. 7733-7742.

85. Payer, S.E., Marshall, S.A., Barland, N., Sheng, X., Reiter, T., Dordic, A., Steinkellner, G., Wuensch, C., Kaltwasser, S., Fisher, K., Rigby, S.E.J., Macheroux, P., Vonck, J., Gruber, K., Faber, K., Himo, F., Leys, D., Pavkov-Keller, T., Glueck, S. M., *Regioselective para-Carboxylation of Catechols with a Prenylated Flavin Dependent Decarboxylase.* Angew Chem Int Ed Engl, 2017. **56**(44): p. 13893-13897.

86. Marshall, S.A., Fisher, K., Cheallaigh, A.N., White, M.D., Payne, K.A.P., Parker, D., A., Rigby, S.E.J., Leys, D., *Oxidative Maturation and Structural Characterization of Prenylated FMN Binding by UbiD, a Decarboxylase Involved in Bacterial Ubiquinone Biosynthesis.* J Biol Chem, 2017. **292**(11): p. 4623-4637.

87. Ghisla, S., .Massey, V., *Mechanisms of flavoprotein-catalyzed reactions.* Eur. J. Biochem, 1989. **181**: p. 1-17.

88. White, M.D., Payne, K.A., Fisher, K., Marshall, S.A., Parker, D., Rattray, N.J., Trivedi, D.K., Goodacre, R., Rigby, S.E., Scrutton, N.S., Hay, S., Leys, D., *UbiX is a flavin prenyltransferase required for bacterial ubiquinone biosynthesis.* Nature, 2015. **522**(7557): p. 502-506.

89. Kurti, L.C., B., *Strategic Applications of Named Reactions in Organic Sytnthesis*. 1 ed. 2005: Academic Press. 864.

90. Waugh, M.W., Marsh, E.N.G. *Solvent isotope effects on alkane formation by cyanobacterial aldehyde deformylating oxygenase and their mechanistic implications.* Biochemistry, 2014. **53**(34): p. 5537-5543.

91. Wuensch, C., Pavkov-Keller, T., Steinkellner, G., Gross, J., Fuchs, M., Hromic, A., Lyskowski, A., Fauland, K., Gruber, K., Glueck, S.M., Faber, K., *Regioselective Enzymatic beta-Carboxylation of para-Hydroxy- styrene Derivatives Catalyzed by Phenolic Acid Decarboxylases.* Adv Synth Catal, 2015. **357**(8): p. 1909-1918.

92. H., J.H., *A Reexamination of the Hammett Equation*, U.S.P.H. Service, Editor. 1953, U.S. Public Health Service: Chapel Hill, North Carolina. p. 191-254.

93. Neims, A.H.D.L., D. C.; Hellerman, L., *Studies on crystalline D-Amino Acid Oxidase. III. Substrate Specificity and sigma-rho Relationship* biochemistry, 1966. **5**(1): p. 203-213.

94. Yorita, K.M., H., Palfey, B. A., Massey, V., *On the interpretation of quantitative structure-function activity relationship data for lactate oxidase.* PNAS, 2000. **97**(6): p. 2480-2485.

95. Gadda, G., P.F. Fitzpatrick, *Solvent isotope and viscosity effects on the steady-state kinetics of the flavoprotein nitroalkane oxidase.* FEBS Lett, 2013. **587**(17): p. 2785-2789.

96. Cook, P.F., *Enzyme Mechanism from Isotope Effects*. Vol. 1. 2000, Boca Raton, FL: CRC Press. 500.

97. Cleland, W.W., *The use of isotope effects to determine enzyme mechanisms.* J Biol Chem, 2003. **278**(52): p. 51975-51984.

98. Chinchilla, R.F., L. R.; Galindo, N.; Nijera, C., *Asymmetric Synthesis of Substituted Prolines by 1,3-Dipolar Cycloaddition Azomethine Ylides from Chiral 6-isopropyl-5-phenylmorpholin-2-ones.* Eur. J. Org Chem, 2001: p. 3133-3140.

99. Jiang, K., Y.-C. Chen, *Organocatalytic reactions involving nitrogen-ylides.* Tetrahedron Letters, 2014. **55**(13): p. 2049-2055.

100. Pérez, P., Domingo, L.R., Aurell, J.M., Contreras, R., *Quantitative characterization of the global electrophilicity pattern of some reagents involved in 1,3-dipolar cycloaddition reactions.* Tetrahedron, 2003. **59**(17): p. 3117-3125.

101. Fadeyi, O.O., Hoth, L.R., Choi, C., Feng, X., Gopalsamy, A., Hett, E.C., Kyne, R.E., Robinson, R.P., Jones, L.H., *Covalent Enzyme Inhibition through Fluorosulfate Modification of a Noncatalytic Serine Residue.* ACS Chem Biol, 2017. **12**(8): p. 2015-2020.

102. Szewczuk, L.M.C., J. C.; Yang, M.; Majumdar, A.; Yu, M.; Cole, P. A., *Mechanisitic Analysis of a Suicide Inactivator of Histone Demethylase LSD1*. Biochemistry, 2007. **46**: p. 6892-6902.

103. Culhane, J., C.; Szewczuk, L., M.; Liu, X.; Da, G.; Marmorstein, R.; and Cole, P., A., *A Mechanism-Based Inactivator for Histone Demethylase LSD1*. J Am Chem Soc, 2006. **126**: p. 4536-4537.

104. Kelly, T.R.K., M. H., *relative Binding Affinity of Carboxylate and Its Isosteres: Nitro, Phosphate, Phosphonate, Sulfonate, and g-Lactone*. J Am Chem Soc, 1994. **116**: p. 7072-7080.

105. Craig, D.H., Peter, T.B., Moody, C. E., Bruce, N.C., Chapman, S.K., Munro, A.W., Scrutton, N.S., *Effects of environment on flavin reactivity in morphinone reductase: analysis of enzymes displaying differential charge the N-1 atom and C-2 carbonyl region of the active-site flavin.* Biochem J., 2001. **359**: p. 315-323.

106. Eckstiein, J.W.H., J. W.; Ghisla, S., *Mechanism of Bacterial Bioluminescence: 4a, 5-Dihydrogenflavin Analogs as Models for Luciferase Hydroperoxide Intermediates and the Effect of Substitutents at the 8-Position of Flavin on Luciferase Kinetics.* Biochemistry, 1992. **32**: p. 404-411.

107. Nanni, E.J.S., D. T., Ball, S. S., Bruice, T. C., *Redox Chemistry of N5-Ethyl-3-methyllumiflavinium Cation and N5-Ethyl-4a-hydroperoxy-3-methyllumiflavin in Dimethylformamide. Evidence for the Formation of the N5-Ethyl-4a-hydroxperoxy-3-methyllumiflavin Anion via Radical-Radical Coupling with Superoxide ion.* J Am Chem Soc, 1981. **103**(10): p. 2797-2802.

108. Arunrattanamook, N., Marsh, E.N.G., *Kinetic Characterization of Prenyl-Flavin Synthase from Saccharomyces cerevisiae.* Biochemistry, 2018. **57**(5): p. 696-700.

APPENDICIES

Appendix A.1. FDC1 & PAD1 Gene Sequence and Mutagenesis Primers

FDC1 Gene Sequence

ATGCGCAAACTGAACCCGGNNNNNNNNTTCCGTGATTTTATCCAAGTCCTGAAAGA
TGAAGATGACCTGATTGAAATTACCGAAGAAATTGATCCGAACCTGGAAGTTGGCG
CAATCATGCGTAAAGCTTATGAATCACACCTGCCGGCGCCGCTGTTTAAAAATCTGA
AAGGTGCCAGTAAAGACCTGTTTAGCATTCTGGGCTGCCCGGCGGGTCTGCGTTCGA
AAGAAAAAGGCGACCATGGTCGCATTGCCCATCACCTGGGCCTGGACCCGAAAACC
ACGATCAAAGAAATTATCG
ACTATCTGCTGGAATGCAAAGAAAAAGAACCGCTGCCGCCGATCACGGTTCCGGTC
AGCTCTGCGCCGTGTAAAACCCATATTCTGAGCGAAGAAAAAATCCACCTGCAGTCT
CTGCCGACGCCGTACCTGCACGTTAGTGATGGCGGTAAATATCTGCAGACCTACGGT
ATGTGGATTCTGCAAACCCCGGACAAAAAATGGACGAACTGGTCCATCGCACGTGG
CATGGTGGTTGATGACAAACACATTACCGGTCTGGTGATCAAACCGCAGCATATTCG
CCAAATCGCGGATAGCTGGGCGGCCATTGGCAAAGCGAATGAAATCCCGTTTGCAC
TGTGCTTCGGTGTGCCGCCGGCAGCTATTCTGGTTAGCTCCATGCCGATCCCGGAAG
GCGTTAGCGAATCTGATTATGTCGGCGCGATTCTGGGTGAAAGTGTTCCGGTCGTGA
AATGTGAAACCAACGACCTGATGGTCCCGGCCACGAGTGAAATGGTGTTTGAAGGT
ACCCTGTCCCTGACCGATACGCATCTGGAAGGCCCGTTTGGTGAAATGCACGGCTAC
GTTTTCAAAAGCCAGGGTCATCCGTGCCCGCTGTATACCGTCAAAGCAATGTCATAC
CGTGATAACGCTATTCTGCCGGTGTCGAATCCGGGCCTGTGTACGGACGAAACCC
ATACGCTGATCGGTAGCCTGGTGGCAACCGAAGCTAAAGAACTGGCAATTGAATCT
GGCCTGCCGATCCTGGATGCTTTTATGCCGTATGAAGCGCAGGCCCTGTGGCTGATT
CTGAAAGTTGACCTGAAAGGTCTGCAAGCCCTGAAAAC
CACGCCGGAAGAATTCTGCAAAAAAGTCGGCGATATTTATTTTCGCACCAAAGTGG
GTTTCATCGTTCACGAAATTATCCTGGTGGCAGATGACATCGACATCTTCAACTTCA
AAGAAGTCATTTGGGCTTACGTGACCCGTCATACGCCGGTTGCGGATCAGATGGCCT
TTGATGACGTCACCTCATTTCCGCTGGCACCGTTCGTGTCACAATCATCGCGCTCGA
AA
ACGATGAAAGGCGGTAAATGCGTGACCAACTGTATTTTTCGTCAGCAATATGAACGC
TCTTTCGATTACATCACCTGTAACTTCGAAAAAGGCTACCCGAAAGGTNNNNNNNN
NNNNNNNAATGAAAACTGGAAACGCTACGGTTACAA

tPAD1 Gene Sequence

TGAGGAATTCCCTCTGAATATTTTGTTTAACTTTAAGAAGGAGATATACCATGGGCA
GCAGCCANCATCATCATCATCACAGCAGCGGCCTGGTGCCGCGCGGCAGCCATATG
AAACGTATTGTGGTTGCGATCACCGGCGCCACGGGTGTTGCACTGGGCATTCGCCTG
CTGCAGGTCCTGAAAGAACTGAGCGTGAAACCCATCTGGTTATCTCTAAATGGGGTG
CGGCCACCATGA
AATATGAAACGGATTGGGAACCGCACGACGTTGCAGCTCTGGCCACCAAAACGTAC
TCAGTTCGTGATGTCTCGGCATGCATTAGCTCTGGCAGCTTTCAACACGACGGTATG
ATCGTCGTGCCGTGTAGTATGAAATCCCTGGCGGCCATTCGTATCGGCTTCACCGAA
GATCTGATTACGCGCGCAGCTGACGTGTCTATCAAAGAAAACCGTAAACTGCTGCTG
GTTACCCGCGAAACGCCGCTGAGTTCCATTCATCTGGAAAATATGCTGAGCCTGTGC
CGCGCTGGCGTCATTATCTTTCCGCCGGTGCCGGCA
TTCTATACCCGTCCGAAAAGTCTGCACGATCTGCTGGAACAGTCCGTGGGTCGCATC
CTGGACTGTTTCGGCATTCACGCTGACACGTTTCCGCGCTGGGAAGGTATCAAATCA
AAATAAGGATCCGAATTCGAGCTCCGTCGACAAGCTTGCGGCCGCACTCGAGCACC
ACCACCACCACCACTGAGATCCGGCTGCTAACAAAGCCCGAAAGGAAGCTGAGTTG
GCTGCTGCCACCGCTGAGCAATAACTAGCATAACCCCTTGGGGGCCTCTAAACGGG
GTCTTGAGGGGTTTTTTTGCTGAAAGGAGGGAACTATATCCGGGATTGGCGAATGGG
ACGCGCCCTGTAGCGGCGCATTAACCGCGGCGGGTGTGGTGGTTACGCGCANCGTN
GACCGCTACACTTGCNAGCGCCCTANCGCCCGCTCCTTTTCGCTTTCTTTCCCTTCCT
TTTCTCGCCACGTTTCGCCCGGGNTT
TCCCNGTCAAGCTCTAAATCGGGGGGGCTCCCTTTAAGGGGTTCCNNATTTTAGNGG
CTTTANCGGNNACCNNCNACCCCAAAAAAANTTGATTAGGGGNGAAGGTTTCNNNT
NAGNNGGGCCANCCCCCCNGAAAAAACGGTTTTTCCCCCTTTGANTTTGGGAAATCN
ANGTTTTTTTAAATANNGGA

Appendix A.1.2. FDC1 Primer Sequences for FDC1 mutants

5’-TGGACGAACTGGTCCATCGCACGTGGCATGGTGGTTGATGACAAACACA-3’
R175A 5’-GACGAACTGGTCCATCGCAGCTGGCATGGTG-3’
R175K 5’-CGAACTGGTCCATCGCAAAGGGCATGGTGGTTGATGAC -3’

5’- CGCATCTGGAAGGCCCGTTTGGTGAAATGCACGGCTACGTTTTCAAAAGCCG - 3’
E285Q 5’-GGAAGGCCCGTTTGGTCAGATGCACGGCTACGTTT-3’
E285A 5’-GGCCCGTTTGGTGCAATGCACGGCTACG-3

Appendix A.2 Representative Purification of FDC1 WT enzyme and mutant FDC1

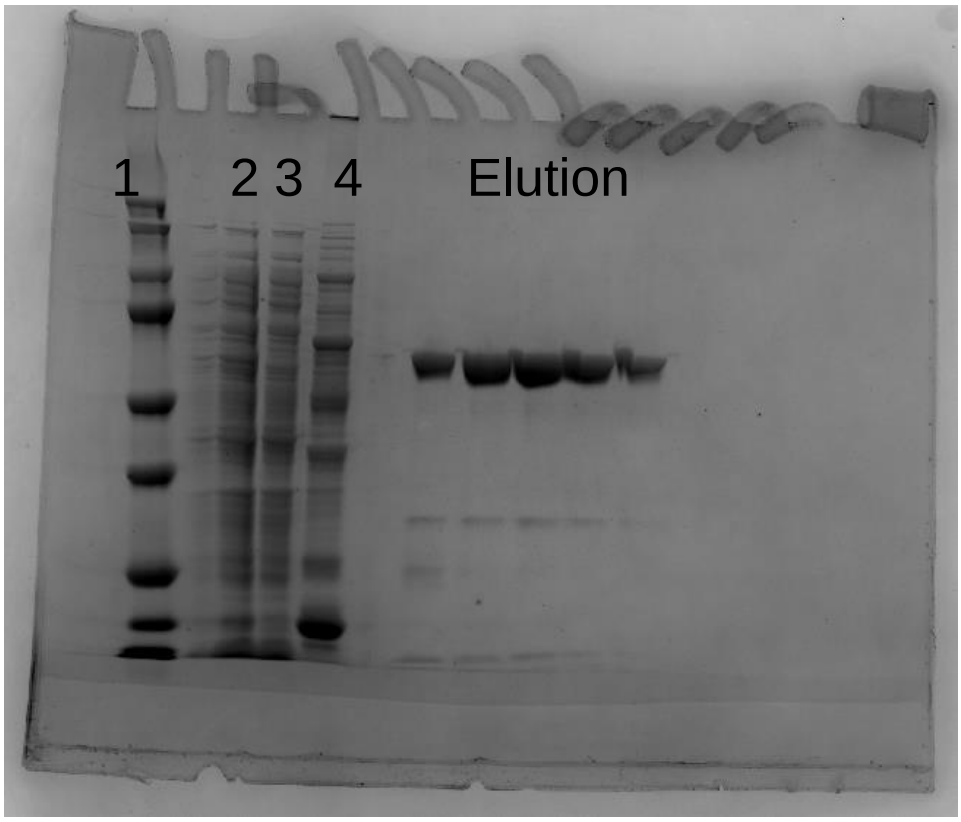

Figure A.1 Typical SDS gel of the FDC1 purification where lane 1 is the ladder, lane 2 is the cell lysate, lane 3 is the flow-through, lane 4 is the wash, and the elution lanes are holo-FDC1 with a typical yield of 10mg/L and a purity of >95%

Appendix A.3 DNA Agarose Gel of FDC1

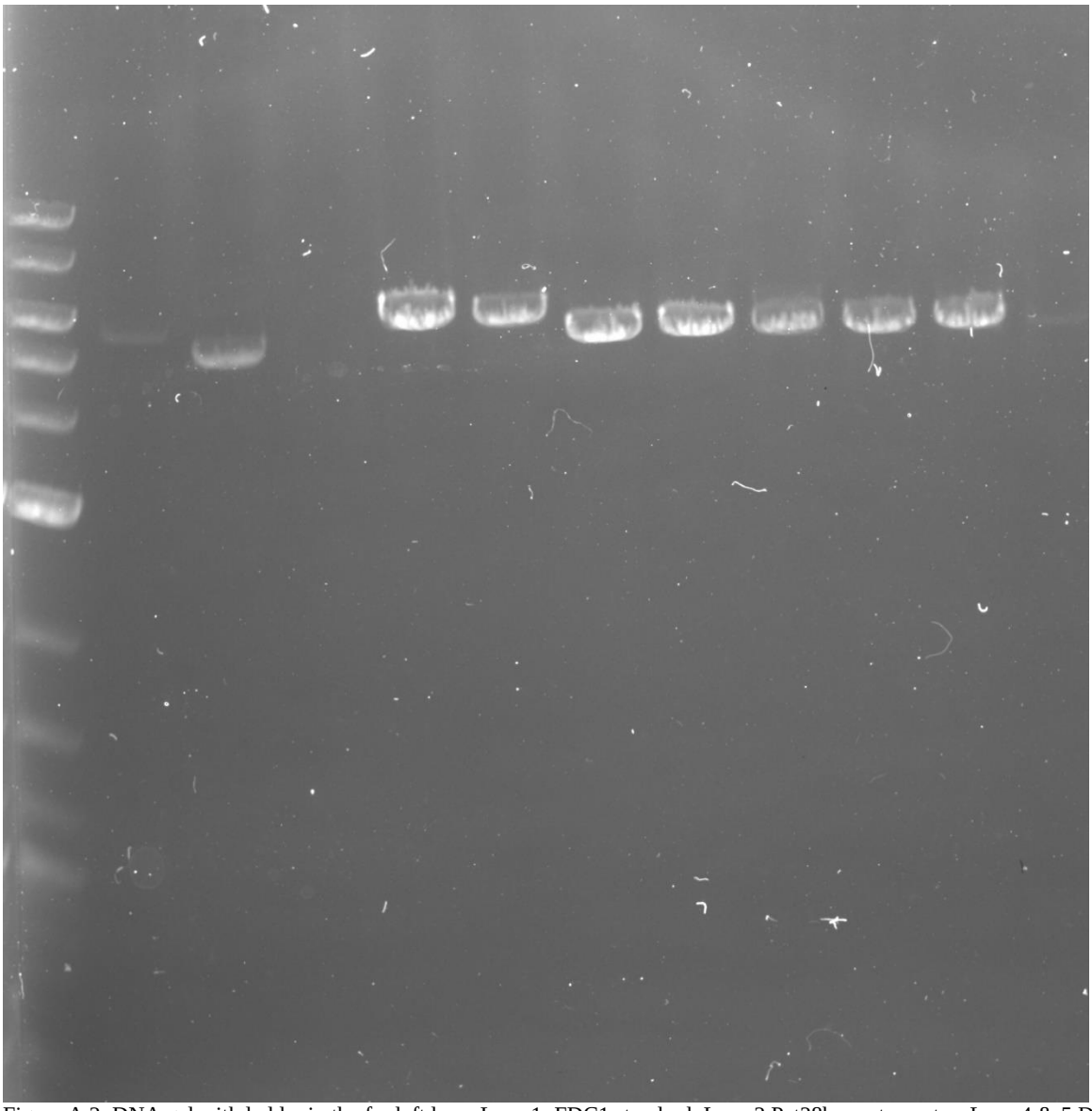

Figure A.2. DNA gel with ladder in the far left lane, Lane 1: FDC1 standard, Lane 2 Pet28b empty vector, Lane 4 & 5 Duel construct Lanes 5-9 FDC1 mutant DNA linearization

Appendix A.4 Typical GC-MS spectrum of TCA and Styrene

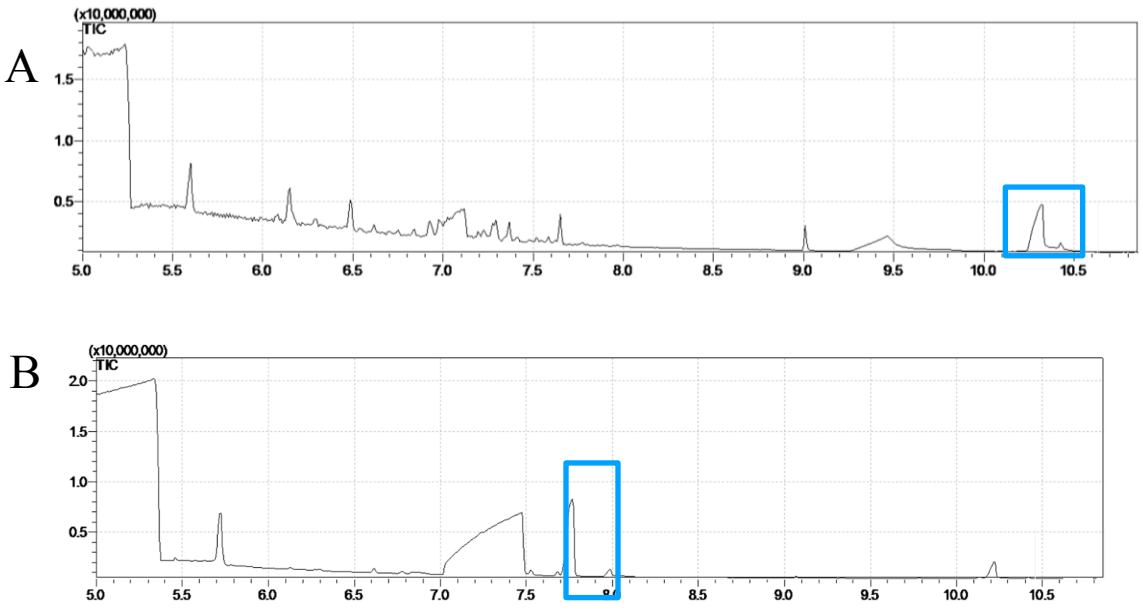

Figure A.3 Typical GC-MS result where A is the no – enzyme control where TCA presents at 10.25 minutes (B) Styrene peak present at 7.8 minutes

Appendix A.4.1 Styrene Calibration Curve for GC-MS

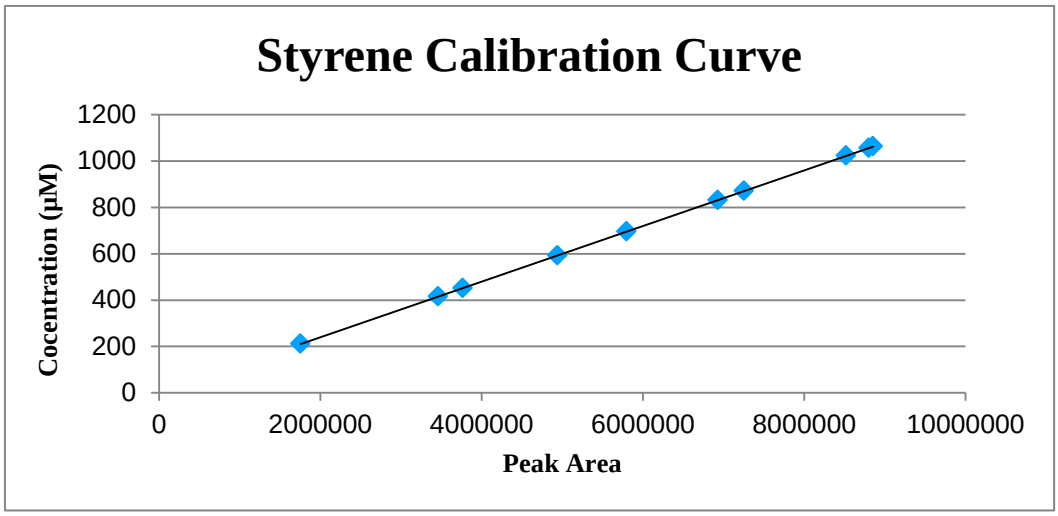

Figure A.4. Styrene Calibration Curve for GC-MSanalysis

Appendix A.5 $_1$d-Cinnamic Acid ^{1}HNMR and Cinnamic Acid Product Standard

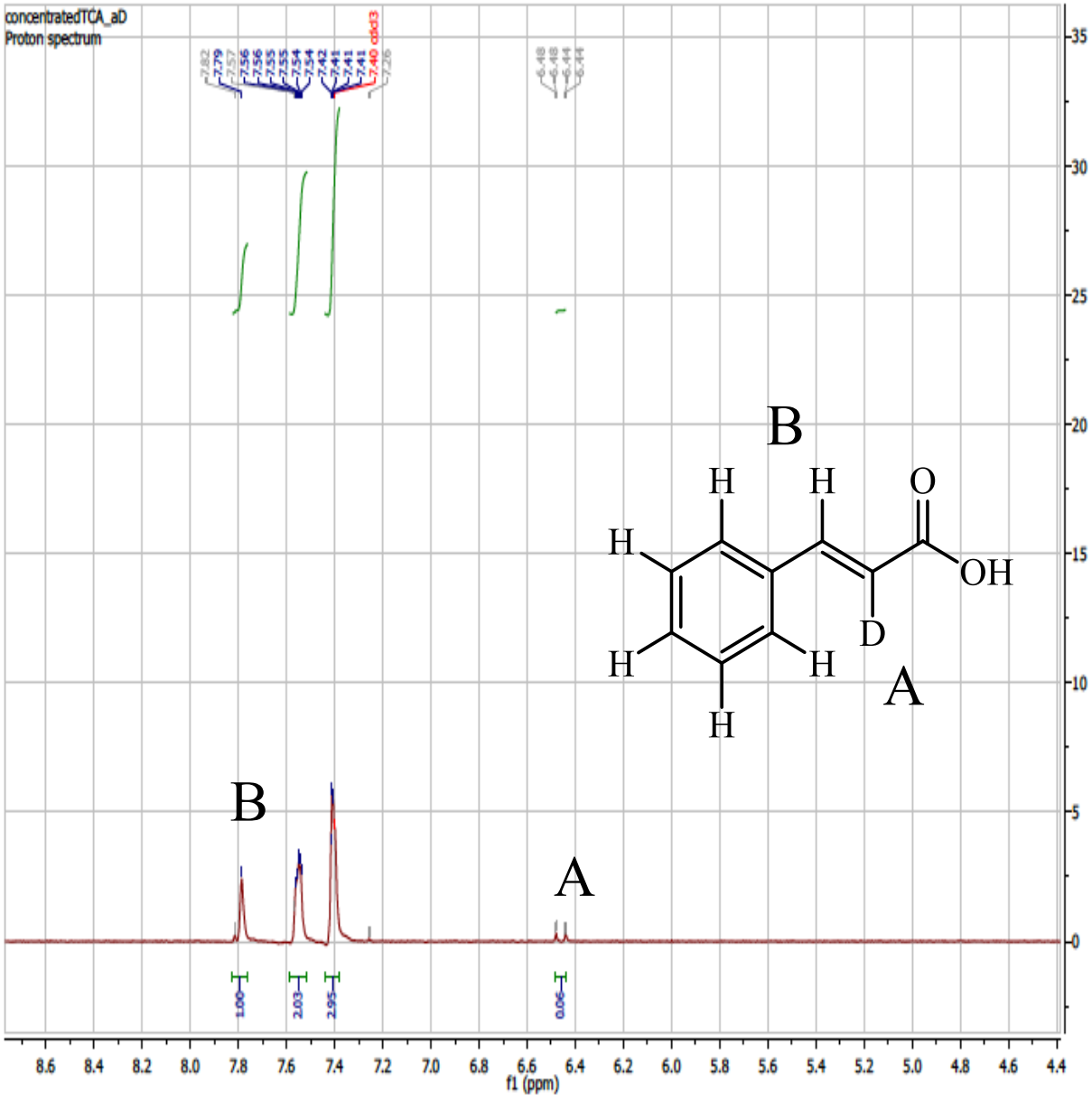

Figure A.5 $_1$d-TCA NMR with a singlet at 7.79 ppm and a disappearance of the doublet a 6.48 and 6.44 ppm

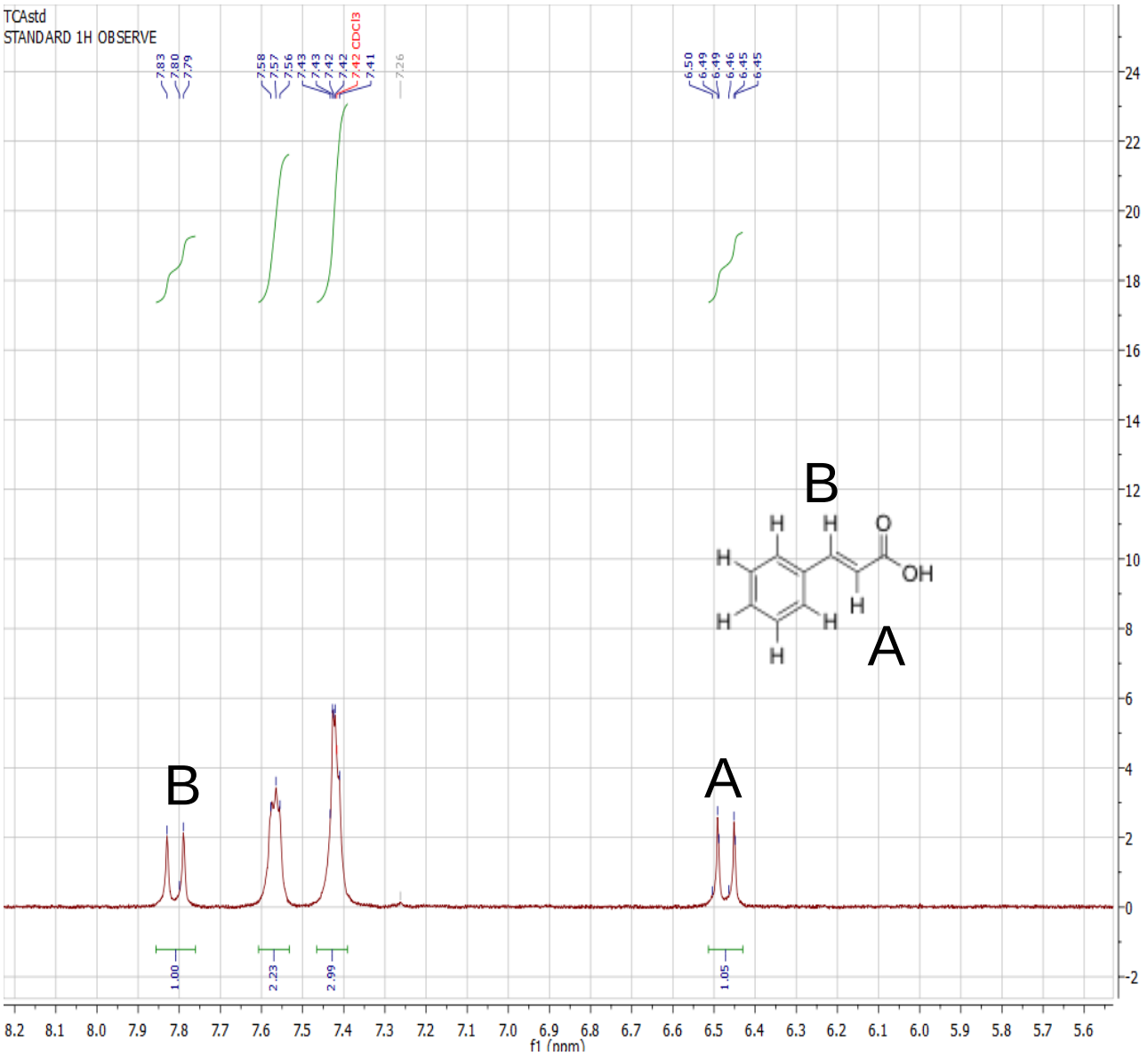

Figure A.6 TCA NMR with a doublet at 7.79 and 7.83 ppm a doublet a 6.48 and 6.44 ppm